D3.5 – Prototypes characterization and durability testing

WP3

Lead Partner: UNIVPM

Partner Contributors: ULSTER, SAES, TVITEC, DAPP, FOCCHI, BGTEC

Dissemination Level: Public

Deliverable due date: M44   Actual submission date: M47

Deliverable Version: V0

Project Acronym	Eensulate
Project Title	Development of innovative lightweight and highly insulating energy efficient components and associated enabling materials for cost-effective retrofitting and new construction of curtain wall facades
Grant Agreement n°	723868
Funding Scheme	Innovation Action
Call	H2020- EEB-2016
Topic	EEB-01-2016 Highly efficient insulation materials with improved properties
Starting Date	1st August 2016
Duration	49 Months

Executive Summary

The document collects the main results achieved in the completion of Task 3.6 of the Eensulate project and specifically the activity for prototype characterization (SubTask 3.6.1) and for durability testing (SubTask 3.6.2).

Concerning the prototype characterization, the fabricated EENSULATE glass system has been characterised in the laboratory for performance evaluation under steady state conditions. Thermal transmittance (U-value) has been determined in a guarded hotbox calorimeter. A methodology to measure the effects of thermal shock has been proposed. Permeation measurements of the sealing and of the getter materials have been performed. In order to assess the effectiveness of the gas barrier outgassing effects have been also monitored.

Concerning the durability testing, specific accelerated ageing procedures have been developed to evaluate the durability of the stimuli-sensitive solar reflective (thermochromic) glass coating. The main objective here was to evaluate the effect of ageing on the radiative properties (solar reflectance and thermal emittance) and therefore on the dynamic response of the coating to the environmental changes, taking into account also the soiling effect due to dust, soot deposition and biological growth.

Table of Contents

List of Figures

List of tables

Abbreviations and Acronyms

[COG] – Center of Glass

[EC] - European Commission

[EOG] – Edge of Glass

[EU] - European Union

[VIG] - Vacuum Insulated Glass

[TGU] – Triple Glass Unit

[UV] - Ultra-Violet

[VIS] - Visible

[NIR] – Near Infra Red

[WP] – Work Package

[D] – Deliverable

[wt] – weight

[a.u.] – adimensional unit

1 Introduction

This deliverable reports the results of Task 3.6 on which activities on prototypes characterization and durability testing have been performed. Specifically the following activities have been carried on and their results described in this deliverable:

- determination of thermal transmittance characteristics in a guarded hotbox calorimeter (Section 2.1);
- determination of the gas permeability and outgassing of the sealant employed for VIG prototype (Section 2.2);
- development of a procedure for the VIG prototype thermal shock assessment (Section 2.3);
- measurement of thermochromic coatings optical properties, i.e. solar and luminous transmittance and reflectance (Section 3);
- development and performance of natural and accelerated aged tests for estimation of durability of thermochromic coatings in terms of optical properties (Section 4);
- check of compliance of design and manufacturing to retrofit strategy (Section 5).

2 Prototype characterization

2.1 Prototype thermal characterization

2.1.1 Introduction

The thermal performance of the building façade curtain walling is primarily influenced by the U-value of both the glazed elements and the framing system, with the former having the most significant impact on building heat loss or heat gain. For an individual glazing element the U-value can be quoted as a centre-of-pane value (which is common practice in industry) or an overall glazing value which includes heat transmission through the glazing edge seal area. In the modelling work in Task 3.1 the thermal performance of the vacuum insulated glass (VIG) was optimised based on limiting mechanical stresses and material performances, therefore an accurate measurement of the U-value of the developed prototype VIG's should be determined and compared to the modelling results. In this work U-value measurements have been undertaken on initial VIG prototype samples sealed with organic resin EPO4.2 using a guarded hotbox calorimeter.

2.1.2 Experimental Guarded Hotbox Procedures

The guarded hotbox used in this work comprises a guard chamber (commonly referred to as the hot chamber) with an inner metering box, and an environmental chamber (commonly referred to as the cold chamber) separated by a central mask wall. An opening provided in the mask wall accommodates the glazing under test. The hotbox is illustrated in Figure 1.

Isothermal baffle plates with matt black coatings of emissivity ≈ 0.9 in the metering box and in the environmental chamber ensure a uniform radiant temperature and view factor to the VIG, preventing local radiative heat exchange between the glazing and other components inside the chambers. Air circulation fans are used in each chamber and metering box to ensure adequate mixing of the air and to help achieve the required surface heat transfer coefficients on the glazing as detailed in appropriate standards. Heaters are used to achieve the required temperatures in the metering box and guard chamber and a chiller provides a well-controlled low temperature environment in the environmental chamber. For the purposes of U-value determination, the metering box and guard chamber setpoint temperature is a nominal 20°C while the environmental chamber setpoint is a nominal 0°C. A series of type T thermocouples are used to monitor the

air temperatures, mask wall and baffle plate temperatures, and the glazing temperatures and logged via a Keithley data acquisition system.

Figure 1. Guarded hotbox calorimeter

To determine the thermal transmittance of a VIG, the prototype is installed in the opening in the centre of the mask wall. When steady-state conditions (±0.1°C) has been achieved the temperature of the air and glazing surface in the metering box/ chambers are measured. A schematic representation of the hotbox is illustrated in Figure 2 showing the principal heat transfer processes. Heat transfer Q_s can be calculated for a given input power, Q_{input} to the heaters inside the metering box. Heat transfer through the VIG prototype sample in the guarded hot box can be determined from:

$$Q_s = Q_{input} - Q_b - Q_m - Q_e$$
1

The temperature difference between the metering box and the surrounding guard chamber is minimised by adjustment of the heater power, therefor heat flow through the metering box, Q_b is controlled to be negligible. Heat transfer through the mask wall, Q_m is determined by measurement of mean mask wall surface temperatures in the guard and environmental chambers and by knowledge of the mask wall material conductivity. The flanking loss, Q_e, i.e. the heat transfer through the exposed edge area of the mask wall adjacent to the VIG test sample, is determined experimentally using standard samples of known thermal properties.

Radiant and air temperatures can be combined into a single environmental temperature T_n, which represents the appropriate weighting of air and radiant temperatures for the purpose of determining the heat flow to the surface, given by:

$$T_n = \frac{T_a \frac{Q_s}{A} + \varepsilon h_r (T_a - T_r) T_s}{\frac{Q_s}{A} + \varepsilon h_r (T_a - T_r)}$$
2

$$h_r = 4\sigma T_m^3 \qquad\qquad 3$$

where

$$T_m = \frac{T_r + T_s}{2} \qquad\qquad 4$$

Where T_r is the mean temperature of the copper baffle; T_s is the mean temperature of the glazing surface. Using equation 2, the environmental temperatures in the hot and cold chambers, T_{n1} and T_{n2} can be calculated. The overall heat transfer coefficient is then given by:

$$U = \frac{Q_s}{A(T_{n1} - T_{n2})} \qquad\qquad 5$$
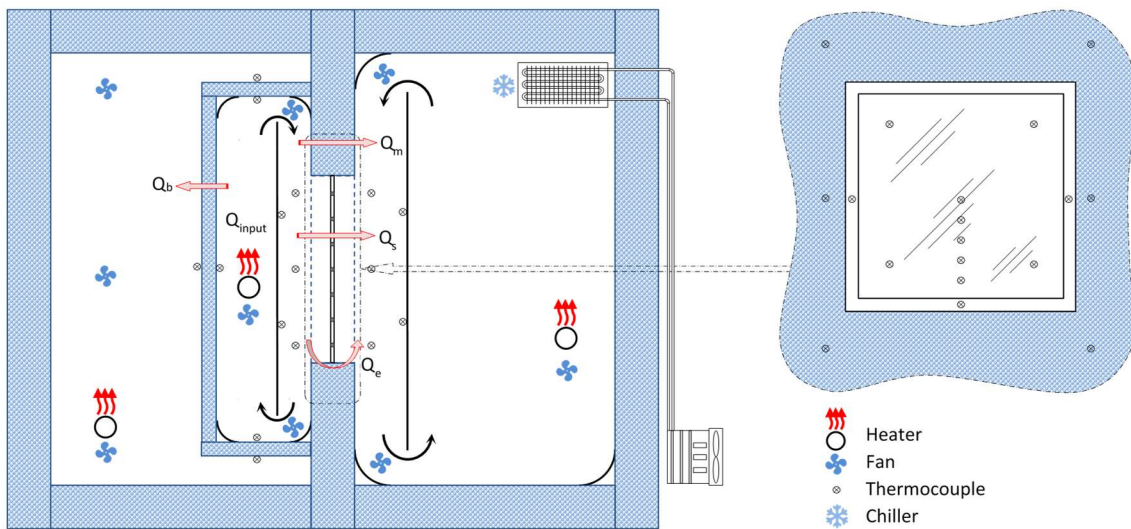
Figure 2. Schematic representation of the guarded hotbox calorimeter

2.1.3 Heat Transfer Measurement

To assess the thermal transmittance (U-value) of the prototype VIG samples the VIG is positioned in the opening in the mask wall between the hot and cold chambers and sealed around the edges to ensure there is no air leakage between chambers. The heaters, circulation fans, chiller and data acquisition are activated. The PID controller for the heater in the guard chamber is set to a nominal 20°C, while the PID controller for chiller in the environmental chamber is set to 0°C. The power to the heater and circulation fans in the metering box is supplied via two DC power supplies. These allow for the accurate adjustment and precise measurement of the power required to maintain a temperature balance between the metering box and the guard chamber. The initial power settings for these are based on hotbox calibration results, the procedure for which is outlined in the following section. The hotbox is allowed to stabilise for 24 hours before the temperature balance between the metering box and the guard chamber is checked and the power adjusted as required to achieve an accurate temperature balance. When equilibrium has been achieved the temperature and power data is logged and a U-value determined using the procedure described in section 2.1.2.

2.1.4 Hotbox calibration

To accurately determine the thermal transmittance U-value of a glazing element it is necessary to calibrate the guarded hotbox calorimeter with materials of known properties. Calibration is commonly undertaken with Styrofoam insulation panels of the same size as the glazing under test and with thicknesses in the same range of the glazing thickness, in this case 10 – 22mm in thickness. Using a calibration panel with a similar thickness to the glazing test specimen allows for a more accurate determination of the flanking losses discussed in section 2.1.2. The calibration panels are positioned and sealed in the opening in mask wall and the process described in section 2.1.3 is used to determine the input power required to achieve steady state conditions for any given thickness of calibration panel. Figure 3 illustrates a typical calibration setup using a polyurethane insulation calibration panel, (note this is a full thickness calibration sample and used for illustration purposes only).

Figure 3. Typical calibration procedures using a material of known properties

2.1.5 Experimental results

The thermal characterisation of the initial vacuum sealed VIG prototypes developed in Task 3.5 was evaluated using the procedures described in the previous sections. Although a significant number of prototype samples were fabricated as discussed in deliverable report D3.2, the challenges in prototype development limited the number of available samples for thermal characterisation. The U-value was measured on prototype VIG's which had a getter activated under static vacuum (after sealing the pump-out hole) and under dynamic vacuum (before sealing the pump-out hole), the results of which are shown in Table 1 below.

Table 1. Prototype VIG U-value measurements

Getter activation under Static Vacuum		Getter activation under Dynamic Vacuum	
Centre-of-pane U-value $Wm^{-2}K$	Overall U-value $Wm^{-2}K$	Centre-of-pane U-value $Wm^{-2}K$	Overall U-value $Wm^{-2}K$
0.7	0.9	0.36	0.44

As can be seen in the results the U-value of the VIG which had the getter activated under dynamic vacuum had the lowest U-value i.e. the best performance. The poorer performance of the VIG which had a getter

activation under static vacuum i.e. after the VIG pump-out port has been sealed is probably due to the presence of contaminants released by the getter during activation at high temperature which subsequently degrade the vacuum pressure to a level where gaseous conduction is present. With further research it is anticipated that a suitable getter activation process can be developed which negates the impact of activation under static vacuum on thermal performance.

The higher U-values measured for the overall glazing area compared to the centre-of-pane area is due to the influences of lateral heat flow to the edge area and the subsequent increased conduction through the edge seal region. For calculating the overall glazing U-value (U_{Total}) we consider average glass surface temperature over the total glazing area, however to calculate the centre-of-pane U-value (U_{centre}) we consider the temperature measured only in the central region of the test sample on both sides of the VIG (using readings from 3 - 4 thermocouples attached to the central region of the glazing on each side). In previous work the edge seal area has been shown to have a significant on overall glazing performance particularly when a modest sample size is considered. This influence diminishes as sample size increases. To obtain an overall U-value the VIG is tested without a frame. In practice however the VIG will be incorporated into a suitably designed framing system covering the edge seal area, therefore the influence of the edge area conduction will be reduced.

The experimental measurements of the initial prototype VIG's compare favourably with the project target U-values of 0.3 $Wm^{-2}K$ for the given assembly conditions i.e. pillar size and spacing and glass thickness. Although the modelling results highlighted a lower U-value was, in theory, achievable, a more precautionary approach was taken with the practical fabrication of the VIG to ensure that the limiting stresses in the assembled VIG did not compromise the integrity of the glazing. This included a small increase in pillar diameter, a small decrease in pillar spacing and a 6mm thick glass pane as opposed to a 5 mm pane, all of which contributed to a modest increase in U-value.

2.2 Prototype thermal shock

2.2.1 Thermal Cyclical Testing VIG Prototypes

The in-situ thermal and mechanical performance of a VIG in any installation may be affected by the temperatures to which it is exposed and the resulting stress gradients which can develop. If severe, these stresses could affect the integrity of the glazing causing a failure of the edge seal, or a failure of the glass particularly in the region of the support pillars where there are significant stress concentrations present. Replicating exposure conditions in a laboratory can give an indication of potential failure. In these proposed tests small scale VIG prototypes, approximately 600 by 600mm, would be evaluated for the effects of differential thermal loading under temperature cycling, which would generate a potential stress gradient in the sealed VIG. In reality the temperature induced stress will be affected by the size of the glazing under test, the larger the glazing the higher the risk of failure due stress and flexure as a result of temperature gradients. Additionally, the framing and support arrangements for the VIG will also impact on the resulting stress generated and control flexure which can influence the incidence of failure. Although these proposed temperature cycling tests do not follow a standardised test protocol, they do provide an indication of the resistance of the VIG to temperature differentials while taking into consideration the size restrictions discussed.

For the proposed test procedure described herein, the VIG prototypes require thermal transmittance U-value characterisation in a guarded hotbox calorimeter using standardised test protocols, as described in Section 2.1, to establish pre-cycling thermal performance. Thermal cycling tests would then be undertaken in the hotbox calorimeter used for U-value measurements.

The VIG is secured using an appropriate framing solution in the centre of the mask wall between the hot and cold chambers of the hotbox in Figure 1.

Testing commences with the glazing exposed to a constant temperature equilibrium of 20°C on both surfaces. One surface of the VIG is then maintained at a constant 20°C throughout the test cycle (representing the indoor environment), while the opposing face is exposed to a transient temperature cycle (representing the outdoor environment). Typically, this temperature is lowered to -20° or below, maintained for a set period (potentially 2 hrs) and then raised to typically 50°C where it is maintained for again for a set period (2 hrs) before returning to 20°C to complete the cycle. This temperature cycling procedure is repeated, following which the U-value of the VIG is remeasured in the hotbox calorimeter to determine any effects of the thermal cycling and the resulting stress on the U-value thermal transmittance.

The time required to undertake these tests would be a minimum of 3-4 weeks, subject to availability and scheduling of the necessary equipment. The testing procedure requires a calibration of the hotbox for the U-value test, the pre-cycle U-value test on the VIG, 1 week of thermal cycles and a post-cycle thermal U-value test. However, these tests cannot be performed due to closure of Ulster University and its laboratories as a result of the Covid-19 pandemic. There is currently no anticipated reopening date for the University.

2.2.2 Fire behavior of small scale VIG prototypes

Small-scale VIG prototypes having dimensions of 600 mm x 600 mm will be tested in an indicated (reduced) scale furnace (1.5 m x 1. 5m x 1.5 m) as shown in the figure below and the fire behaviour of the VIG sample will be compared with that of traditional TGUs. The furnace gas temperature will be controlled to follow the standard ISO 834 curve typically found in compartment fires. The temperature at different locations on the unexposed face of the specimen will be measured using k-type thermocouples. The whole tests will also be recorded to identify the failure of the components as well as of the whole assembly including the cracking and possible fall-out of the glazing and associate times to evaluate the overall fire performance of the VIG prototypes against that of TGUs.

Figure 4. Indicative furnace

It is expected that the work related to this task including the preparation of the test, testing and preparation of the report would take approximately two weeks, however, it was not possible to perform these tests due to the fact that Ulster University including all laboratories is currently closed and it is not possible to know when the University will re-open.

2.3 Prototype permeation characterization

2.3.1 Introduction

This section describes in details characterizations performed onto sealant resin according with specifically designed and/or standardized tests.

In a VIG, the sealant resin is placed peripherally between glasses and actually defines the edges of the inner evacuated chamber. Differently from glasses that are virtually impermeable to all gases (He excluded), because of its polymeric nature, sealant represents the major front of access for gasses and its definition has actually represented one of the main challenge of the whole project.
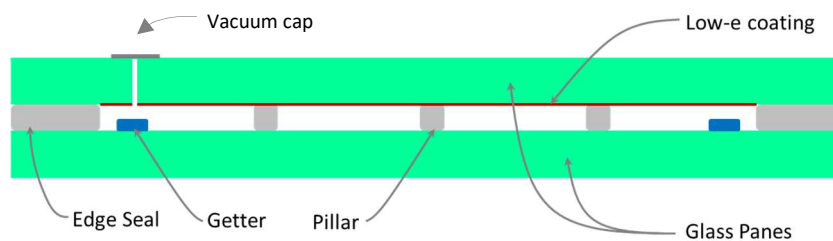
Figure 5. Cross-section scheme of EENSULATE VIG configuration

As a matter of fact, no polymeric sealant was described for VIG sealing in previous scientific literature: the stringent vacuum requirements, together with mechanical strength and durability, were supposed not be addressable with an organic resin.

The definition of coarse formulation as well as fine tuning of recipe and process steps have required a careful characterization of the material in terms of permeation performances that, in ultimate analysis, has driven sealant development.

The theme of vacuum level within the VIG in relationship with thermal properties has been largely discussed in previous documentation, but here we remind that higher the pressure, higher is the thermal conduction in the gap. At given boundary conditions (geometrical and temperature factors), heat flow through a gas at lower pressures is demonstrated to be linearly dependent with the pressure itself and gives a contribution to the overall glazing conductance ranging from 0.02 up to 0.2 $W \cdot m^2 \cdot K^{-1}$ per mTorr of residual gas [1]. In other terms, few mTorr of pressure within the evacuated chamber will give a conductance contribution comparable with the sum of all other parts making the VIG.

Such requirement on pressure has to hold for decades of service life of the VIG device, thus is clear how critical the permeability characterization is.

It is worth to note that just recently (2018) the International Organization for Standardization made available an evaluation method for VIG namely the "ISO 19916-1:2018 Glass in building — Vacuum insulating glass" but just the first section "Basic specification of products and evaluation methods for thermal and sound insulating performance" is complete and available, while the second and third sections, respectively concerning "Mechanical behaviour" and "Test methods for evaluation of performance under temperature differences" are still at drafting stage. The early stage of regulation remarks from one side the novelty of the technology and on the other side the presence of a technical and scientific community actively interested in drawing a common base for VIG evaluation and commercialization.

Because of the lack of standards in characterizations for VIGs vacuum level, we mainly took advantage of standards and methodologies generally developed for permeation through barriers.

In order to characterize the effectiveness of a gas barrier two main effects have to be considered, namely permeation and outgassing. Two sub-sections are devoted to describe methods and results. Here we remind

the general idea, already provided in previous deliverables, that vacuum is not statically defined within the chamber but is rather a dynamic balance between sources and wells. The incoming fluxes are actually determined by the permeation (i.e. the gas flow coming from outer volume) and the outgassing (i.e. the lightweight molecules already trapped into the close volume, onto the inner surfaces or in their close proximity, that during time escape from the solid state to the volatile state, generating a consequent gas load). The outcoming terms are represented by the pumping elements: the real pump during the VIG production and the getter or drier pumps during operation.

Details of tested formulations are provided in D3.2 but for confidentiality reasons cannot be fully reported here. We instead report the following table as reference:

Table 2. List of materials formulated and screened during the project

Code	Name/Component
HM1	H-Dry® (SAES product)
HM2	Butyl rubber (isoprene and polyisobutylene)
HM3	Butyl rubber (isoprene and polyisobutylene)
PIB1	Polyisobutylene
PIB2	Polyisobutylene
PIB3	Polyisobutylene
PSF	Polysulfide
EPO1	Curing agent 1 + Epoxy resin 1
EPO2	Curing agent 2 + Epoxy resin 1
EPO2.2	Curing agent 2 + Epoxy resin 2
EPO2.3	Curing agent 2 + Epoxy resin 3
EPO3	Curing agent 3 + Epoxy resin 1
EPO4	Curing agent 4 + Epoxy resin 1
EPO4.2	Curing agent 4 + Epoxy resin 2
EPO4.3	Curing agent 4 + Epoxy resin 3
EPO5	Curing agent 5 + Epoxy resin 1 + Rubber component + Epoxy resin hardener Epoxy resin promoter + Others

2.3.2 Permeation measurements

Among different measurements, permeation can be considered the most important characteristic of a vacuum sealant because indicates how easily a given gas can pass through the sealant itself.

More rigorously, permeability P is:

$$P = \frac{j}{|p_{out} - p_{in}| \cdot \delta}$$

6

Where j is the flux of gas passing through the surface, δ is the thickness and p_{out} and p_{in} are the pressures across the sealant. There are several units of measure for the permeability and, in most of the cases, their difference deals with the way the flux is defined (e.g. mass, moles, or gaseous volume at standard pressure and temperature). We adopt as unit the Barrer $\left(1\,barrer = 10^{-10}\,\frac{cm^3_{STP}\cdot cm}{cm^2\cdot s\cdot cmHg}\right)$ that, even if not belonging to the International System, is still very popular.

Transmission rate (TR), that is very related quantity sometimes used interchangeably with permeability, is not normalized for the barrier thickness δ. The characteristic of a barrier toward Oxygen and water are typically given as TR (respectively as Oxygen Transmission Rate – OTR – or Water Vapours Transmission Rate -WVTR) but when possible we prefer to express permeation normalized for thickness (e.g. units of Barrer) and with the same unit for different gases, also to make easier the data comparison. Worth to note that for a given permeability value, the incoming flux is proportional to the pressure difference and inversely proportional to sealant thickness.

Permeation is traditionally regarded as the product of two terms: the Solubility factor that describes the amount of gas able to penetrate the matrix at a certain gas pressure (and account for the chemical affinity between the permeant and the matrix) and the Diffusion factor that describes the mobility of the permeant in the matrix [2]. For the purpose of our tests we limited the analysis to the global factor Permeability.

Being the permeation a characteristic of the material, typical measurements are performed on a specific geometry, such as a membrane where the thickness is very limited with respect to exposed area. This arrangement is preferred in order to maximize instrument sensitivity and throughput. Especially for well performing sealants, such as the ones produced within Eensulate, testing the real configuration would have required months of dedicated machine time. We took advantage of the fact the geometrical shape of the specimen does not affect the permeation, that is actually re-scaled for the area and thickness.

Permeability, in both the Solubility and Diffusion terms, is gas-dependent thus its value relates to the specific gas under analysis. For this reason we should in principle test all possible gases.

Luckily the set of the most relevant gases to evaluate for permeation is pretty limited and can be listed in: N_2, O_2, Ar, CO_2, CO, He plus Water moisture. In deliverable D3.1 we showed that Rowe and co-workers [3] defined a set of correlation rules based on a large database of permeability values, to estimate the permeability of most of gases from a limited number of experimental data. These correlation rules allowed us to reduce the number of required measurements. Details and description on different gases are provided in the following sub-paragraphs.

To speed up screening process and to provide a double check on these sensitive measurements, tests were performed both in external laboratories as well as internal laboratory. In particular the majority of tests performed according ASTM D 1434 on He, Ar and O_2 were performed at "Inter-departmental Center of Advanced Industrial Mechanical Research and Materials" of University of Bologna. Tests performed according ASTM F 1927 on O_2 have been run internally in SAES with a commercial instrument, namely OX-TRAN® Model 2/22 from MOCON. The analysis is highly automated, thus no much effort by operator is required. For these reasons we do not spend much words here but for more details refer on the vendor website.

On the contrary, experimental equipment used for permeation tests according with the standard ASTM D 1434.1 were home-made, thus we will describe with some details the operation principles and data extraction that, with some extent, are also valid for O_2 measurements . Worth to mention that sample outgassing conditioning described below is also valid for O_2 measurement performed with MOCON.

The core of the permeation system is a closed system, where the volumes are known and it is possible to detect pressure rise in the chamber located downstream of the membrane (see Figure 6). In its essence, the system consists of two closed volumes separated by a cell containing the film to be characterized.

On the downstream volume there is a capacitive pressure gauge, with full scale 10 mbar and resolution 10^{-3} mbar. To promote desorption of all volatile chemical species dissolved into polymer, the polymer sheet is initially conditioned in a vacuum oven at 120°C for 24 hours, then mounted on the sample holder cell and dynamic vacuum is applied overnight with a high vacuum rotary pump. When the film is mounted into the

system, during both vacuum step as well as during the permeation measurement, the temperature is kept constant and uniform at 35°C through the PID controller of the incubator where the entire system is housed.
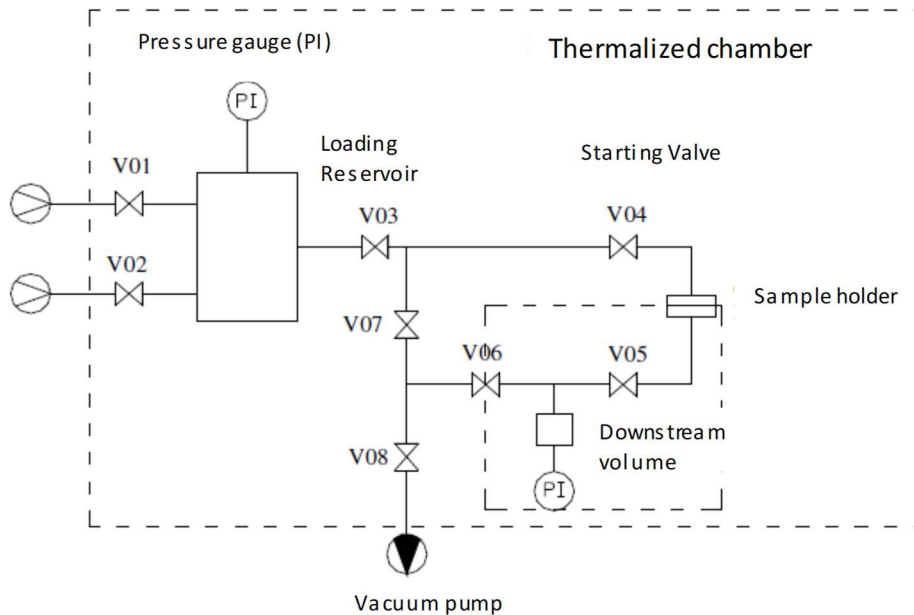
Figure 6. Scheme of permeation test bench

Once the preliminary operations are completed, the vacuum pump is disconnected and upstream volume is set at a given pressure (through valves V03 and V04) provided by the loading reservoir (1 Bar). The pressure in the downstream volume increases as effect of permeation of gas through the membrane. After an initial transitional phase, the steady state is approached and a linear trend of the downstream pressure is observed, thus the test can be considered concluded. An example of the experiment output is shown in Figure 7. The same procedure was repeated several times (at least 2 or 3) for each sample to ensure repeatable and reliable results.
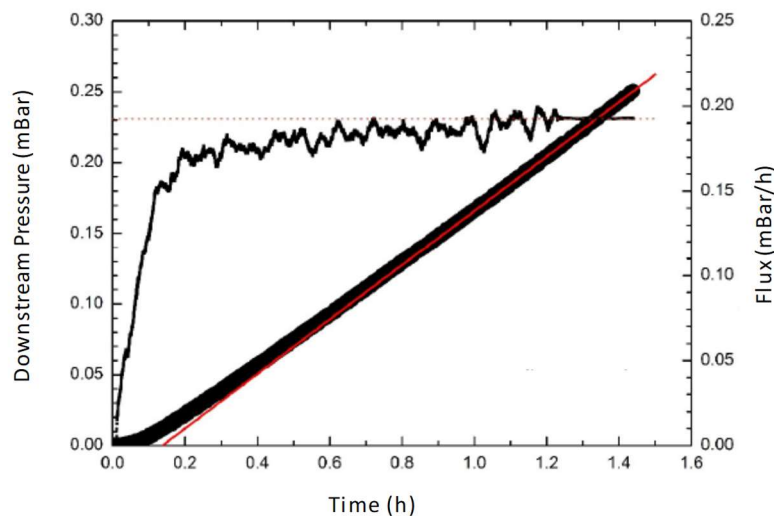
Figure 7. Example of measurement output from permeation test bench

The permeation P can be determined with the following relationship:

$$P = \frac{dp_{down}}{dt}\bigg|_{t\to\infty} \cdot \frac{V}{R \cdot T} \cdot \frac{\delta}{A} \cdot \frac{1}{(p_{up} - p_{down})} \qquad 7$$

Where p is the pressure, measured in the upstream (*up*) and downstream (*down*) chambers, V is the volume of the downstream chamber at the given temperature T, R is the gas constant , δ and A are respectively the average film thickness and its exposed area.

Table below reports permeability measurements for selected gases collected on different resins according with several standard procedures. Discussion and comments on the values are given in the following sub-paragraphs.

Table 3. Summary of permeability data measured for different sealants. In the case of EPO 4.2 moisture permeability two values are reported: * value corresponding at WVTR of 2.85 g/m^2/d for a film 0.25mm thick at RH 90% and T=38°C measured for the EPO 4.2 matrix; **value estimated for EPO 4.2 I, i.e. the EPO 4.2 when an active drier is embedded.

Code	Ar [Barrer]	He [Barrer]	O$_2$ [Barrer]		H2O [Barrer]
Standard	ASTM D 1434	ASTM D 1434	ASTM D 1434	ASTM F 1927	ASTM F 1249
HM1	9				
HM2	0.5				
HM3	0.5				
PIB1	0.3				
PIB2	0.4				
PIB3	0.5				
PSF	1				
EPO2.2	$9 \cdot 10^{-3}$	1.7			
EPO2.3					
EPO4	$7 \cdot 10^{-2}$	1.7		$2 \cdot 10^{-2}$	
EPO4.2	$3 \cdot 10^{-3}$	1.3	$1 \cdot 10^{-2}$	$1 \cdot 10^{-2}$	$230*/<10^{-5}**$
EPO4.3	$2 \cdot 10^{-3}$			$4 \cdot 10^{-3}$	
EPO5	0.3			0.6	

All values reported in Table 3 are given for sample at 35°C or 38°C. Relative Humidity (RH) is 0% for all gases except, of course, for the column of H$_2$O. In that case carrier is nitrogen and RH is 90% (corresponding to 59.4 mBar). In the case of EPO 4.2, where O$_2$ permeability has been recorded with two different techniques, we observe a very good matching between the two data.

2.3.2.1 Noble gases

At ordinary conditions all noble gases have as common and distinctive property to be chemically inert. Because of their chemical nature, they tend not to interact with matter and for this reason they cannot be trapped with any getter device.

As obvious consequence, all noble gases that penetrate into VIG by permeation cannot be removed anymore and their accumulation produces a detrimental and unwanted pressure increase.

Argon is by far the most abundant noble gas in the atmosphere and for this reason is regarded as one of the main target of our analysis; the permeation of the sealant to Ar is one of the limiting factors affecting the lifetime of the VIG device or, in other terms, the effectiveness of selected sealing resin. From previous analysis (see for instance D3.1), the permeability target for Ar was 10^{-2} Barrer or below. As reported in the Table 3, EPO 2.2, EPO4.2 and EPO4.3 satisfy this condition.

Heavier noble gases (Kr, Xe, Rn), because of higher mass, would exhibit lower diffusivity (thus lower permeability) that combined with their scarcity make them not critical for inner VIG pressure raise.

Helium is also present in atmosphere, but at trace level (i.e. 5.2 ppmV). It is particularly harmful because its high kinetic mobility make it a high thermally conductive gas and, at the same glance, a fast permeant (as reported in the Table 3 P_{He} is 10 to 300 time higher than P_{Ar} for different resins). However combining He scarcity together with the experimentally determined barrier properties of EPO 4.2, it comes out that for 1 m^2 VIG, the inner pressure increases due to He contribution is just of $2 \cdot 10^{-5}$ mBar per year, thus fully compatible with the target.

Neon is also present in traces in air, i.e. 18 ppmV (3.5 times the helium), but is heavier (4 times) than He, thus it is expected to give a comparable contribution with He.

2.3.2.2 Getterable gases

Getterable gases are defined as the permanent gases (i.e. not able to condensate at standard pressures and temperature) that can be trapped by a getter. As mentioned before, the group of relevant getterable gases are N_2, O_2, CO_2, CO.

Nitrogen and Oxygen are so far the most abundant gases in the atmosphere and for this reason both of them are regarded as potentially detrimental source of contamination.

Thanks to the correlation of Rowe and co-workers [3] we have been able to use the measurement of O_2 permeation to estimate also N_2 permeation.

For determination of OTR, and consequently O_2 permeability, SAES already possess a best in class instrument, namely OX-TRAN® Model 2/22 from MOCON, able to operate according with ASTM F 1927 protocol. This system relies on a coulometric sensor that requires no calibration, offers a high selectivity toward the target gas (O_2) and is well recognized for its robustness in a wide dynamic range. For this reason we decided to focus our attention to O_2 data collection.

CO_2, CO, that are also typically present as contaminants in a vacuum device, exhibit a much higher permeability value than O_2 and N_2 (till a factor 6x higher than O_2) but since they are not so abundant as O_2 and N_2, they are not likely to heavily affect total getter gas load. CO_2, CO are generated within the vacuum device as effect of direct outgassing and/or oxidation of outgassed organic compounds (such as CH_4 and other hydrocarbons). In any case the dimensioning of the getter, intended to cope with very large amounts of N_2 and O_2, is supposed to offer enough rooms also for CO_2, CO, regardless their origin.

Concerning hydrocarbons, or other volatile organic compounds in general, their presence in atmosphere is typically so low with respect to the corresponding permeability, to be not considered as noxious sources of permeation.

2.3.2.3 Water Vapour and Drier

Water vapours are among the most permeable gases the organic matrix have to deal with. In general water vapours tend to robustly dissolve into matrix and this gives a large contribution to the permeability through the solubility term. Moreover the plasticizer effect due to water swelling typically favours permeation also to other gases that in moisty conditions can exhibit higher transmission rate [4]. For these reasons water vapours are particularly important in sealant formulation.

For Water vapour permeation measurements we used a HiBarSens from SEMPA SYSTEMS GmbH, in a configuration analogous to the one described by ASTM F 1249. Vapour permeation test system uses the common permeation measurement setup, consisting of a permeation cell, divided into an upper and a lower compartment, which are separated by the barrier sample. The sensor is directly placed into the lower compartment. The detection principle is based on the measuring of the attenuation of the laser light intensity, caused by the excitation of the permeated water molecules. To further enhance the sensitivity, the laser diode spectrometer uses a wavelength modulation technique with second harmonic detection. All details of measurement scheme are given at this reference [4].

Measurements taken on a 250 µm thick film for different temperatures are summarized below.

Repeated tests give very comparable results.

Table 4. WVTR Tests performed

T(°C)	RH	p (mBar)	WVTR (g /m² day)	Permeability (Barrer)
38	90%	59,40	2,850	230
25	90%	28,53	1,197	200
12	90%	12,62	0,458	175

As reported in Table 3 and Table 4, water actually represents the worst gas to block because of its permeability and abundance in ordinary conditions. All three measurements here reported have been collected at 90% RH, that for different temperatures, correspond to different partial pressure of water.

Figure 8 reports an Arrenhius plot for permeability measurements. The ordinary linear trend is observed and this also confirms, as observed in a separated set of data, that Permeability is constant with respect water pressure for a wide range (at least 10 – 60 mBar).
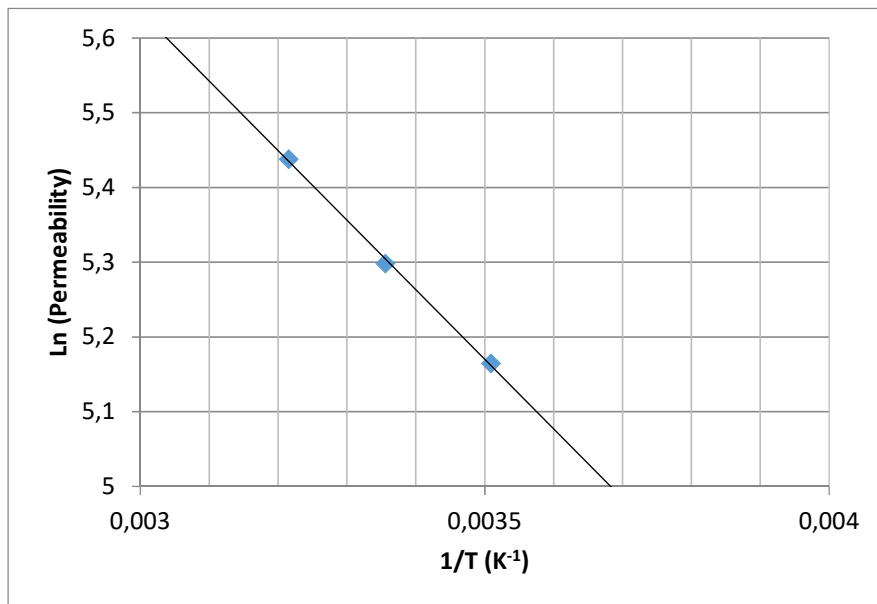
Figure 8. Arrhenius plot of water permeability measurements

A simple, effective and elegant way to dramatically reduce the water permeation is the introduction of an active filler into the matrix able to trap the water (i.e. a drier). The presence of this additional element completely changes the mass transport phenomenon within the polymeric barrier.

Mathematically the new situation can be modelled with a modified Fick law with a "well" contribution. It can be demonstrated that, with the suitable drier, the effective permeation is dramatically reduced for a long period of time. Just when all the drier in the matrix is completely saturated, i.e. not able to trap water

anymore, the effective permeation jump up to its pristine value. The time necessary to saturate the drier, i.e. restore pristine matrix permeation, is called lag time [2].

Lag time is related to the drier capacity (see Figure 9 and Figure 10below), its mass load within the matrix, pristine permeability of the matrix and external water vapour pressure conditions. On the other side the effective, or apparent, permeability relates to the drier kinetic pumping speed, i.e. how fast is in removing incoming water.

In this section we show some of the characterizations done on the drier to evaluate lag time and effective permeability. The following picture indicates the water uptake at 38°C, 90% RH and show both a large capacity (about 30% wt/wt) and relatively high speed (full saturation in 10 hours).
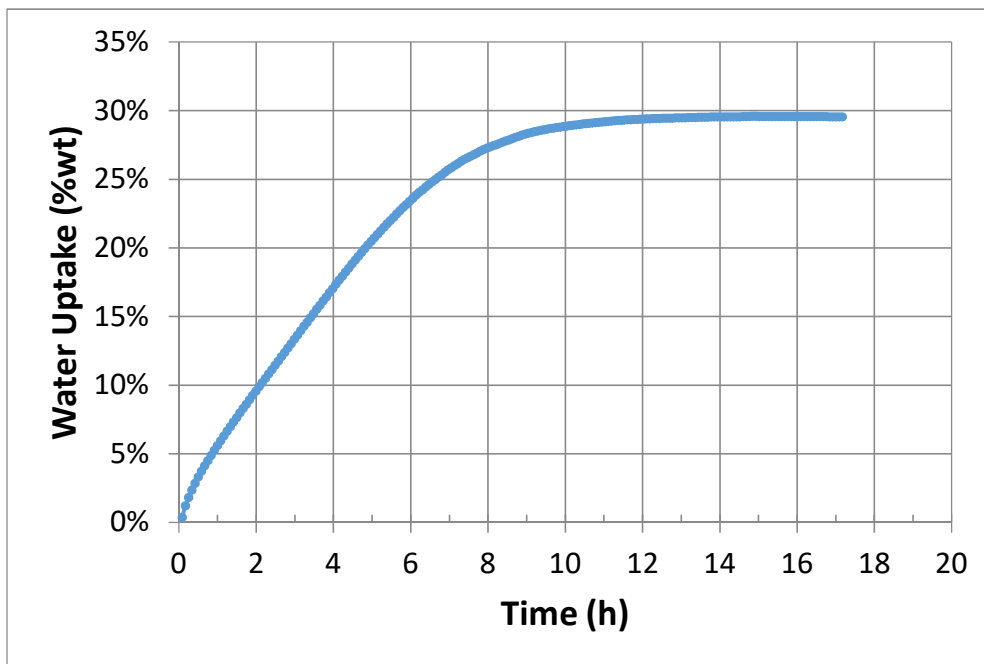
Figure 9. Water uptake of active filler at 38°C and 90%RH
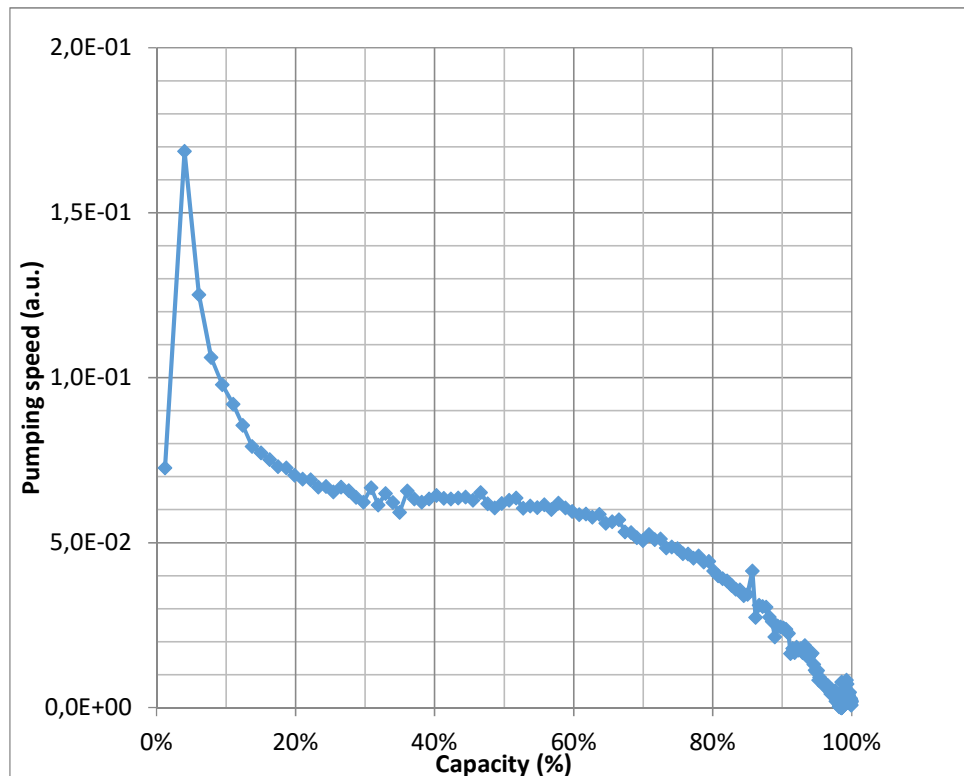
Figure 10. Active filler performance of water sorption (pumping speed vs exploited capacity)

Figure 10 shows how fast the drier removes water (i.e. pumping speed) as function of its exploited capacity. When the drier is fresh has a peak that is followed by a long plateau that account for about 80% of the total capacity. Just above that value there is a drop in the absorption rate. This kind of profile is independent of temperature and gives valuable information for sealant modelling [6].

The information related to the temperature are already given above (see Figure 8).

On the basis of information collected by aforementioned characterization, we estimated the pressure evolution within the VIG as effect of water vapour pressure to be negligible as effect of the drier. Unfortunately because of COVID emergency, so far it was not possible to collect a direct measurement of the effective moisture permeability. Compatibly with other activities, in the next months, we hope to perform a volumetric measurement in a closed system and collect the resulting data in the project final report.

2.3.3 Outgassing

As anticipated in the introductory section, outgassing is the second source of possible contamination in and depends on the property of the surfaces to release gas previously trapped and/or dissolved onto the surface or in its close proximity. Virtually all glasses as well as metal for high-vacuum applications are prone to outgassing but: i) the outgassing rate is typically not severe and ii) according with the application, they are prepared through outgassing steps prior to the sealing. Glasses are generally regarded as good vacuum material and, in particular tempered glass, can withstand to chemical or thermal step for preliminary degassing. In other terms, outgassing contribution is largely related to the preparation conditions and, if the precautions and good practice are applied, glasses can be considered as high-vacuum grade materials.

Moreover in our VIG production a long pumping period at moderately high temperature (≈ 150°C) is foreseen, thus we guess that the glass surface would be clean enough to give minor outgassing contributions.

Such minor outgassing contributions would be faced by the getter that has been purposely dimensioned. Moreover the fact traditional VIG are entirely composed of glass and (with minor getter load) they demonstrated their operation for decades, strengthens our conviction that glass panes are appropriate in terms of outgassing.

More concern is related to the use of the organic sealant which is new for the application.

For this reason specific tests with Gas Chromatography – Mass Spectroscopy (GC-MS) have been run.

The GC-MS system is composed by these three modules: 7697A Headspace Sampler; 7890 A GC system; 5975 C inert MSD with triple axis detector, all from Agilent.

In standard vials are inserted cured samples of EPO2, EPO4 and EPO5 of comparable size and dimension (few hundred mg weight), incubated at 60°C for 2 hours and then headspace is automatically sampled and analysed via the CG-MS system. Results are presented below.
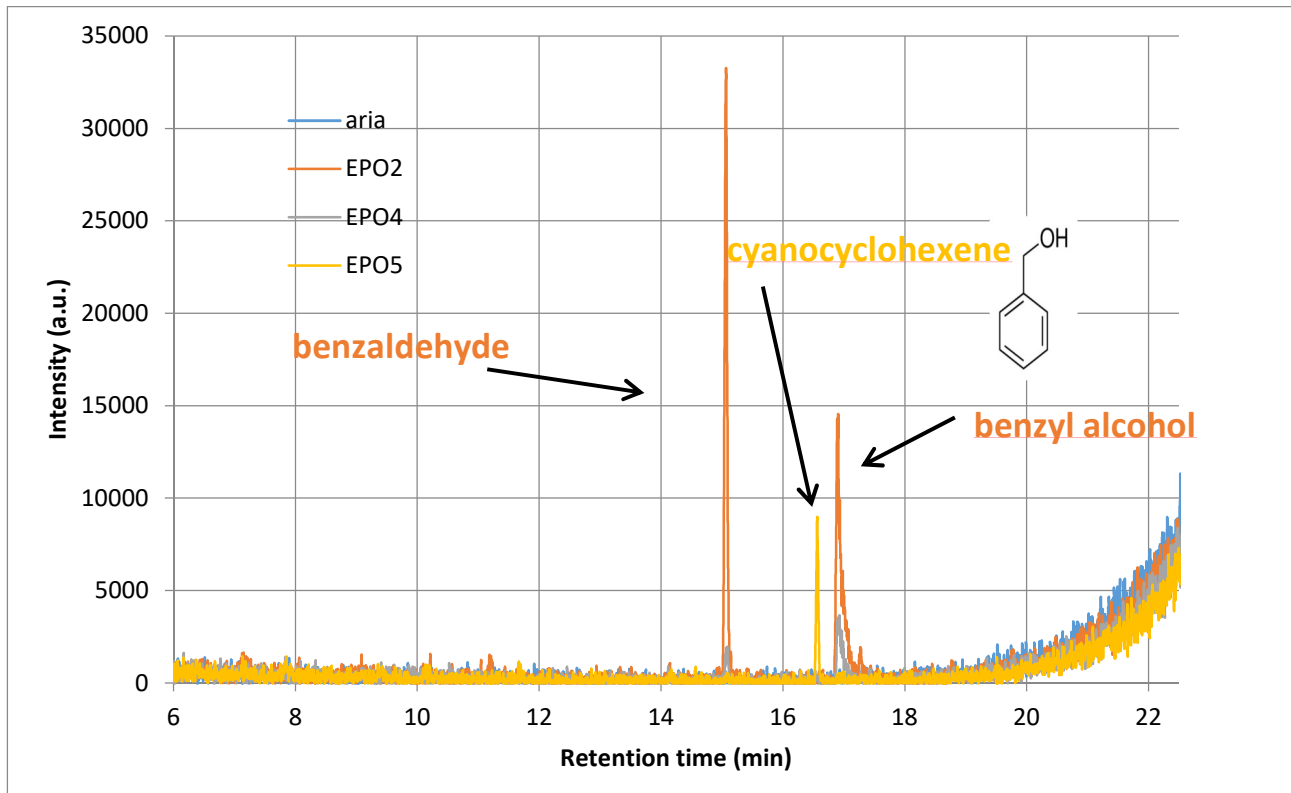
Figure 11. GC-MS results of outgassing tests of polymeric sealants EPO2, EPO4, EPO5.

Same protocol has been applied to different formulations. Below is reported the data collected for the EPO4.2 in comparison with blank vial used as reference. The conclusion is that there is no outgassing within GC-MS detection limit. Considering the superb sensitivity of the technique, the result can be considered extremely encouraging.
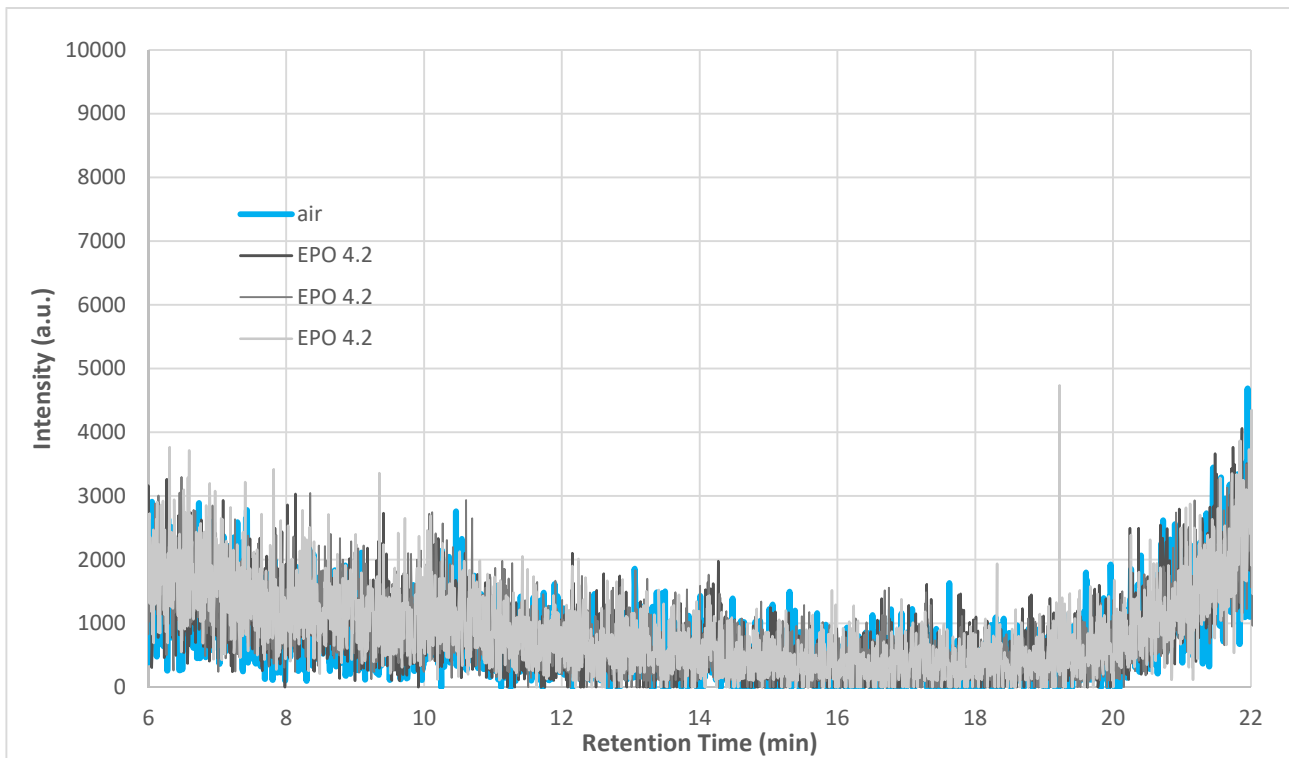
Figure 12. GC-MS results of outgassing tests of polymeric sealants EPO4.2.

Another important information concerning outgassing comes from permeability measurements taken for O_2. In particular we have data coming from two different methods: ASTM D 1434.1 and ASTM F 1927. We remind that the former set-up collects the overall pressure in the downstream chamber (the gauge is a capacitive, thus is sensitive to every gas), thus the signal comes from the permeation plus outgassing if any. On the other side, ASTM F 1927 is gas dependent, thus the results are influenced just by oxygen contribution. If the results are so well matched at a such low value of permeability, the outgassing contribution has to be low and negligible with respect the permeability contribution.

2.3.4 Residual Gas Analysis (RGA)

Residual gas analysis, in short RGA, is a method to assess the gas amount and the composition of the atmosphere sealed within a closed device.

It is a destructive technique, where the device under analysis is connected with a high-vacuum bench equipped with a vacuum gauges and (quadrupole) mass spectrometer. After careful preparation of the sample, the device wall is pierced and the gas filling the target volume is let to expand into the vacuum bench, where is measured and analysed. In this way it is possible to determine the total pressure within the cavity and the relative partial pressures composing the atmosphere. The set-up and technique are well established for decades, and more details can be found in [7]. Figure 13 sketches the main elements of the system.
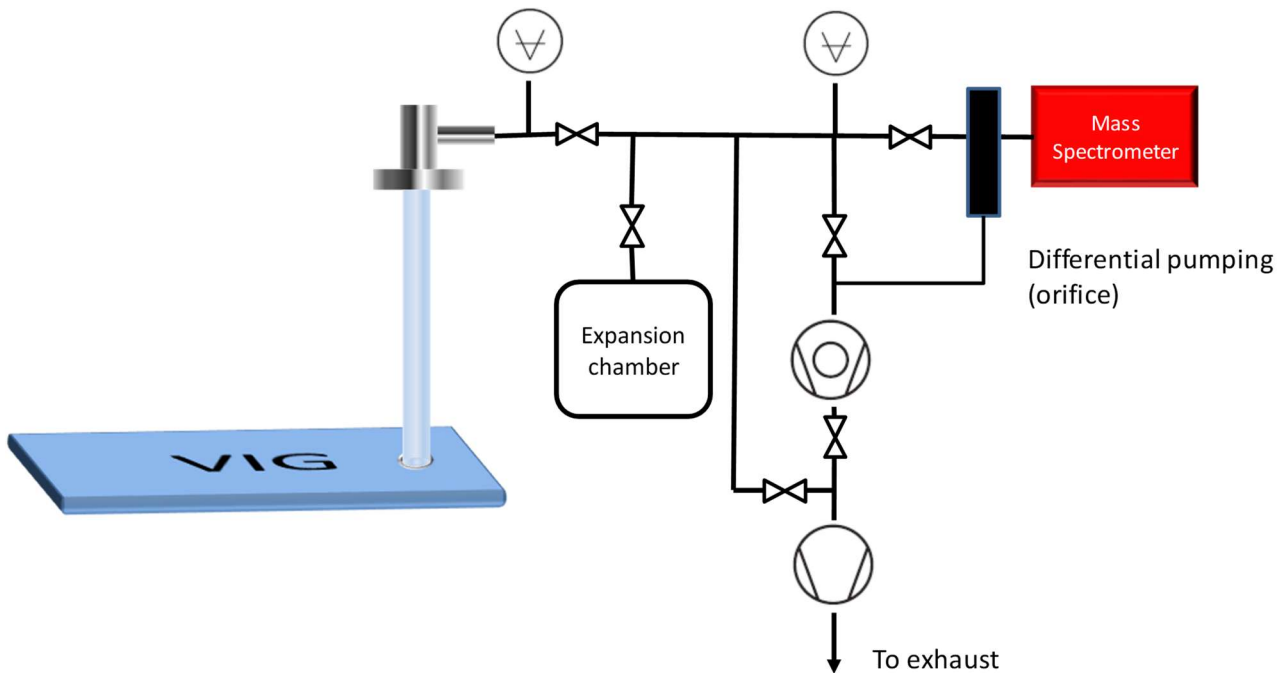
Figure 13. Scheme of RGA test bench.

A couple of tests for applying RGA to VIG prototypes have been performed. Unfortunately, because prototypes were made of tempered glass, none of the trials got useful results (see Figure 14 below). The state of stress into the VIG made not possible drilling the glass pane for connecting the VIG with RGA system. As soon as the ultrasonic horn used for thinning the glass pane penetrated of few millimetres, the stresses induced the break of the whole surface and the vacuum was definitively lost. In order to understand if stresses were concentrated into the single pane, because of the tempering process, or in the VIG because of the vacuum sandwiched structure, ultrasonic drilling was applied also on the single tempered glass sheet. Results were catastrophic as well, thus it was concluded that piercing the tempered pane was intrinsically not feasible (as also confirmed by subsequent interview with glass experts).
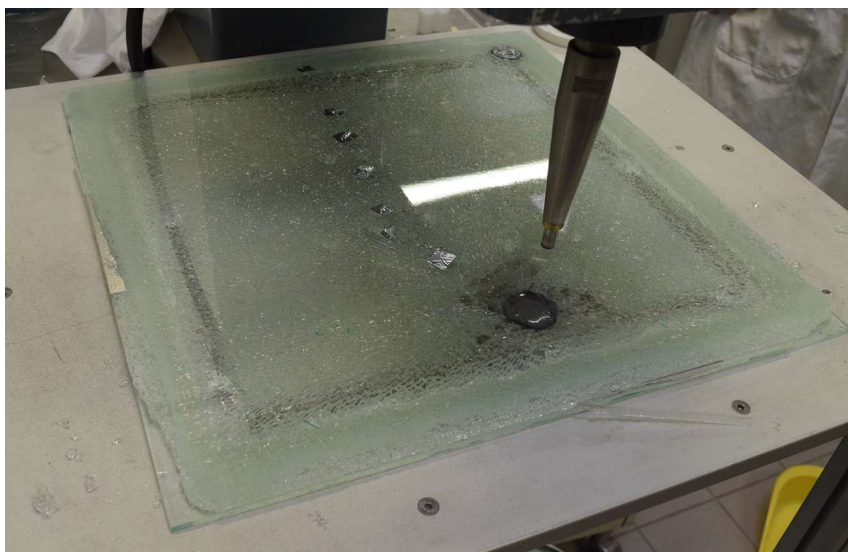
Figure 14. Failing of VIG drilling because VIG made of tempered glasses.

Also the option to make a prototype with float glass (stress-free process) was considered, but it was argued that such variation would affect too much on the process to let the same residual gas quantity and composition as in the original process. Thus considering the final target is to produce VIGs made of tempered glass, the RGA has been abandoned. However, just recently, we considered the possibility to connect the vacuum systems through the vacuum cup (see Figure 5) and if feasibility tests will be positive will be able to complete RGA onto prototype.

3 Prototype coating optical properties characterization

3.1 Introduction

Thermochromic materials are part of a larger class of intelligent or "smart" materials. Smart materials are the ones which can change their properties according to some external stimulus. In the case of thermochromism, the optical properties of a material change depending on the value of the temperature. Consequently, features such as transmittance and reflectance of the materials can be different at different temperature. This change is generally due to a structural phase change in the material itself and takes place at a particular temperature (transition temperature or critical temperature Tc) and is typically completely reversible. Thermochromic materials can be applied on glassy windows; in this way, the amount of light and energy transmitted and reflected through the window will be different depending on the temperature (i.e. on the external atmospheric conditions).

3.2 Experimental setup

3.2.1 Test item

Different sets of glazed samples have been realized by UCL with the aim to optimise the coating structure and process parameters. In particular, 3 sets of glazed samples were analysed which differ in:
- geometry shape and size;
- deposition techniques of the coating during the manufacturing process;
- combination of thin films coatings on glass substrates.

The first set consisted on 9 glazing samples (see Figure 4a) with dimensions of 20 mm × 20 mm × 4 mm (height × width × thickness) coated with a film containing a percentage of vanadium dioxide (VO_2) going from 0.5 to 1 % of the weight. The deposition has been realised with the spin deposition process at a speed going from 3000 to 5000 rpm.

The second set consisted of 4 glazing samples (see Figure 15b) of semi-circular shape and thickness of 0.5 mm. All the samples have been realised with the same spin deposition process, they had a VO_2 coating of 100 nm thickness and thy have been tested for assessing the process reproducibility. Samples 3 and 4 have been passivated with a silica barrier layer (SiO_2) with a thickness of 80 nm.

The third set consisted of 10 glazing samples (see Figure 15c) where 4 of 26x76 mm rectangular shape and a thickness of 1 mm (except the sample ML-1 with a thickness of 2 mm) and 6 of circular shape with 25 mm of diameter and a thickness of 1 mm (except the sample V96-4 with a thickness of 2 mm). The samples have been coated with different combination of thin films coatings as shown in the Figure 16.

(a)

(b)

(c)

Figure 15. Glazed sample sets: (a) set n. 1, (b) set n. 2 and (c) set n. 3

Sample	TiO2/nm	VO2/nm	TiO2/nm	Norland	Glass
Quartz Sample					
V96-2	53	105	-	-	-
V96-4	54	114	-	-	-
V96-1	55	108	103	-	-
V96-3	55	108	99	-	-
V83-2	55	127	106	Yes	-
V89-3	52	117	103	Yes	-
Microscopic slide					
ML3	Yes	Yes			
ML4	Yes	Yes	Yes		
ML2	Yes	Yes	Yes	Yes	
ML1	Yes	Yes	Yes	Yes	Yes

Figure 16. Characteristics of the coating used for the glazed samples of the set n. 3

Currently all the glazed samples belonging to the 3 sets have undergone measurements for the characterization of the thermochromic properties of the coatings moreover natural and accelerated aging tests have been partially performed and planned to run up to the end of the project. The schedule of the tests is reported in Table 5. The circular samples (Vxx-x) with the similar characteristics will be destined one to natural tests and one to accelerated tests while the rectangular samples (Mx), thanks to their sizes, can be cutting in two, and sent one part to natural aging test and one part to accelerated aging test. The solar radiation with soling exposure (that could be more aggressive than thermal fatigue) will be performed on the samples that have protective layers (ML1, ML2, V89-3).

Table 5. Schedule of experimental tests

| N. set | Samples | Optical properties measurements | | Natural ageing tests | Accelerated ageing tests | Accelerated ageing tests |
		Transmittance measurements	Reflectance measurements		Thermal fatigue	Soling and Solar radiation
1	1	yes	yes	-	-	-
	2	yes	yes	-	-	-
	3	yes	yes	-	-	-
	4	yes	yes	-	Done	-
	5	yes	yes	-	-	-
	6	yes	yes	Done 6 month	-	-
	7	yes	yes	Done 6 month	-	-
	8	yes	yes	-	-	-
	9	yes	yes	-	-	-
2	1	yes	yes	-	-	-
	2	yes	yes	-	-	-
	3	yes	yes	-	Done	-
	4	yes	yes	-	-	-
3	ML-1	yes	yes	planned	-	planned
	ML-2	yes	yes	planned	-	planned
	ML-3	yes	yes	In progress From February 2020	In progress (done 86 cycles)	-
	ML-4	yes	yes	In progress From February 2020	Done	-
	V96-1	yes	yes	planned	-	-
	V96-2	yes	yes	In progress From February 2020	-	-
	V96-3	yes	yes	-	planned	-
	V96-4	yes	yes	-	Done	-
	V83-2	yes	yes	planned	-	-
	V89-3	yes	yes	-	-	planned

The optical properties of the samples have been measured using a UV/VIS/NIR, double beam spectrophotometer Jasco V670 (Figure 17), equipped with a 60 mm diameter integrating sphere. The instrument measures in a broad spectral range 190-2700 nm thanks to a double light source (Deuterium lamp for the UV and Halogen lamp in the VIS/NIR), a dual grating (1200 lines/mm for UV/VIS and 300 lines/mm for the NIR) and a dual detector (Photomultiplier tube and Peltier cooled PbS detector). All the tests have been performed in the spectral range of 300-2500 nm which is the range of the AM1:5 solar irradiance spectrum, with a resolution of 2 nm.

In order to perform the transmittance measurement at different controlled temperatures, a thermostated cell holder has been employed equipped with a system maintaining the test sample at constant temperature in the range of 20 to 90 °C.

Figure 17. UV/VIS/NIR, double beam spectrophotometer Jasco V670 – Measurements of transmittance

For the reflectance measurements the Jasco V670 spectrophotometer has been equipped with a dedicated aluminium holder allowing to test the sample at different controlled temperatures. The drawn of the holder and its connection to the spectrophotometer are illustrated in Figure 18. The temperature is regulated using a TLK 33 from ASCON TECNOLOGIC which is a single-loop digital microprocessor-based controller for Peltier elements with PID dual action (direct and reverse) control and measured with a K type thermocouple mounted in close contact with the sample. A Peltier Cell is employed to generate the heating and to achieve and maintain the desired temperature on the glazed sample which is connected to the Peltier Cell via an aluminium plate behaving as a heating transmission element (see Figure 18d).
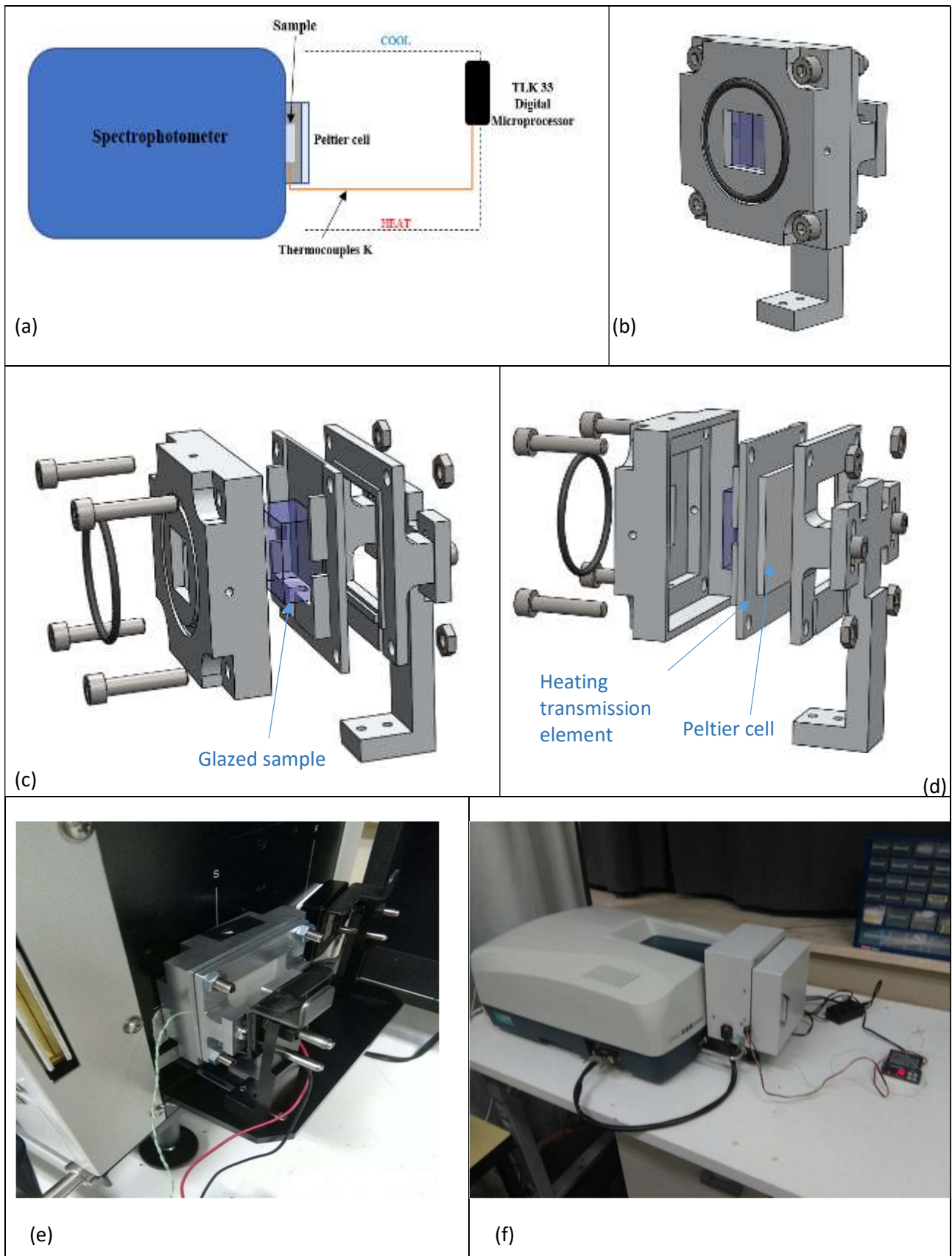
Figure 18. Dedicated holder for measurements of reflectance: (a) experimental set-up, (b) assembly, (c) exploded view, (d) experimental test bench

3.3 Thermochromic properties assessment procedure

The procedure exploited to measure the optical properties of the glass coating and to gather its thermochromic properties will be described hereafter considering the sample number 1 of the set reported in Figure 15a.

First of all the optical transmittance and reflectance have been measured, by using the Jasco V670 spectrophotometer and the thermostatic systems described in the previous section, at different temperatures between 20 and 90 °C. In order to account for the possible coating hysteresis two sets of measurements have been performed: one by varying the temperature in an incremental way and one in decremental way. The measurement have been started after two minutes of waiting time in order to overcome the thermal transient and to insure that the temperature was stable.

Figure 19a and Figure 19b shows static measurements of reflectance and transmittance, respectively, realised with incremental (heating) or decremental (cooling) temperature. The data have been filtered with a median filter to remove noise.
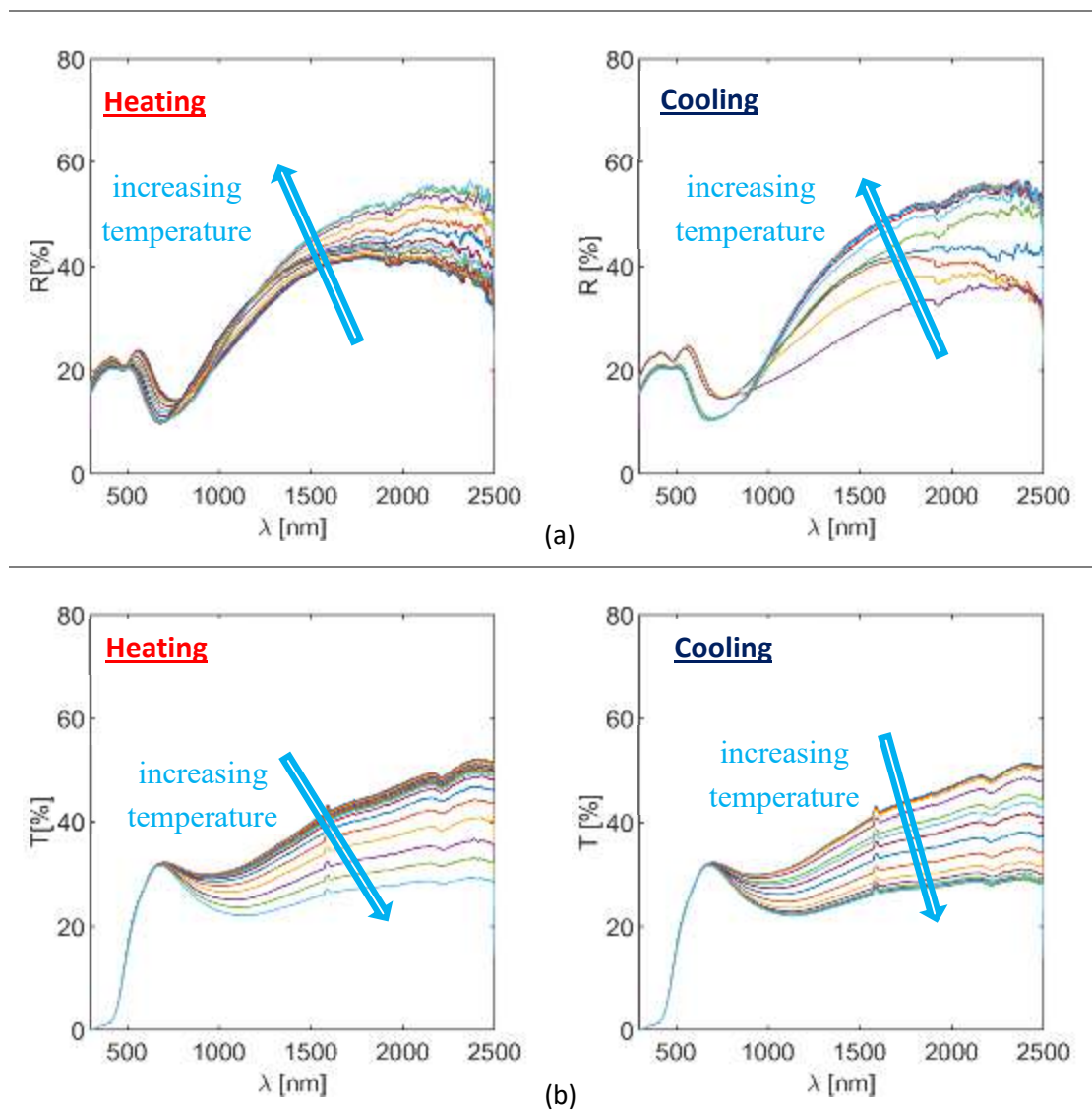
Figure 19. Spectral (a) reflectance and (b) transmittance of VO2 (arrows indicate direction of increasing temperature).

While the reflectance manifests changes in all the spectral regions, visible (400-800nm), near-infrared (800-1100nm), and the infrared (1100-2500nm), the transmittance changes are concentrated entirely in the infrared.

As expected from the literature [1], the reflecatance increases with the temperature while the transimittance decreases and this effect makes the thermochormic coating interesteng for the modulation of the solar radiant heat that is transmitted into a building depending upon the ambient environmental conditions. This effect is more evident if the relative reflectance and transmittance variation with respect to the reflectance and transmittance at 20 °C (R_0 and T_0) are considered, as reported in Figure 20.

(a)
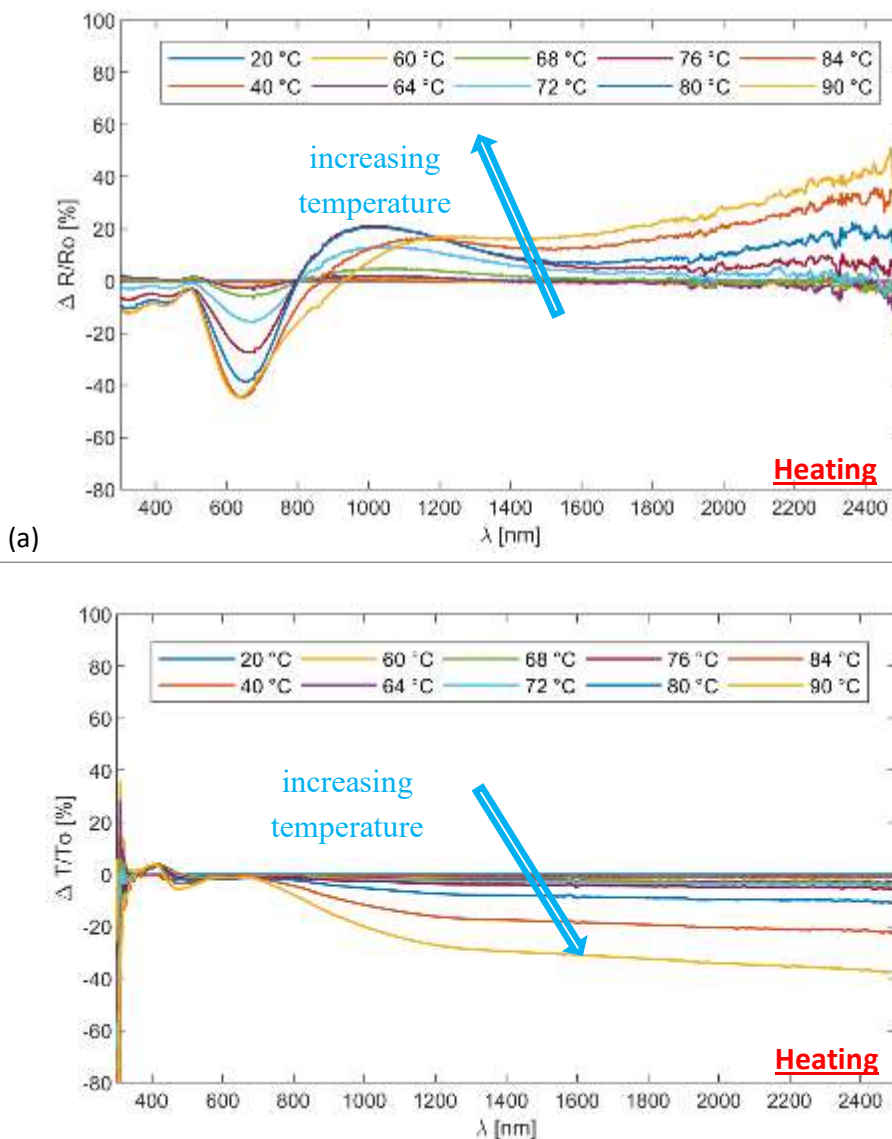
Figure 20. (a) Relative change in reflectance (R – R0)/ R0 and (b) relative change in transmittance (T – T0)/ T0 with temperature

Hysteresis measurements of either transmittance or reflectance are also essential. Indeed, another important factor for evaluating glazing efficiency is the width of the hysteresis cycle. This affects the temperature at which the thermochromic transition occurs on heating and cooling the window.

Figure 21 shows hysteresis measurements of VO_2 thin-film performed in reflectance and transmittance at the spectrum wavelength of 2000 nm: it is evident that the coating reflectance and transmittance switch

form a lower value to a higher value respectively when the temperature increases (heating) and vice versa when the temperature decreases (cooling). Moreover the switch occurs at different temperature in the case of heating or cooling. This phenomenon is due to the hysteresis of the coating.

The hysteresis curves of the transmission and reflection were plotted at 2000 nm that is a significative wavelength for the thermochromic behaviour according to [9], [10].

(a)
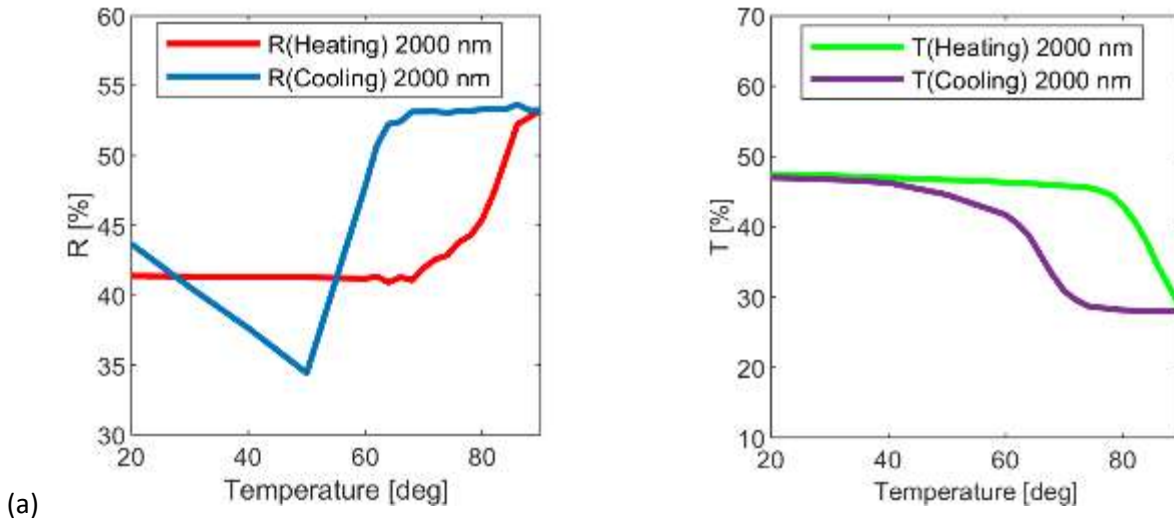
Figure 21. Hysteresis measurements @ 2000 nm (a) Reflectance and (b) Transmittance

Even though the optical hysteresis is commonly given at the wavelength of 2000 nm, in the case of glazed systems it is essential to understand the phenomenon in two different wavelength ranges: the visible one, which is the region affecting the lighting performance of the glass, and the infrared one, which is the region affecting the thermal behaviour of the glass and therefore the energy performance of the window. In order to quantify the amount of visible light useful for human vision under normal conditions the photopically averaged transmittance T_{lum} and reflectance R_{lum} has to be calculated with the first formulation of equation 8. The amount of solar thermal energy entering a building or reflected by its envelope are called solar averaged transmittance T_{sol} and reflectance R_{sol} and are given by the second formulation of equation 8 [11].

$$T_{lum}^{\sigma} = \frac{\int_{\lambda=380\,nm}^{780\,nm} \bar{y}(\lambda)T^{\sigma}(\lambda)d\lambda}{\int_{\lambda=380\,nm}^{780\,nm} \bar{y}(\lambda)d\lambda} \qquad\qquad T_{sol}^{\sigma} = \frac{\int_{\lambda=300\,nm}^{2500\,nm} AM_{1.5}(\lambda)T^{\sigma}(\lambda)d\lambda}{\int_{\lambda=300\,nm}^{2500\,nm} \overline{AM_{1.5}}(\lambda)d\lambda} \qquad 8$$

$$\Delta T_{lum} = T_{lum}^{cold} - T_{lum}^{hot} \qquad\qquad \Delta T_{sol} = T_{sol}^{cold} - T_{sol}^{hot} \qquad 9$$

In equation 8 σ represents the temperature state of the window (i.e. hot or cold state). The CIE photopic luminous efficiency of the human eye [12], $\bar{y}(\lambda)$, and the $AM_{1.5}$ solar irradiance spectrum [13] are used as weighting functions for the wavelength dependent transmittance coefficients, see Figure 21. The wavelength range used for the photopically averaged calculations was 380 nm ≤ λ ≤780 nm corresponding to the limits of human vision. The $AM_{1.5}$ weighting spectrum was chosen for solar averaged transmittance calculations as it represents an overall yearly average for mid-latitudes including diffuse light from the ground and sky on a south facing surface tilted 37° from horizontal. The wavelength range used for these calculations was 300 nm ≤ λ ≤2500 nm.
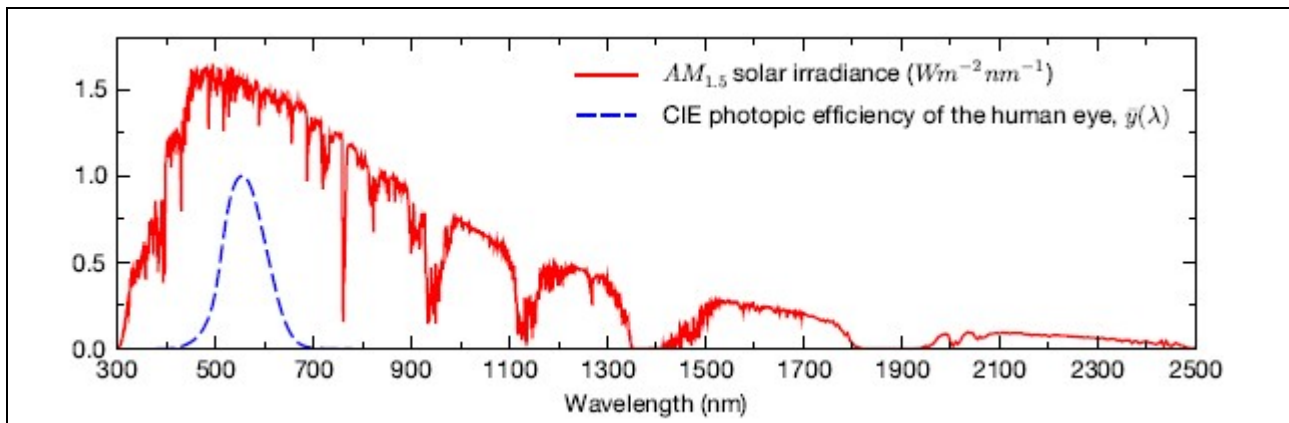
Figure 22. Spectra used to weight the transmittance functions. The photopic luminous efficiency of the human eye, $\overline{y}(\lambda)$, and the AM1:5 solar irradiance spectrum

The luminous reflectance and transmittance of the sample number 1 and its solar reflectance and transmittance are reported in Figure 23 and Figure 24. The hysteresis is manifested on all the optical properties except on the luminous transmittance (Figure 23b). This fact is positive because it means that the transparency of the glass to the light does not change with temperature allowing a lighting comfort independent from the external weather conditions. It can be observed that the solar reflection curves are almost flat due to the fact that the reflectance behaves in opposite way in the visible and solar ranges, see Figure 20a: the reflectance decreases between 300 and 800 nm and increases with temperature beyond 800 nm. Since the curves have been obtained by integrating the whole optical range (as in the second equation of 8) the two effects will cancel each other.
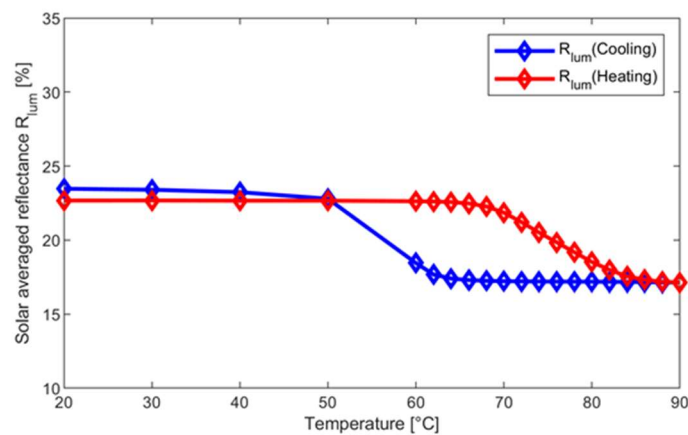
(a)
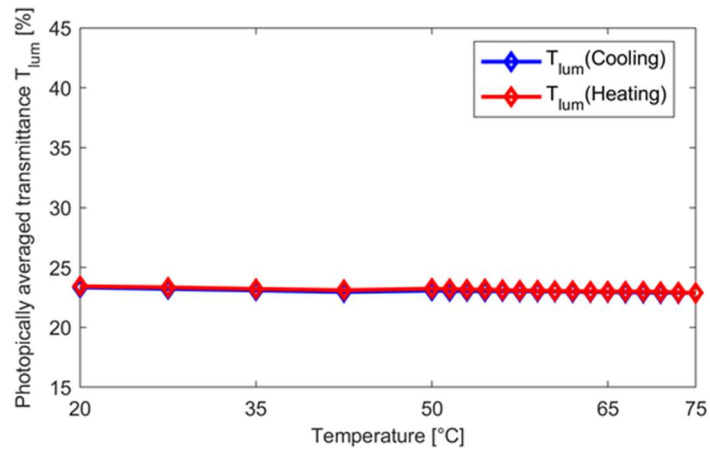
(b)

Figure 23. Photopically averaged reflectance R$_{lum}$ (a) and transmittance T$_{lum}$ (b)
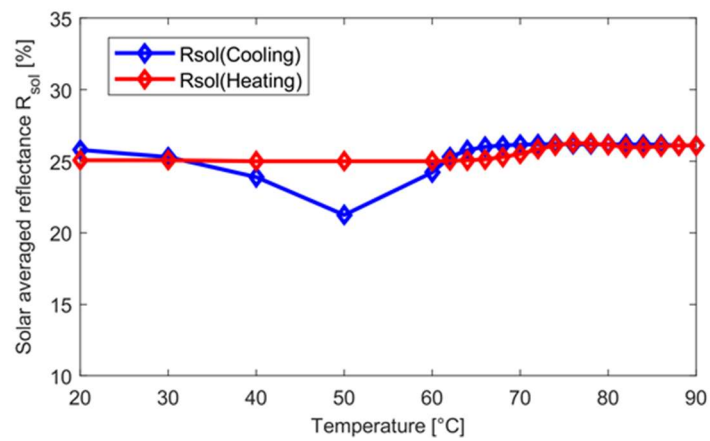
(a)
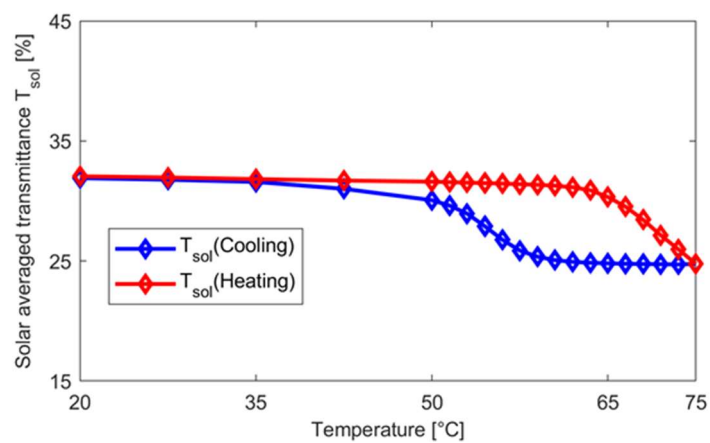
(b)

Figure 24. Solar averaged reflectance R$_{sol}$ (a) and transmittance T$_{sol}$ (b)

3.4 Results and discussion

In this chapter the optical properties measured for all the samples are reported in terms of luminous and solar reflectance and transmittance.

Spectral reflectance	*Spectral transmittance*

The change in in reflectance (R – R₀)/ R₀ and the change in transmittance (T – T₀)/ T₀ highlight temperature dependent changes of VO₂ by comparing to their value at room temperature (T₀ and R₀).

Reflectance hysteresis loop @2000 nm	*Transmittance hysteresis loop @2000 nm*
Photopically averaged transmittance T_lum	*Solar averaged transmittance T_sol*
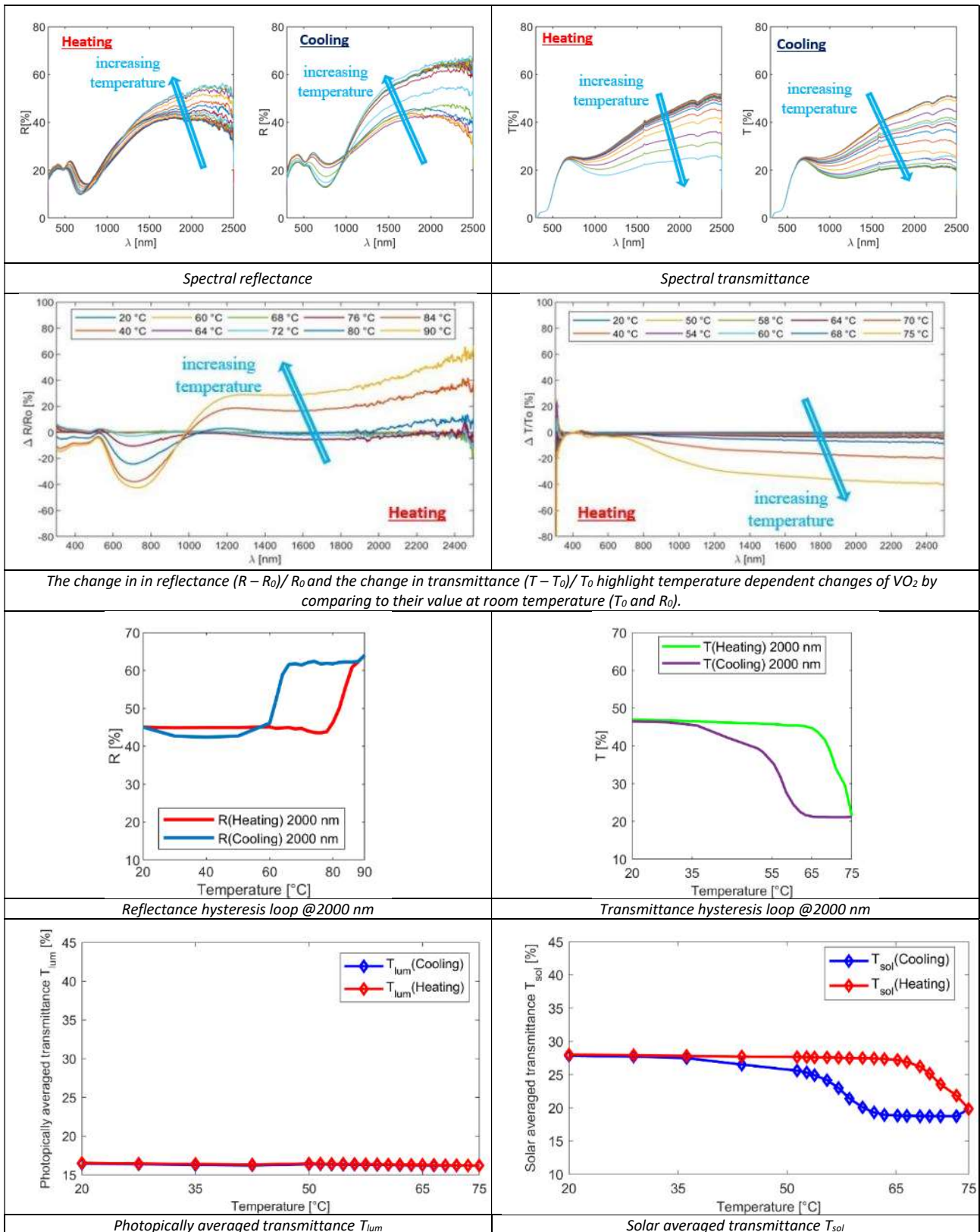
Figure 25. Thermochromic optical properties measured for the sample 2 – set n. 1

Spectral reflectance

Spectral transmittance

The change in in reflectance (R – R₀)/ R₀ and the change in transmittance (T – T₀)/ T₀ highlight temperature dependent changes of VO₂ by comparing to their value at room temperature (T₀ and R₀).

Reflectance hysteresis loop @2000 nm

Transmittance hysteresis loop @2000 nm

Photopically averaged transmittance T_lum

Solar averaged transmittance T_sol

Figure 26. Thermochromic optical properties measured for the sample 3 – set n. 1

Spectral reflectance

Spectral transmittance

The change in in reflectance (R – R₀)/ R₀ and (b) the change in transmittance (T – T₀)/ T₀ highlight temperature dependent changes of VO₂ by comparing to their value at room temperature (T₀ and R₀).

Reflectance hysteresis loop @2000 nm

Transmittance hysteresis loop @2000 nm

Photopically averaged transmittance T_lum

Solar averaged transmittance T_sol

Figure 27. Thermochromic optical properties measured for the sample 4 – set n. 1
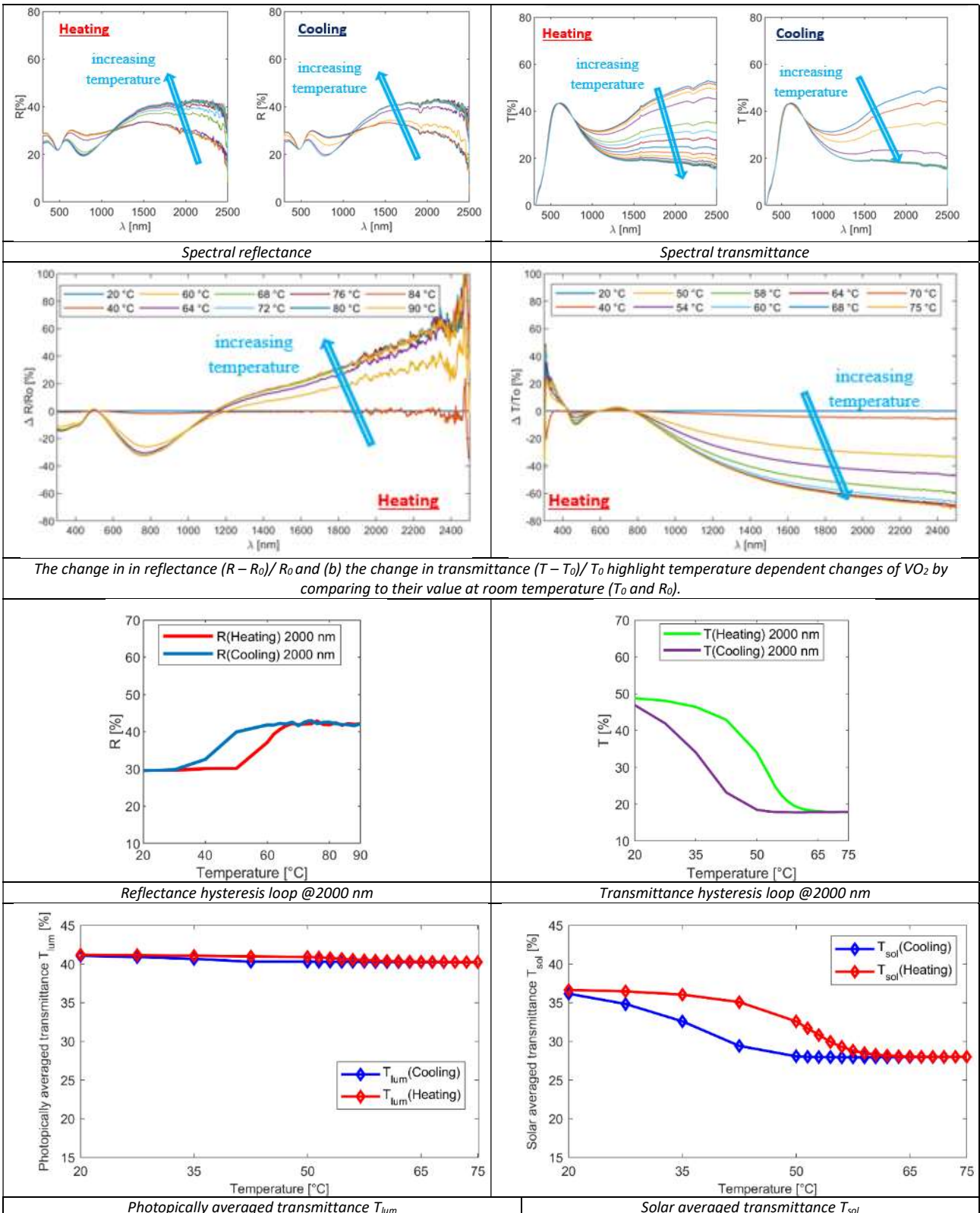
Figure 28. Thermochromic optical properties measured for the sample 5 – set n. 1

| Spectral reflectance | Spectral transmittance |

The change in in reflectance $(R - R_0)/ R_0$ and (b) the change in transmittance $(T - T_0)/ T_0$ highlight temperature dependent changes of VO_2 by comparing to their value at room temperature (T_0 and R_0) .

| Transmittance hysteresis loop @2000 nm | Reflectance hysteresis loop @2000 nm |

| Photopically averaged transmittance T_{lum} | Solar averaged transmittance T_{sol} |

Figure 29. Thermochromic optical properties measured for the sample 6 – set n. 1

Spectral reflectance | Spectral transmittance

The change in in reflectance (R – R₀)/ R₀ and (b) the change in transmittance (T – T₀)/ T₀ highlight temperature dependent changes of VO₂ by comparing to their value at room temperature (T₀ and R₀).

Reflectance hysteresis loop @2000 nm | Transmittance hysteresis loop @2000 nm

Photopically averaged transmittance T_lum | Solar averaged transmittance T_sol
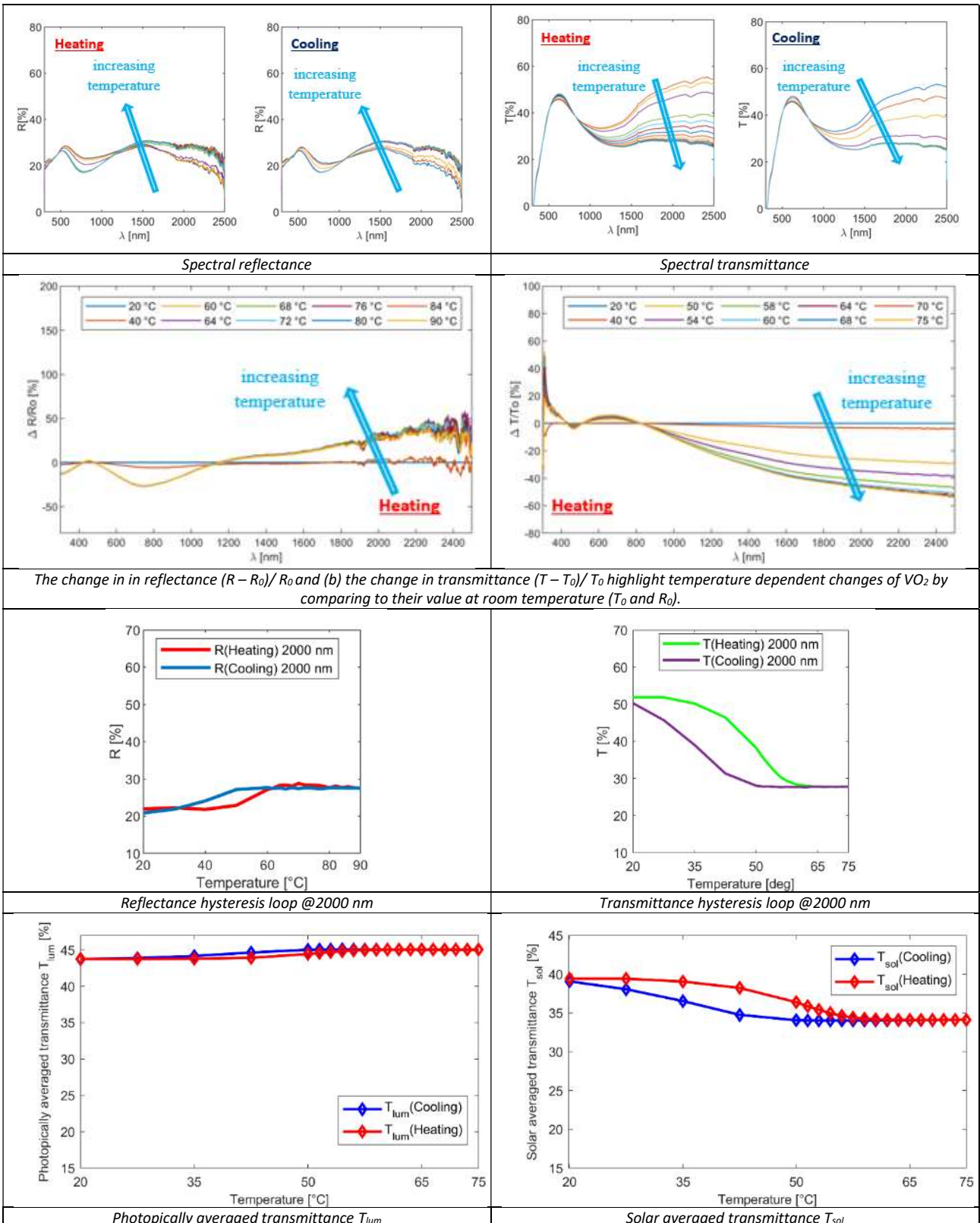
Figure 30. Thermochromic optical properties measured for the sample 7 – set n. 1
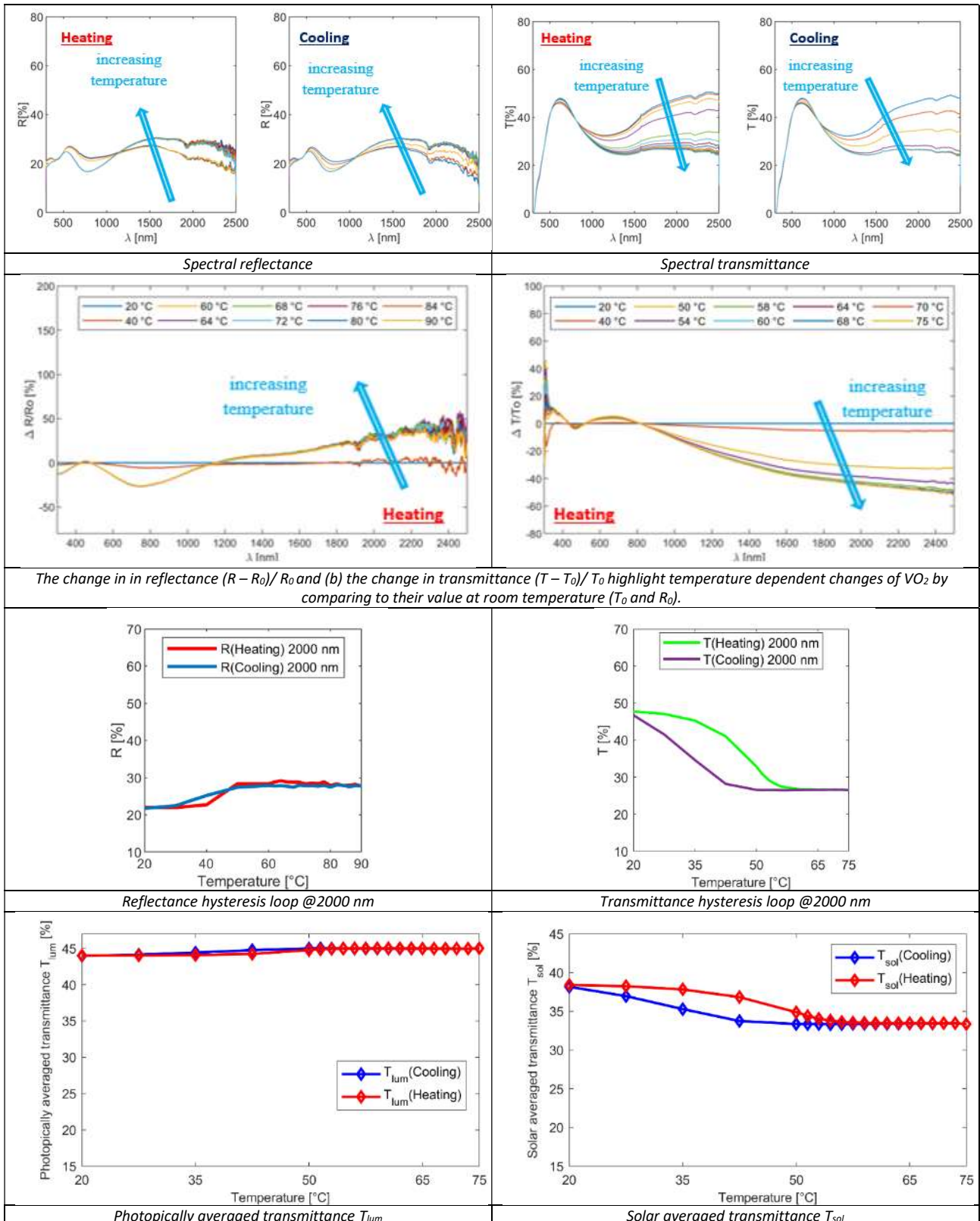
Figure 31. Thermochromic optical properties measured for the sample 6 – set n. 1
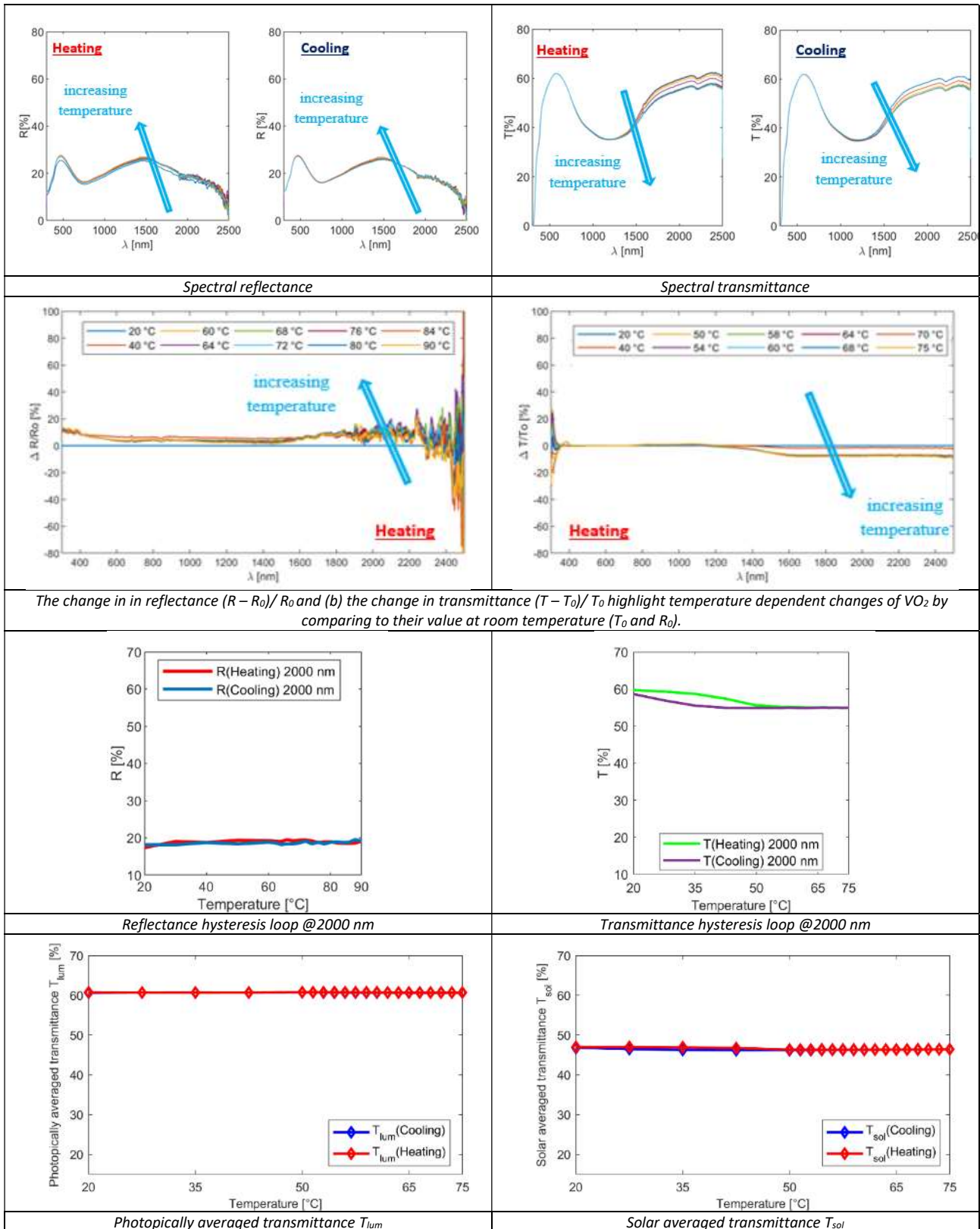
Figure 32. Thermochromic optical properties measured for the sample 7 – set n. 1

Table 6 summarizes the values of solar averaged transmittance (T_{sol}) and photopically averaged transmittance (T_{lum}) calculated according to the Equation (8) and the luminous transmittance modulation (ΔT_{lum}) and solar energy modulation (ΔT_{sol}) defined by the Equation (9) for all 9 glazing samples belonging to set n. 1 analysed.

Table 6. Luminous and solar transmittance of the 9 glass samples belonging to set n. 1

Samples	% of weight	Spin [rpm]	hot state		cold state		ΔT_{sol} [%]	ΔT_{lum} [%]
			T_{sol} [%]	T_{lum} [%]	T_{sol} [%]	T_{lum} [%]		
1	1	3000	24.7	22.8	32.1	23.4	7.4	0.6
2	1	4000	19.8	16.9	28.0	17.5	8.2	0.6
3	1	5000	25.3	32.1	35.1	33.0	9.8	0.9
4	0.75	3000	30.6	36.4	36.0	36.7	5.4	0.3
5	0.75	4000	28.1	40.2	36.7	41.2	8.6	1.0
6	0.75	5000	27.0	37.0	36.0	37.3	9	0.3
7	0.5	3000	34.1	45.0	39.4	43.8	5.3	-1.2
8	0.5	4000	33.3	45.0	38.4	44.0	5.1	-1.0
9	0.5	5000	46.4	60.7	47.0	60.8	0.6	0.1

Table 7 shows the percentage of reflection and transmission values of the samples evaluated in the hot and cold state conditions at the wavelength of 2000 nm and the respective variation ΔR and ΔT.

Table 7. Reflectance and transmittance properties at the wavelength of 2000 nm of the 9 glass samples belonging to set n. 1

Samples	% of weight	Spin [rpm]	hot state	cold state	ΔR [%]	hot state	cold state	ΔT [%]
			R@2000 [%]	R@2000 [%]		T@2000 [%]	T@2000 [%]	
1	1	3000	53.2	41.5	11.7	28.2	47.4	19.2
2	1	4000	64.0	45.0	19.0	21.5	46.9	25.4
3	1	5000	48.5	36.8	11.7	23.7	52.8	29.1
4	0.75	3000	47.6	36.5	11.1	28.5	56.1	27.6
5	0.75	4000	42.1	29.5	12.6	17.9	48.8	30.9
6	0.75	5000	43.5	35.3	8.2	23.4	56.1	32.7
7	0.5	3000	27.5	21.9	5.6	27.7	51.9	24.2
8	0.5	4000	27.7	21.7	6.0	26.6	47.7	21.1
9	0.5	5000	19.0	17.3	1.7	54.9	59.7	4.8

The bar histograms shown in Figure 33 and Figure 34 highlight the influence of the process parameters (percentage of vanadium dioxide (VO_2) and spin deposition) on the values of solar modulation (ΔT_{sol}) and visible light transmission (ΔT_{lum}) where it is possible to see how the solar modulation improves both by increasing the percentage of vanadium dioxide (VO_2) and the speed of deposition. While the transmittance of the visible light remains almost unchanged. The histograms in Figure 35and Figure 36 show the reflection

and transmission modulation between the cold and hot state at 2000 nm as a function of the process parameters.
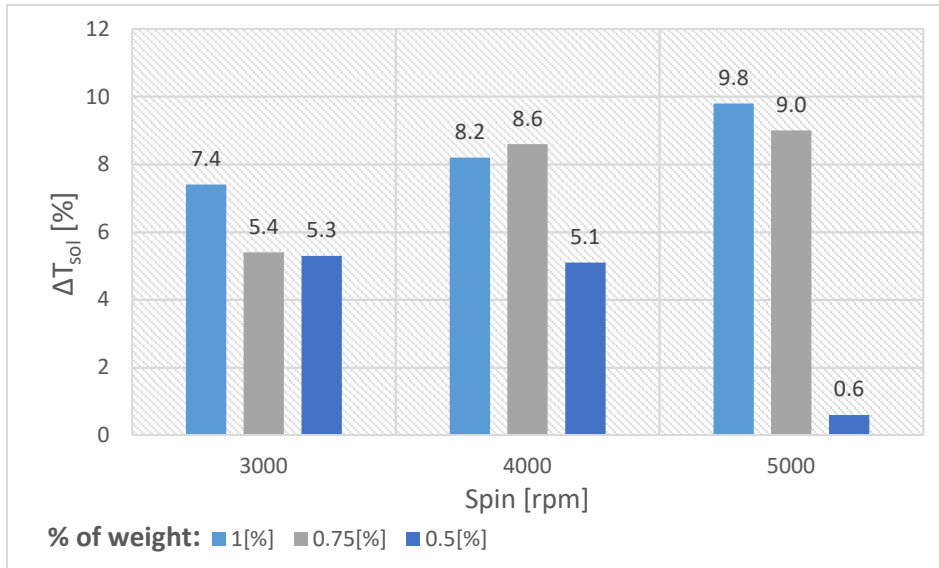
Figure 33. Solar modulation ability ΔT_{sol}
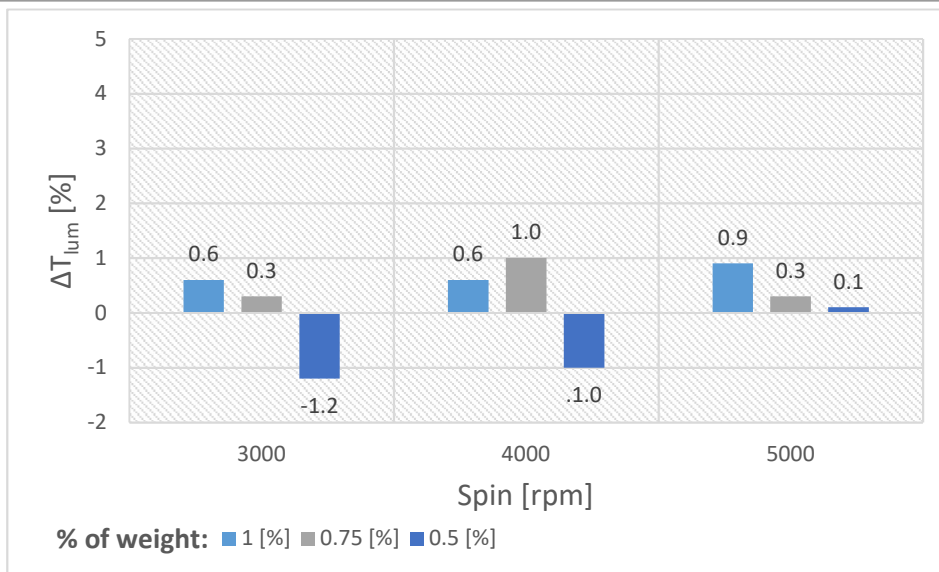
Figure 34. Luminous modulation ΔT_{lum}
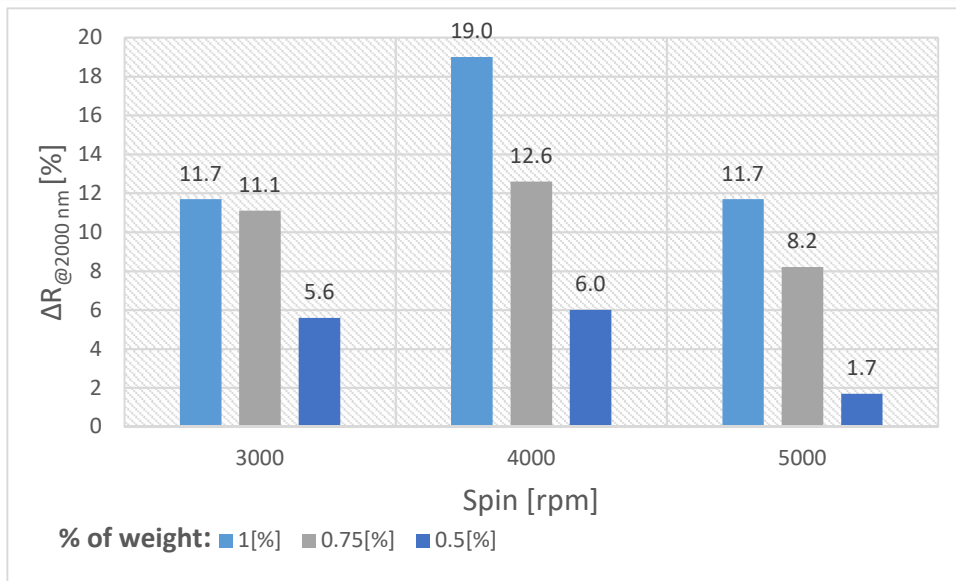
Figure 35. Variation of reflection coefficient between hot and cold state in the infrared region at the spectrum wavelength of 2000 nm.
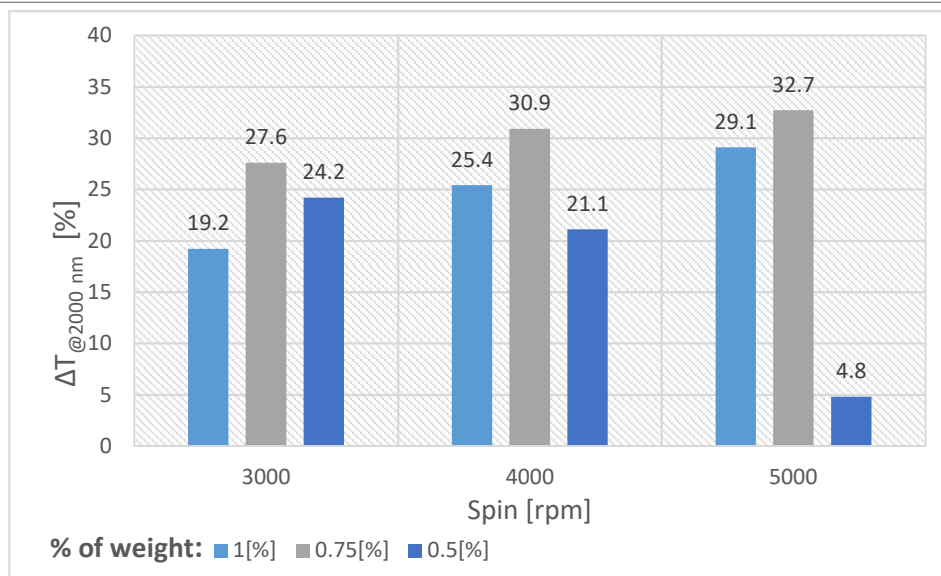
Figure 36. Variation of transmittance coefficient between hot and cold state in the infrared region at the spectrum wavelength of 2000 nm

Figure 37 shows the optical properties, i.e. transmission and reflectance spectra and hysteresis of a standard glazed sample without thermochromic coating. For the hysteresis plots, given at the wavelength of 2000 nm, it is evident that the system does not manifest optical properties modulation with varying the temperature. Also the reflectance and transmittance spectra measured at different temperatures in ascending or descending order are almost identical apart from noise. This demonstrates that the glass optical properties are not affected by the temperature variations.

Sample without coating - Reflectance
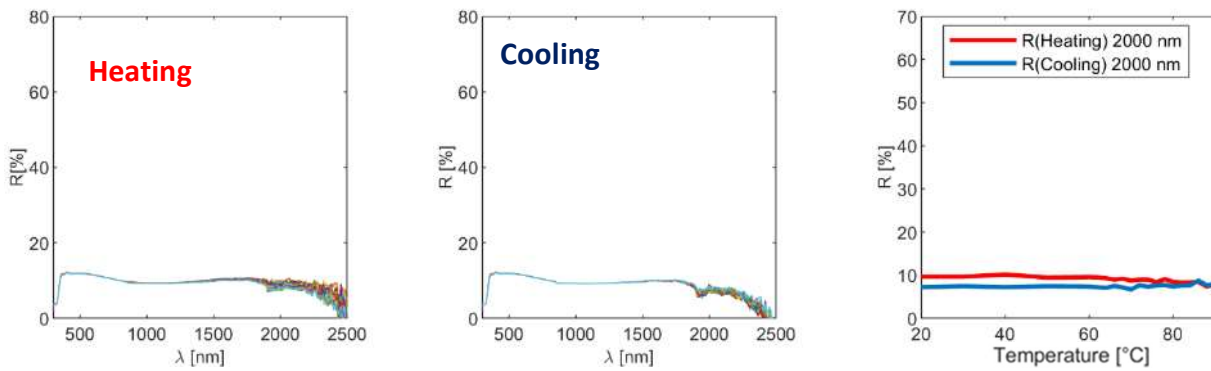
Sample without coating - Trasmittance
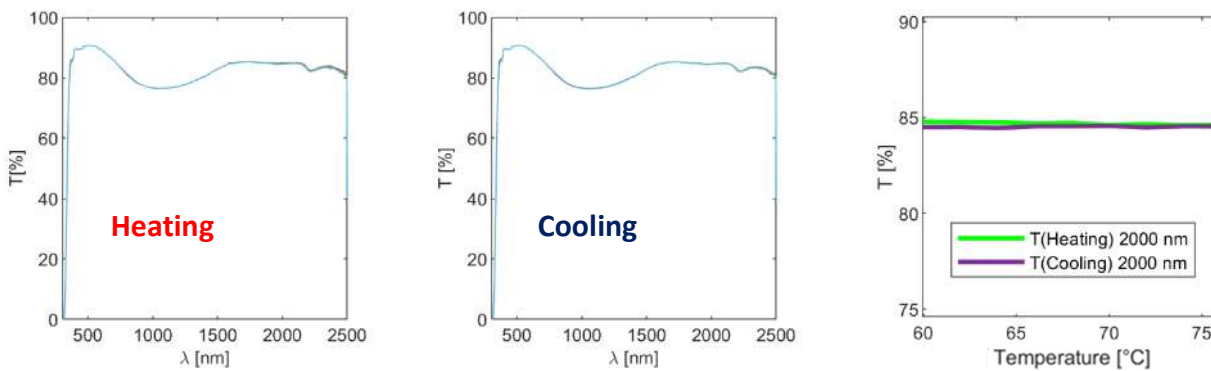
Figure 37. Optical proprities of a glazed sample without VO$_2$ coating

3.4.2 Result of the tests performed on set n. 2

The optical properties measured for the 4 glass samples listed in Figure 15b are reported in terms of luminous and solar transmittance and reflectance at 2000 nm.
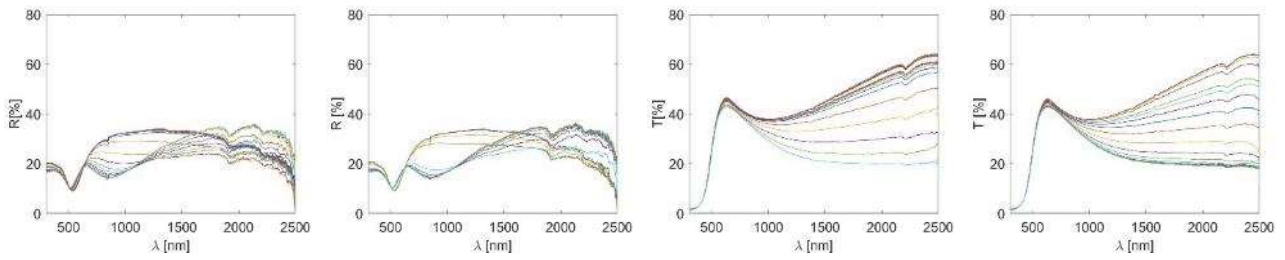
Spectral reflectance   *Spectral transmittance*
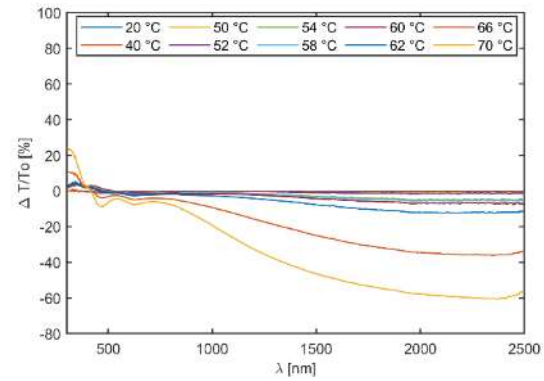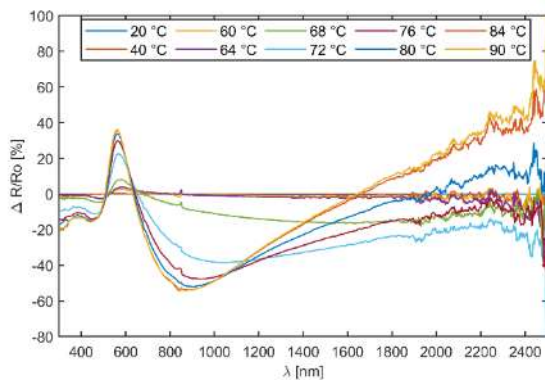
The change in in reflectance (R – R₀)/ R₀ and (b) the change in transmittance (T – T₀)/ T₀ highlight temperature dependent changes of VO₂ by comparing to their value at room temperature (T₀ and R₀).
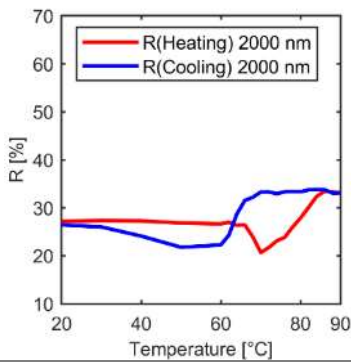
Reflectance hysteresis loop @2000 nm   *Transmittance hysteresis loop @2000 nm*
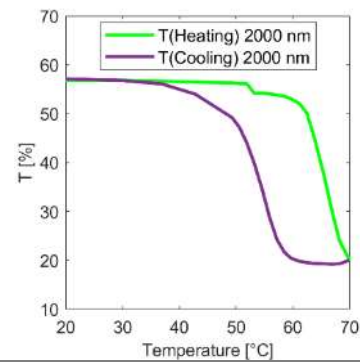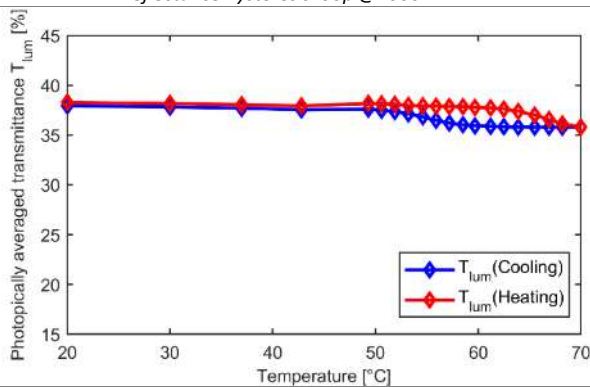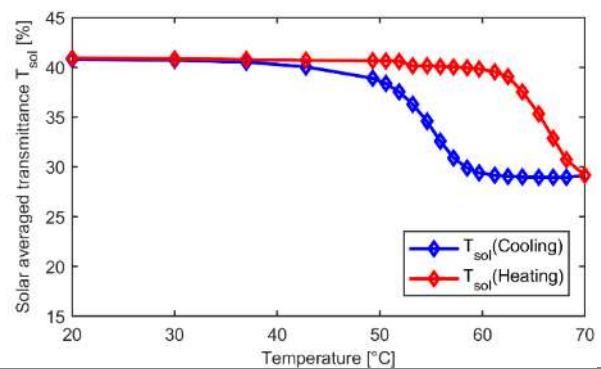
Photopically averaged transmittance T_{lum}   *Solar averaged transmittance T_{sol}*

Figure 38. Thermochromic optical properties measured for the sample 1– set n. 2

Spectral reflectance   Spectral transmittance

The change in in reflectance (R – R₀)/ R₀ and (b) the change in transmittance (T – T₀)/ T₀ highlight temperature dependent changes of VO₂ by comparing to their value at room temperature (T₀ and R₀).

Reflectance hysteresis loop @2000 nm   *Transmittance hysteresis loop @2000 nm*

Solar averaged transmittance Tₛₒₗ   *Photopically averaged transmittance Tₗᵤₘ*

Figure 39. Thermochromic optical properties measured for the sample 2– set n. 2
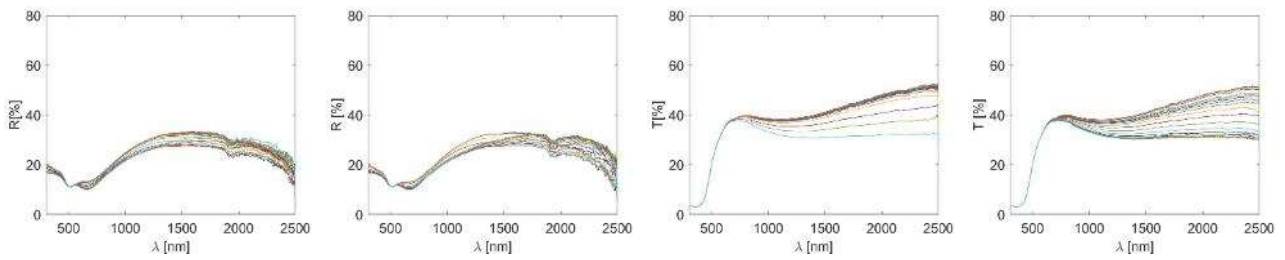
Spectral reflectance	*Spectral transmittance*
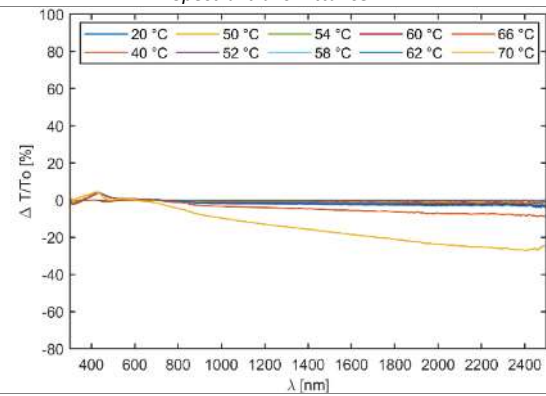
The change in in reflectance (R – R₀)/ R₀ and (b) the change in transmittance (T – T₀)/ T₀ highlight temperature dependent changes of VO₂ by comparing to their value at room temperature (T₀ and R₀).

Reflectance hysteresis loop @2000 nm	*Transmittance hysteresis loop @2000 nm*
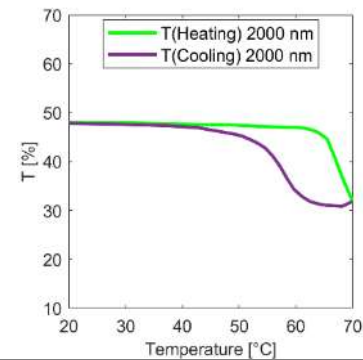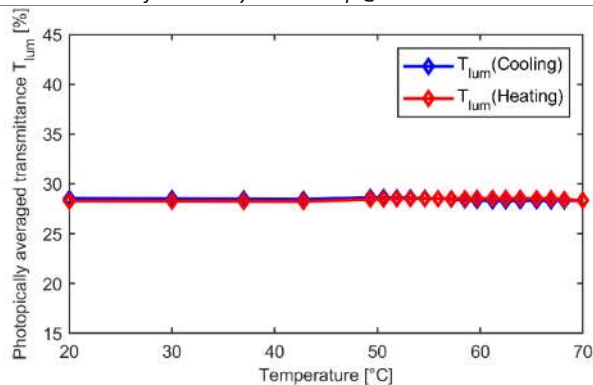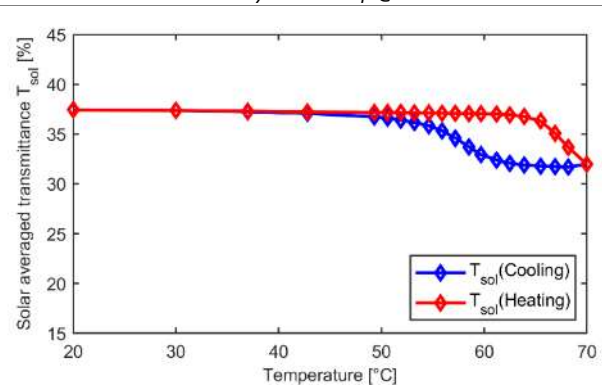
Solar averaged transmittance T_sol	*Photopically averaged transmittance T_lum*

Figure 40. Thermochromic optical properties measured for the sample 3– set n. 2

| Spectral reflectance | Spectral transmittance |

| Solar averaged transmittance T_{sol} | Photopically averaged transmittance T_{lum} |

| Reflectance hysteresis loop @2000 nm | Transmittance hysteresis loop @2000 nm |

Figure 41. Thermochromic optical properties measured for the sample 4– set n. 2

Table 8 summarizes the values of solar averaged transmittance (T_{sol}) and photopically averaged transmittance (T_{lum}) calculated according to the Equation (8) and the luminous transmittance modulation (ΔT_{lum}) and solar energy modulation (ΔT_{sol}) defined by Equation (9) for the 4 glazing samples of the set n. 2.

Table 8. Luminous and solar transmittance of the 4 glass samples belonging to set n. 2

Samples		hot state		cold state		ΔT_{sol}	ΔT_{lum}
		T_{sol} [%]	T_{lum} [%]	T_{sol} [%]	T_{lum} [%]	[%]	[%]
1	VO$_2$	29.1	35.8	40.9	38.3	**11.8**	**2.5**
2	VO$_2$	29.6	37.1	41.9	39.6	**12.3**	**2.5**
3	VO$_2$ – SiO$_2$	31.9	28.3	37.4	28.4	**5.5**	**0.1**
4	VO$_2$ – SiO$_2$	43.0	40.0	48.9	40.6	**5.9**	**0.6**

Table 9 shows the percentage of reflection and transmission values of the samples evaluated in the hot and cold state conditions at the wavelength of 2000 nm and the respective variation ΔR and ΔT.

Table 9. Reflectance and transmittance properties at the wavelength of 2000 nm of the 4 glass samples belonging to set n. 2

Samples		hot state	cold state	ΔR	hot state	cold state	ΔT
		R@2000 [%]	R@2000 [%]	[%]	T@2000 [%]	T@2000 [%]	[%]
1	VO$_2$	33.2	27.2	6.0	57.1	20.0	37.1
2	VO$_2$	47.1	35.1	12.0	57.7	18.9	38.8
3	VO$_2$ – SiO$_2$	30.0	29.3	0.7	47.8	31.8	16.0
4	VO$_2$ – SiO$_2$	42.4	35.6	6.8	61.1	43.2	17.9

The results summarized in the histogram graphs in the Figure 42, Figure 43, Figure 44, and Figure 45 shown how the SiO$_2$ used as a barrier layer reduced the thermochromic behaviour when compared to single VO$_2$ films.
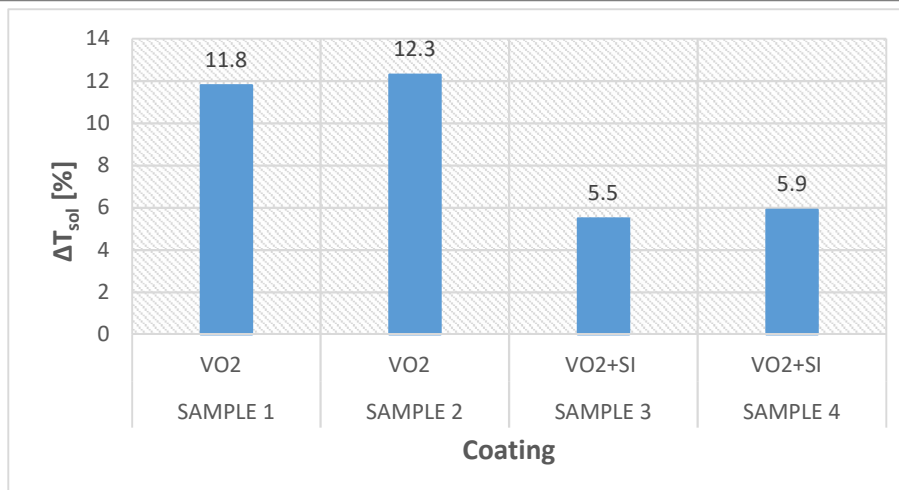
Figure 42. Solar modulation ability ΔT_{sol}
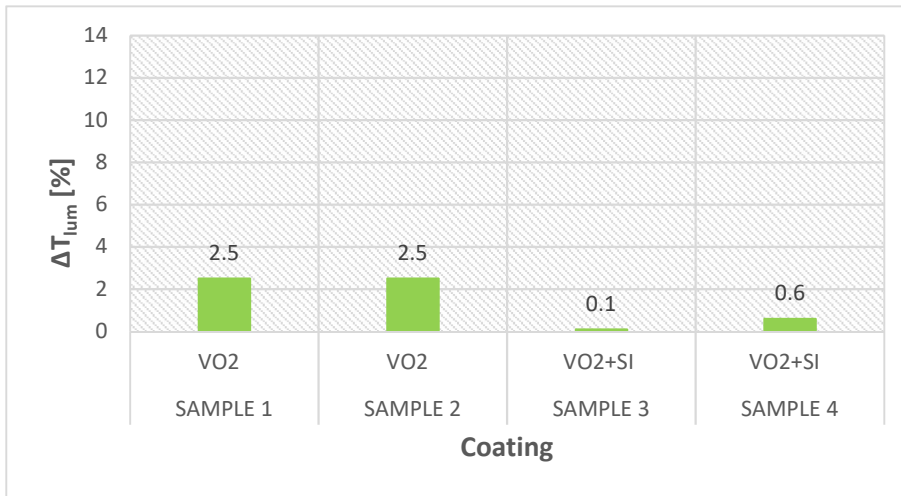
Figure 43. Luminous modulation ΔT_{lum}
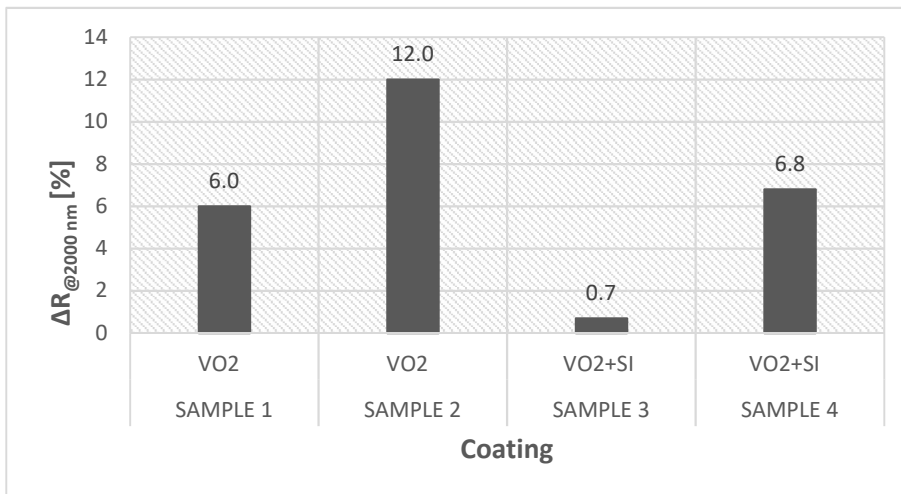
Figure 44. Variation of reflection coefficient between hot and cold state in the infrared region at the spectrum wavelength of 2000 nm
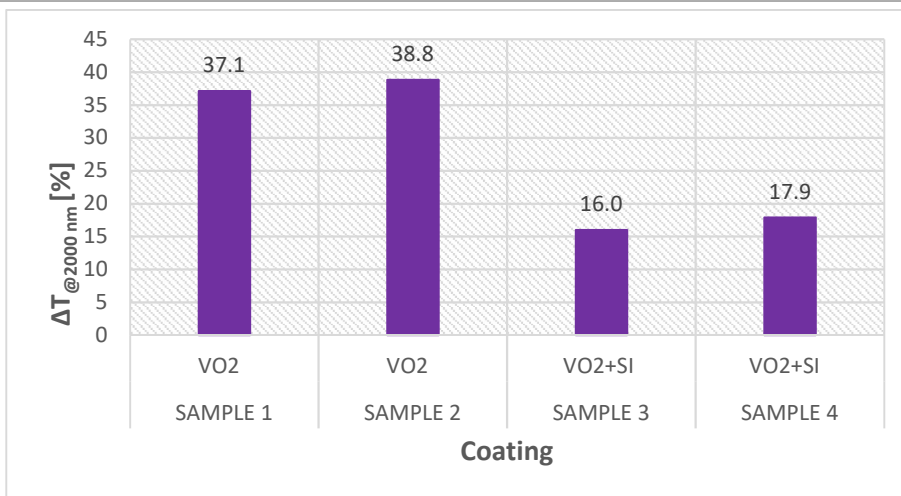
Figure 45. Variation of transmittance coefficient between hot and cold state in the infrared region at the spectrum wavelength of 2000 nm

The glass samples belonging to set n. 3 (see Figure 15c) have been tested in terms of reflectance and transmittance properties. Figures from Figure 46 to Figure 55 reports the hysteresis loops of the transmittance calculated at 2000 nm, the solar and the luminous transmittance.

Transmittance hysteresis loop @2000 nm	Solar averaged transmittance T_{sol}	Photopically averaged transmittance T_{lum}

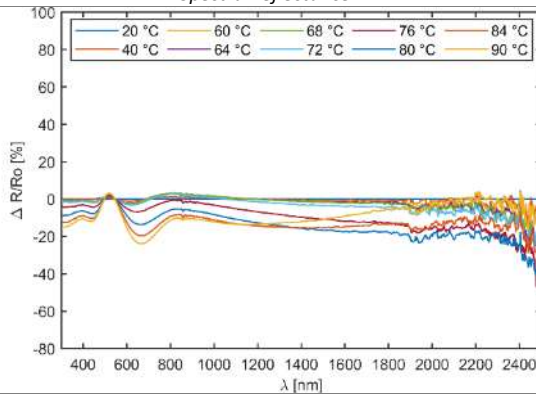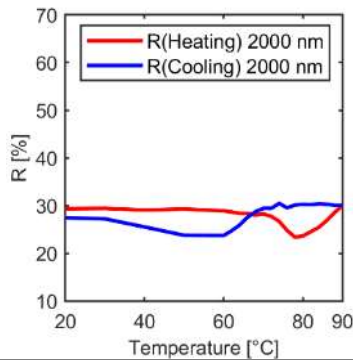Figure 46. Thermochromic optical properties measured for the sample V96-1– set n. 3

Transmittance hysteresis loop @2000 nm	Solar averaged transmittance T_{sol}	Photopically averaged transmittance T_{lum}
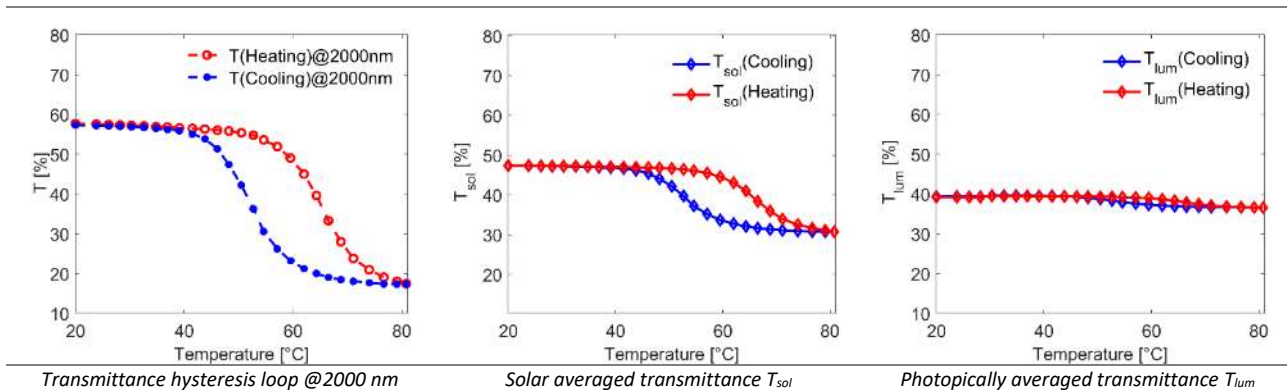
Figure 47. Thermochromic optical properties measured for the sample V96-2– set n. 3

Transmittance hysteresis loop @2000 nm	Solar averaged transmittance T_{sol}	Photopically averaged transmittance T_{lum}
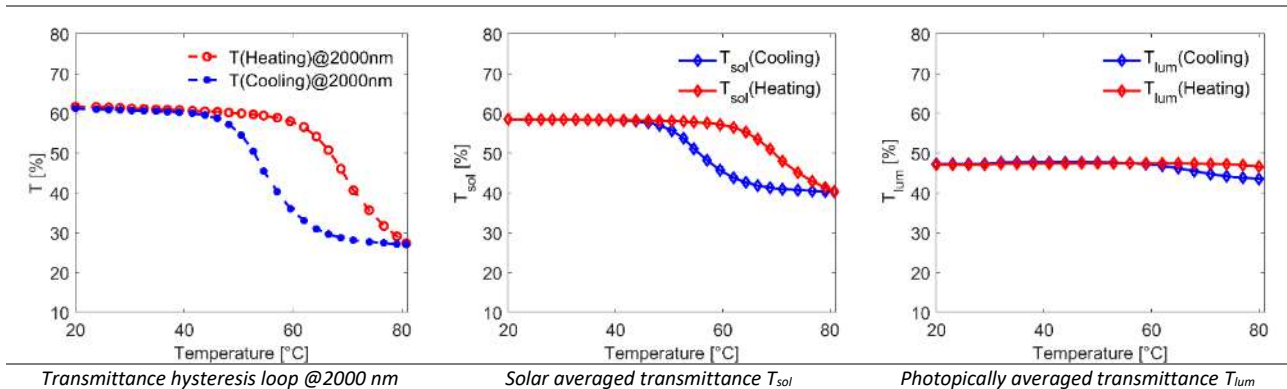
Figure 48. Thermochromic optical properties measured for the sample V96-3– set n. 3

Transmittance hysteresis loop @2000 nm | *Solar averaged transmittance T_{sol}* | *Photopically averaged transmittance T_{lum}*
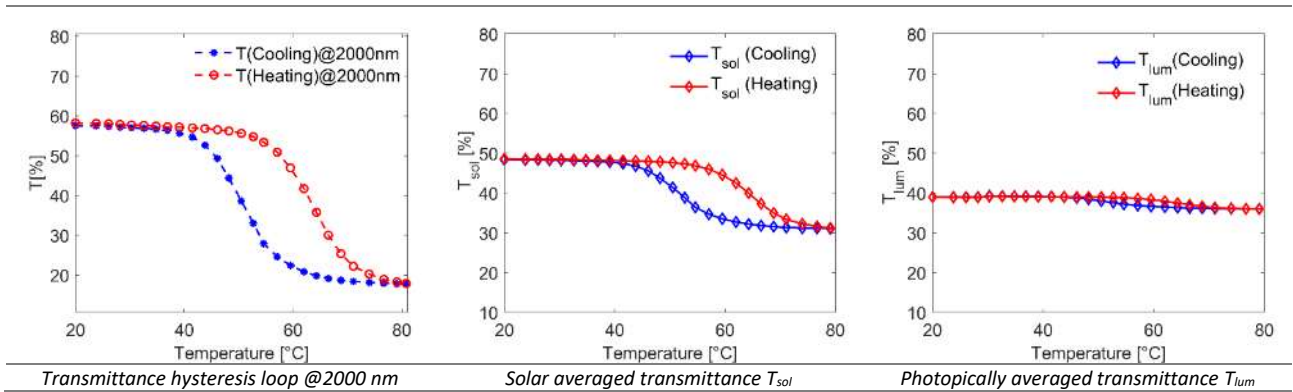
Figure 49. Thermochromic optical properties measured for the sample V96-4– set n. 3

Transmittance hysteresis loop @2000 nm | *Solar averaged transmittance T_{sol}* | *Photopically averaged transmittance T_{lum}*
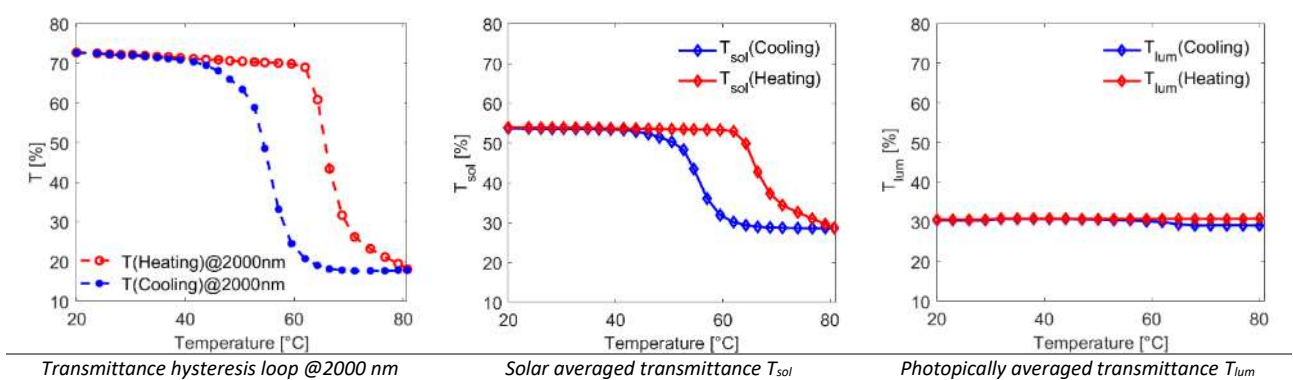
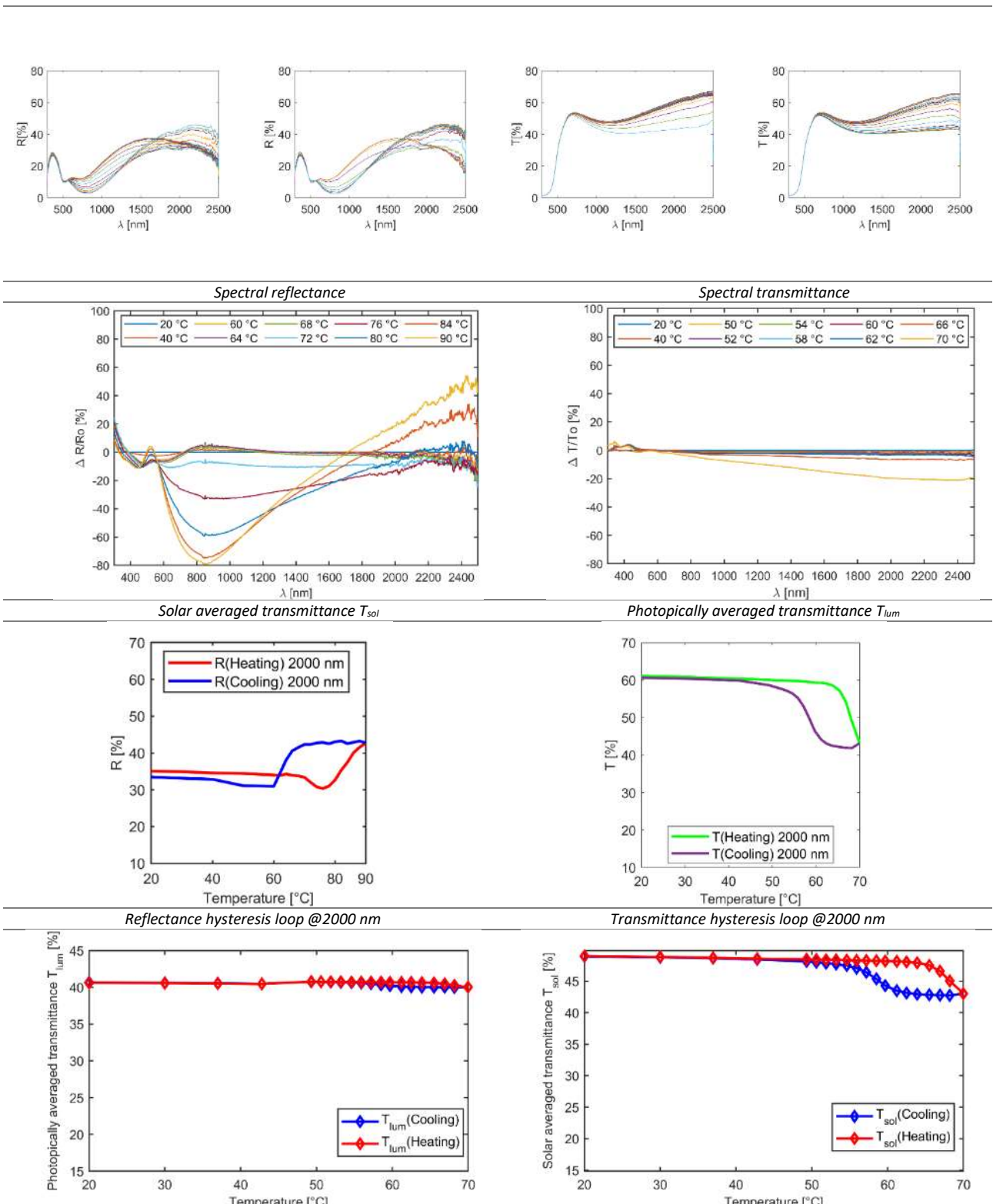Figure 50. Thermochromic optical properties measured for the sample V83-2– set n. 3

Transmittance hysteresis loop @2000 nm | *Solar averaged transmittance T_{sol}* | *Photopically averaged transmittance T_{lum}*
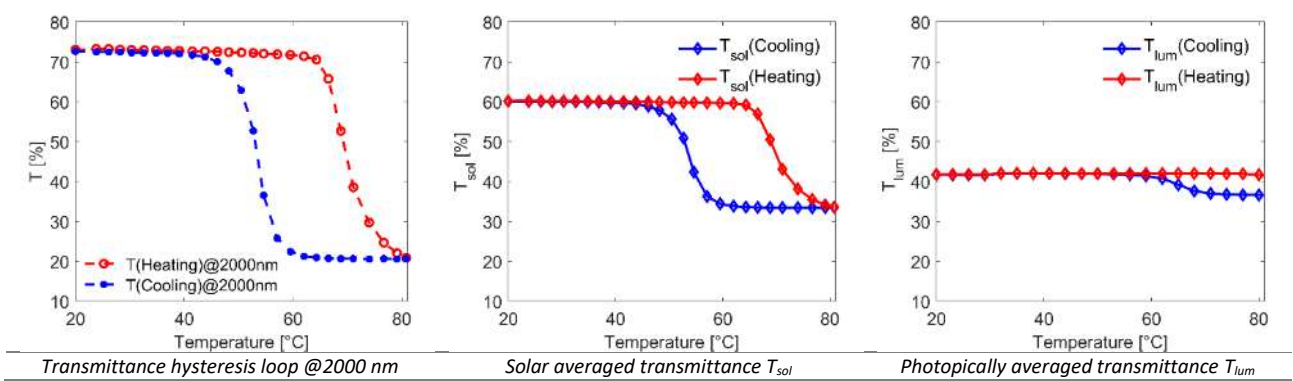
Figure 51. Thermochromic optical properties measured for the sample V89-3– set n. 3

Transmittance hysteresis loop @2000 nm | *Solar averaged transmittance T_{sol}* | *Photopically averaged transmittance T_{lum}*
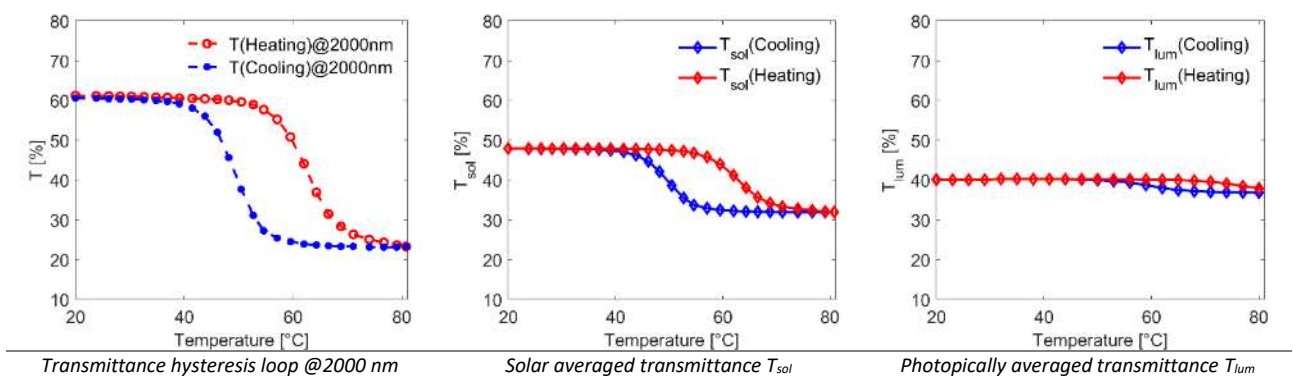
Figure 52. Thermochromic optical properties measured for the sample ML-1– set n. 3

Transmittance hysteresis loop @2000 nm | *Solar averaged transmittance T_{sol}* | *Photopically averaged transmittance T_{lum}*
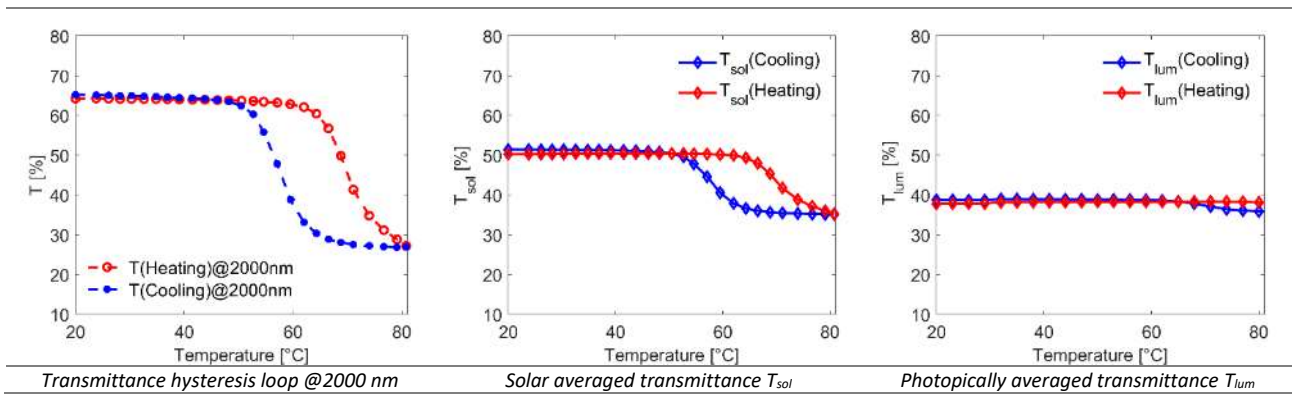
Figure 53. Thermochromic optical properties measured for the sample ML-2– set n. 3

Transmittance hysteresis loop @2000 nm | *Solar averaged transmittance T_{sol}* | *Photopically averaged transmittance T_{lum}*
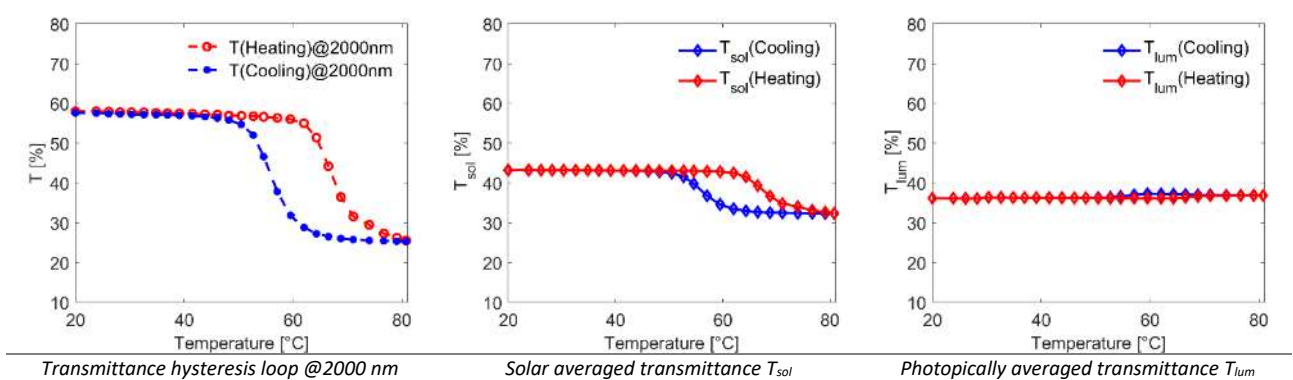
Figure 54. Thermochromic optical properties measured for the sample ML-3– set n. 3

Transmittance hysteresis loop @2000 nm | *Solar averaged transmittance T_{sol}* | *Photopically averaged transmittance T_{lum}*
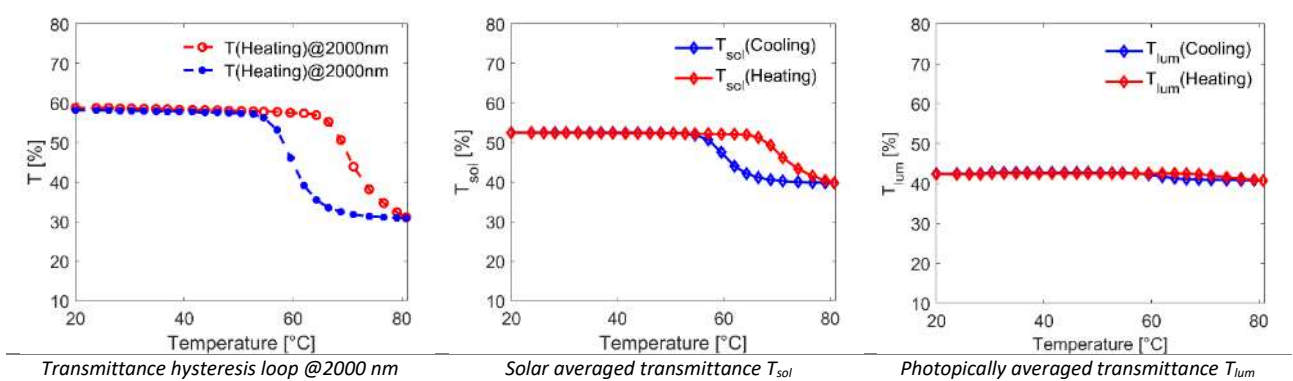
Figure 55. Thermochromic optical properties measured for the sample ML-4 – set n. 3

Table 10 summarizes the values of solar averaged transmittance (T_{sol}) and photopically averaged transmittance (T_{lum}) calculated according to the Equation (8) and the luminous transmittance modulation (ΔT_{lum}) and solar energy modulation (ΔT_{sol}) defined by the Equation (9) for the glazing samples of the set n.3. The transmittance modulation is illustrated in the histograms of Figure 45, 46 and 47 in terms of $\Delta T_{@2000nm}$, ΔT_{sol} and ΔT_{lum}.

Table 10. Luminous, solar transmittance and transmittance @ 2000 nm of the 10 glass samples belonging to set n. 3

| Samples	Coating	hot state			cold state			$\Delta T_{@2000}$ [%]	ΔT_{sol} [%]	ΔT_{lum} [%]
		$T_{@2000}$ [%]	T_{sol} [%]	T_{lum} [%]	$T_{@2000}$ [%]	T_{sol} [%]	T_{lum} [%]			
ML-1	$TiO_2+VO_2+TiO_2+VO_2+$ Norland+Glass	23.2	31.9	37.9	60.6	47.9	40.1	37.4	16.0	2.2
ML-2	$TiO_2+VO_2+TiO_2+VO_2+$ Norland	27.0	35.3	38.1	65.2	50.3	37.8	38.2	15.0	-0.3
ML-3	TiO_2+VO_2	25.4	32.4	36.9	57.6	43.3	36.2	32.2	10.9	-0.7
ML-4	$TiO_2+VO_2+TiO_2$	32.4	40.4	40.9	58.7	52.4	42.3	26.3	12.0	1.4
V83-2	$TiO_2+VO_2+TiO_2+VO_2+$ Norland	17.8	28.8	30.9	72.6	54.0	30.6	54.8	25.2	-0.3
V89-3	$TiO_2+VO_2+TiO_2+VO_2+$ Norland	20.6	33.6	41.7	72.6	60.2	41.8	52.0	26.6	0.1
V96-1	$TiO_2+VO_2+TiO_2$	27.1	39.7	46.2	61.5	58.0	42.1	34.4	18.3	-4.1
V96-2	TiO_2+VO_2	17.3	30.8	36.5	57.3	47.4	39.1	40.0	16.6	2.3
V96-3	$TiO_2+VO_2+TiO_2$	27.1	40.4	46.7	61.3	58.5	47.1	34.2	18.1	0.5
V96-4	TiO_2+VO_2	17.9	31.2	35.9	58.2	48.6	38.9	40.3	17.4	3.0
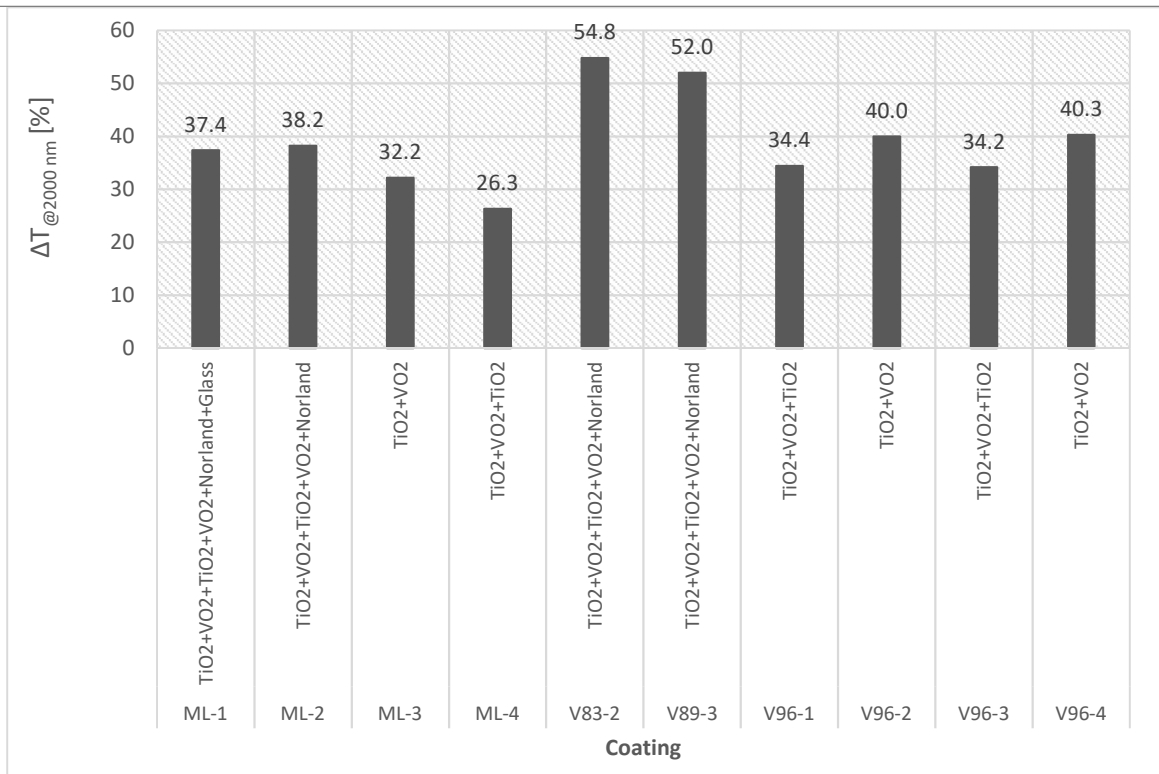
Figure 56. Variation of reflection coefficient between hot and cold state in the infrared region at the spectrum wavelength of 2000 nm

Figure 57. Solar modulation ability ΔT_{sol}

Figure 58. Luminous modulation ΔT_{lum}

Figures from Figure 59 to Figure 68 report the hysteresis loops of the reflectance calculated at 2000 nm, the solar and the luminous reflectance.
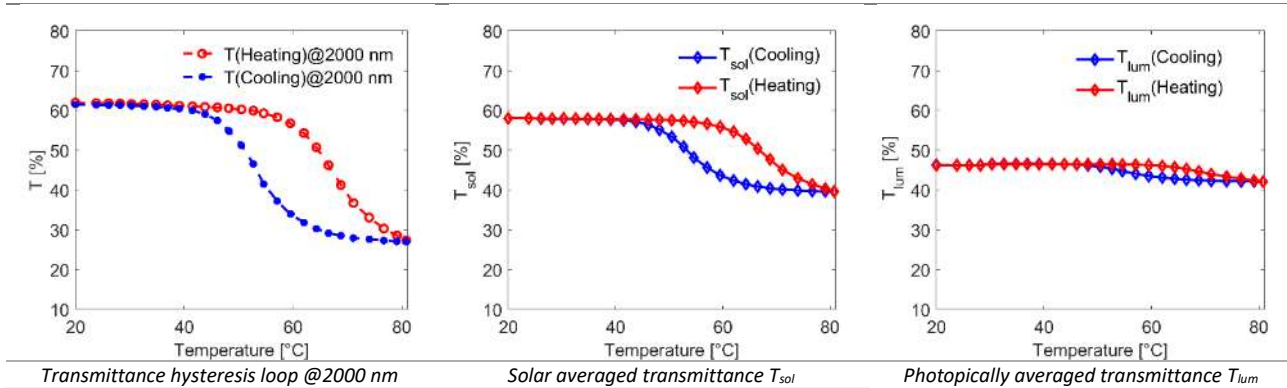

Reflectance hysteresis loop @2000 nm — *Solar averaged reflectance R_{sol}* — *Photopically averaged reflectance R_{lum}*
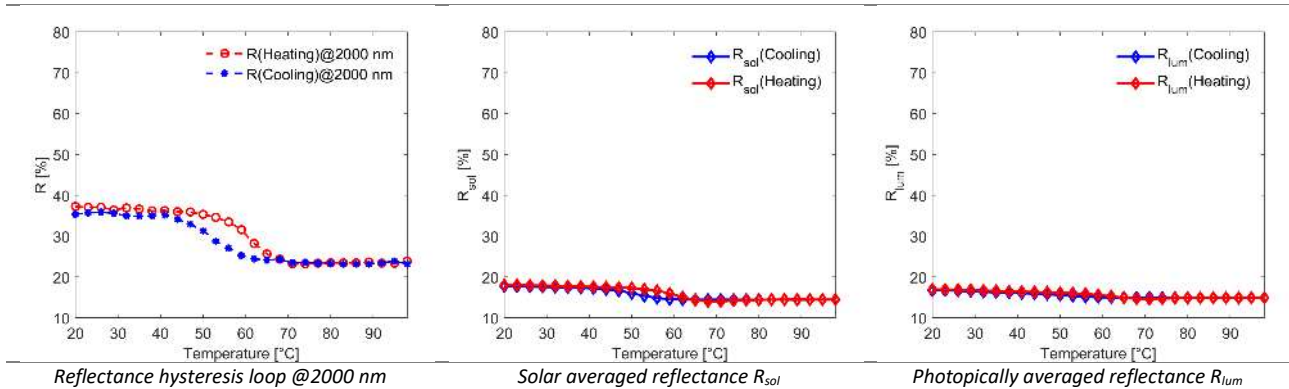
Figure 59. Thermochromic optical properties measured for the sample V96-1 – set n. 3

Reflectance hysteresis loop @2000 nm — *Solar averaged reflectance R_{sol}* — *Photopically averaged reflectance R_{lum}*
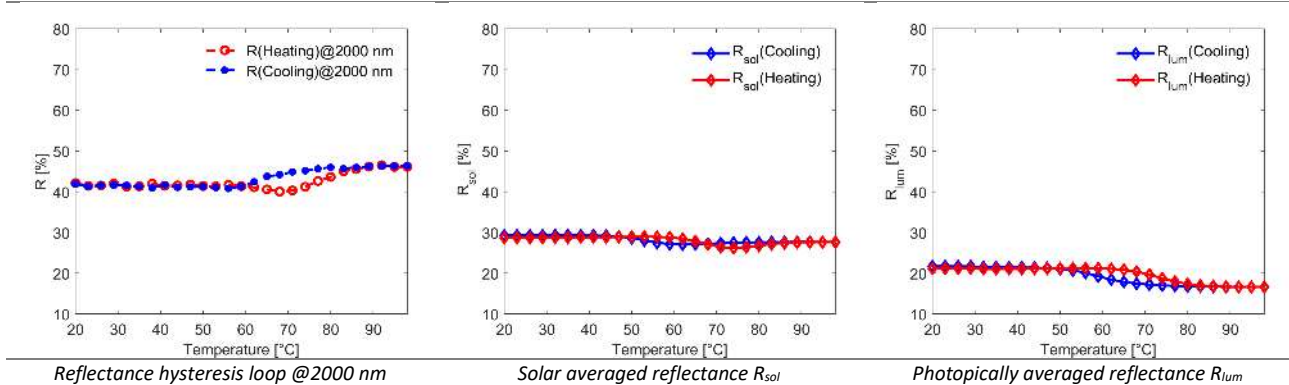
Figure 60. Thermochromic optical properties measured for the sample V96-2 – set n. 3

Reflectance hysteresis loop @2000 nm *Solar averaged reflectance R_{sol}* *Photopically averaged reflectance R_{lum}*
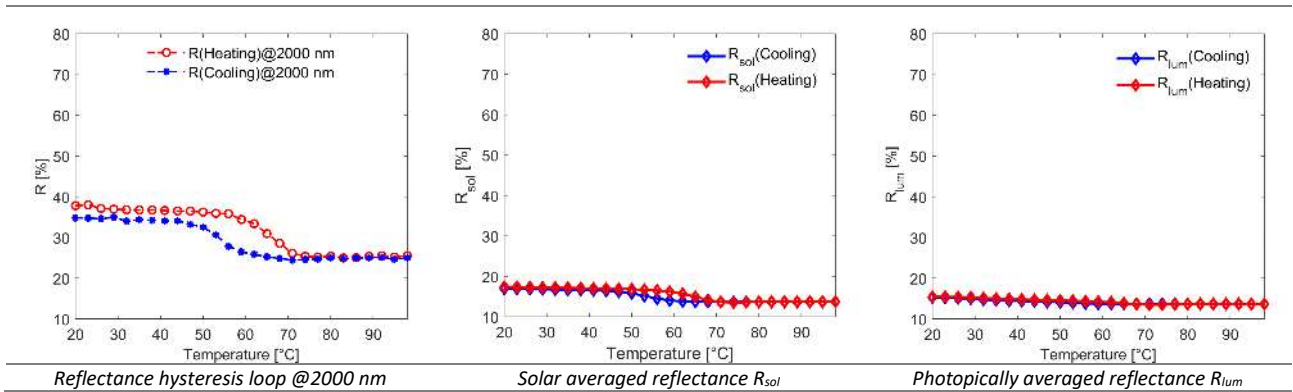
Figure 61. Thermochromic optical properties measured for the sample V96-3 – set n. 3

Reflectance hysteresis loop @2000 nm *Solar averaged reflectance R_{sol}* *Photopically averaged reflectance R_{lum}*
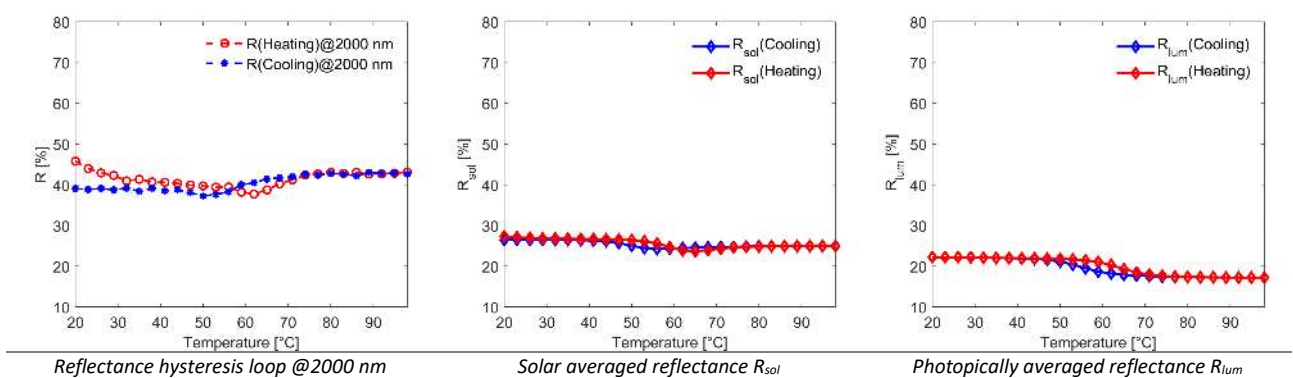
Figure 62. Thermochromic optical properties measured for the sample V96-4 – set n. 3

Reflectance hysteresis loop @2000 nm *Solar averaged reflectance R_{sol}* *Photopically averaged reflectance R_{lum}*
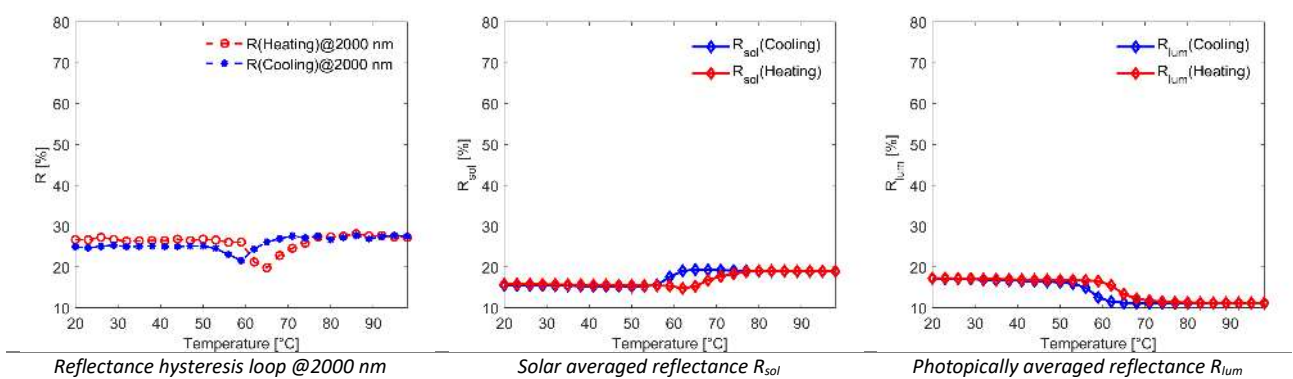
Figure 63. Thermochromic optical properties measured for the sample V82-3 – set n. 3

Reflectance hysteresis loop @2000 nm *Solar averaged reflectance R_{sol}* *Photopically averaged reflectance R_{lum}*
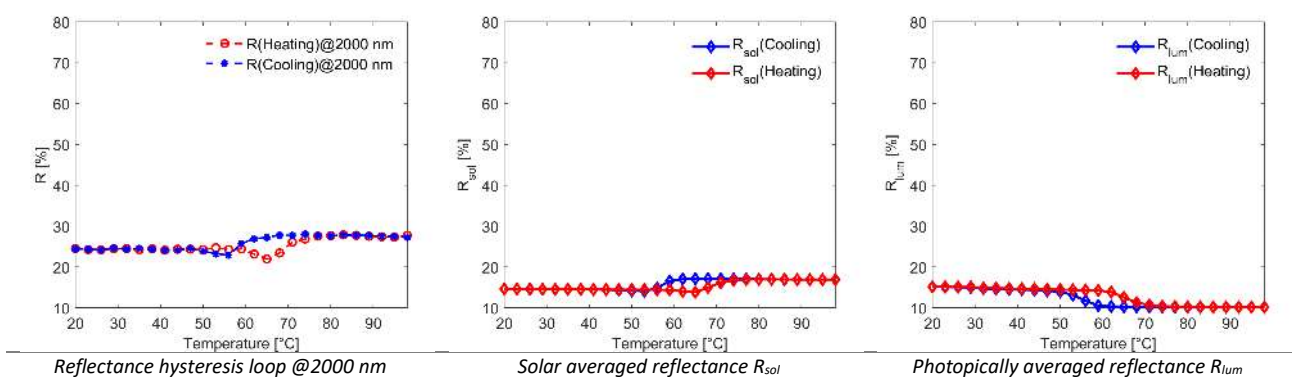
Figure 64. Thermochromic optical properties measured for the sample V89-3 – set n. 3

Reflectance hysteresis loop @2000 nm | *Solar averaged reflectance R_{sol}* | *Photopically averaged reflectance R_{lum}*
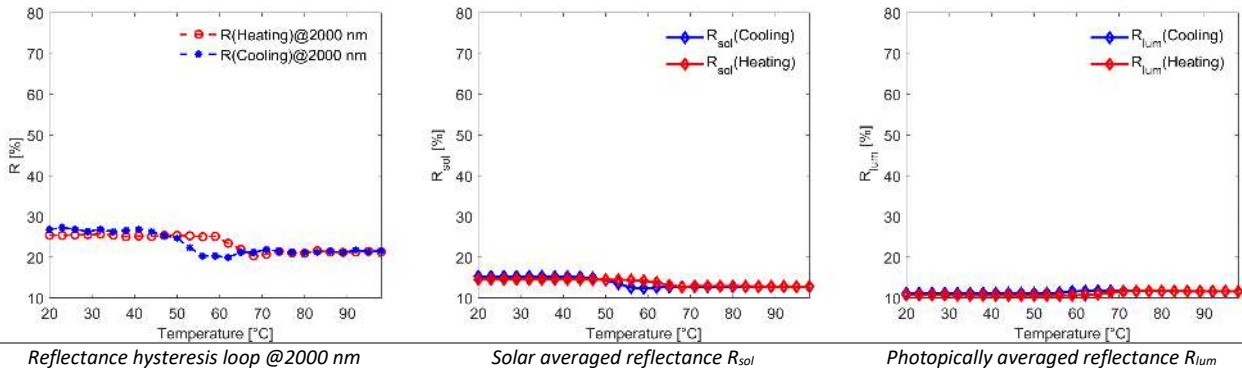
Figure 65. Thermochromic optical properties measured for the sample ML-1 – set n. 3

Reflectance hysteresis loop @2000 nm | *Solar averaged reflectance R_{sol}* | *Photopically averaged reflectance R_{lum}*
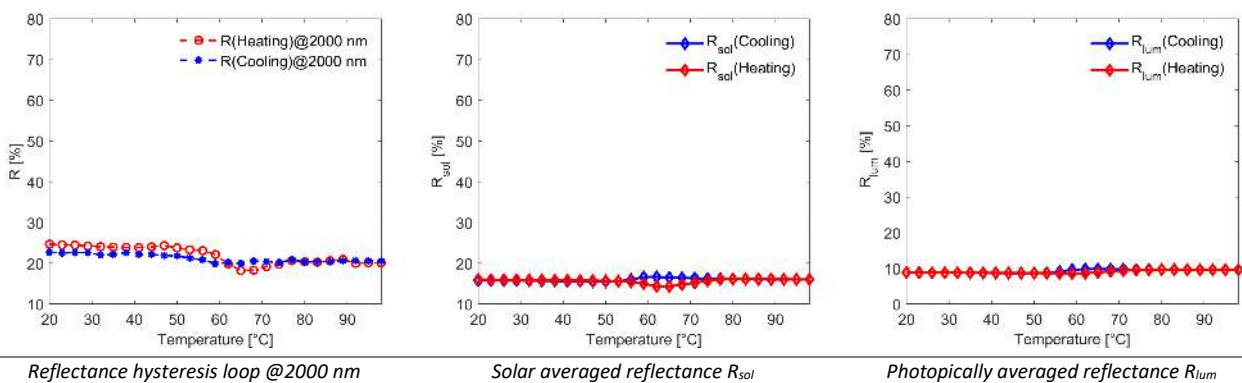
Figure 66. Thermochromic optical properties measured for the sample ML-2 – set n. 3

Reflectance hysteresis loop @2000 nm | *Solar averaged reflectance R_{sol}* | *Photopically averaged reflectance R_{lum}*
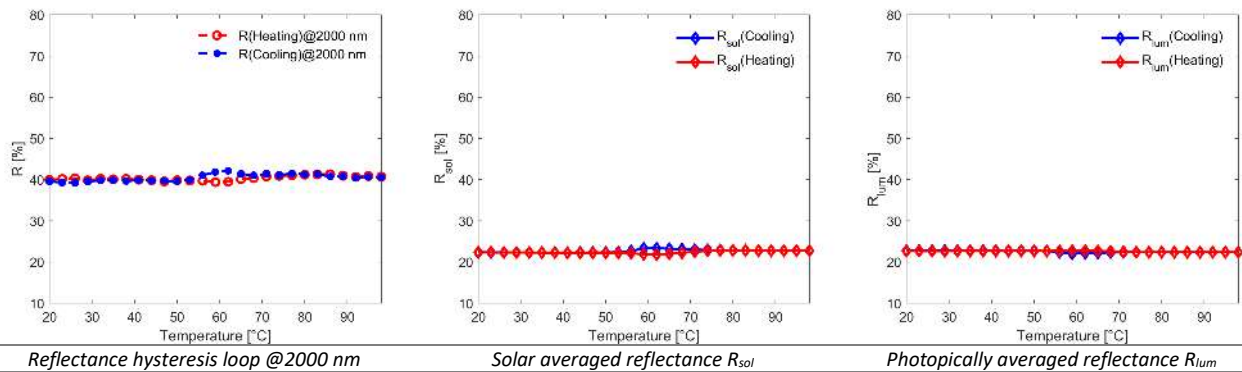
Figure 67. Thermochromic optical properties measured for the sample ML-3 – set n. 3

Reflectance hysteresis loop @2000 nm | *Solar averaged reflectance R_{sol}* | *Photopically averaged reflectance R_{lum}*
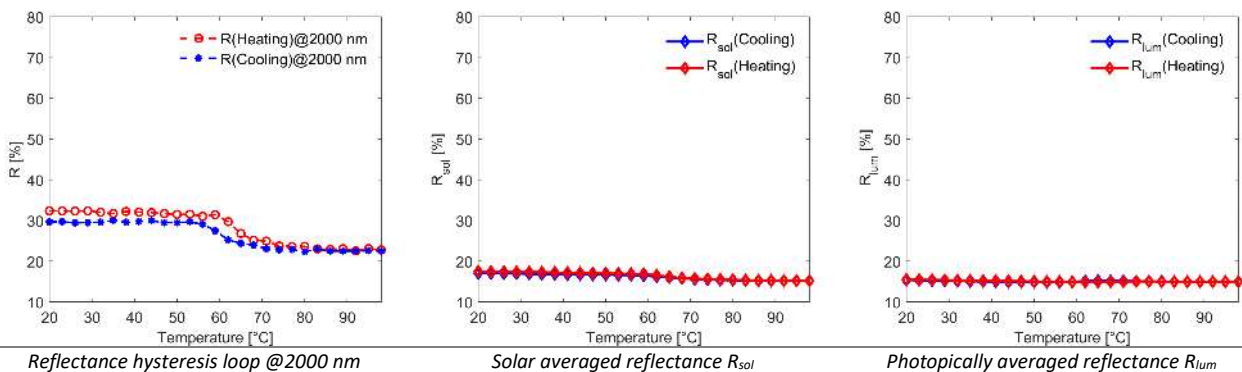
Figure 68. Thermochromic optical properties measured for the sample ML-4 – set n. 3

Table 10 summarizes the values of the reflectance at the wavelength of 2000 nm, the solar averaged reflectance (R_{sol}) and the photopically averaged reflectance (R_{lum}) calculated according to the Equation (8) for the glazing samples of the set n.3. In addition the reflectance modulation (ΔR_{lum} and ΔR_{sol}) defined by the Equation (9) is given. The reflectance modulation is illustrated in the histograms of Figure 69, Figure 70 and Figure 71 in terms of $\Delta R_{@2000nm}$, ΔR_{sol} and ΔR_{lum}.

Table 11. Luminous, solar reflectance and reflectance @ 2000 nm of the 10 glass samples belonging to set n.3

| Samples	Coating	hot state			cold state			$\Delta R_{@2000}$ [%]	ΔR_{sol} [%]	ΔR_{lum} [%]
		$R_{@2000}$ [%]	R_{sol} [%]	R_{lum} [%]	$R_{@2000}$ [%]	R_{sol} [%]	R_{lum} [%]			
ML-1	$TiO_2+VO_2+TiO_2+VO_2+$ Norland+Glass	21.6	12.8	11.7	26.8	14.6	10.7	-5.2	-1.8	1.0
ML-2	$TiO_2+VO_2+TiO_2+VO_2+$ Norland	20.6	16.1	9.6	24.7	16.0	8.8	-4.1	0.1	0.8
ML-3	TiO_2+VO_2	40.6	22.8	22.4	40.0	22.4	22.7	0.6	0.4	-0.3
ML-4	$TiO_2+VO_2+TiO_2$	22.6	15.2	15.0	32.4	17.5	15.5	-9.8	-2.3	-0.5
V83-2	$TiO_2+VO_2+TiO_2+VO_2+$ Norland	27.5	19.0	11.2	26.7	15.8	17.3	0.8	3.2	-6.1
V89-3	$TiO_2+VO_2+TiO_2+VO_2+$ Norland	27.3	16.9	10.2	24.4	14.6	15.2	2.9	2.3	-5.0
V96-1	$TiO_2+VO_2+TiO_2$	23.9	14.5	14.9	37.3	18.0	17.0	-13.4	-3.5	-2.1
V96-2	TiO_2+VO_2	46.3	27.7	16.7	41.9	28.7	21.8	4.4	-1.0	-5.1
V96-3	$TiO_2+VO_2+TiO_2$	25.3	13.8	13.7	37.8	17.5	15.5	-12.5	-3.7	-1.8
V96-4	TiO_2+VO_2	42.7	24.9	17.2	45.7	27.3	22.2	-3.0	-2.4	-5.0
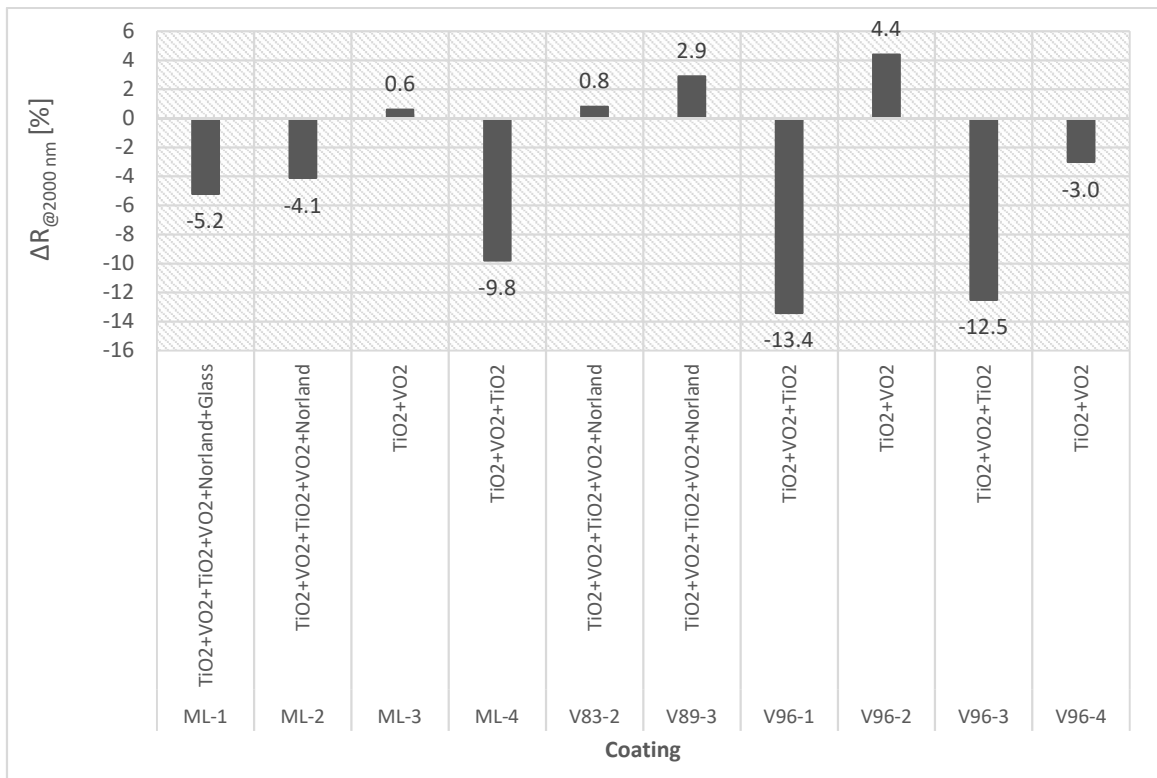
Figure 69. Variation of reflection coefficient between hot and cold state in the infrared region at the spectrum wavelength of 2000 nm
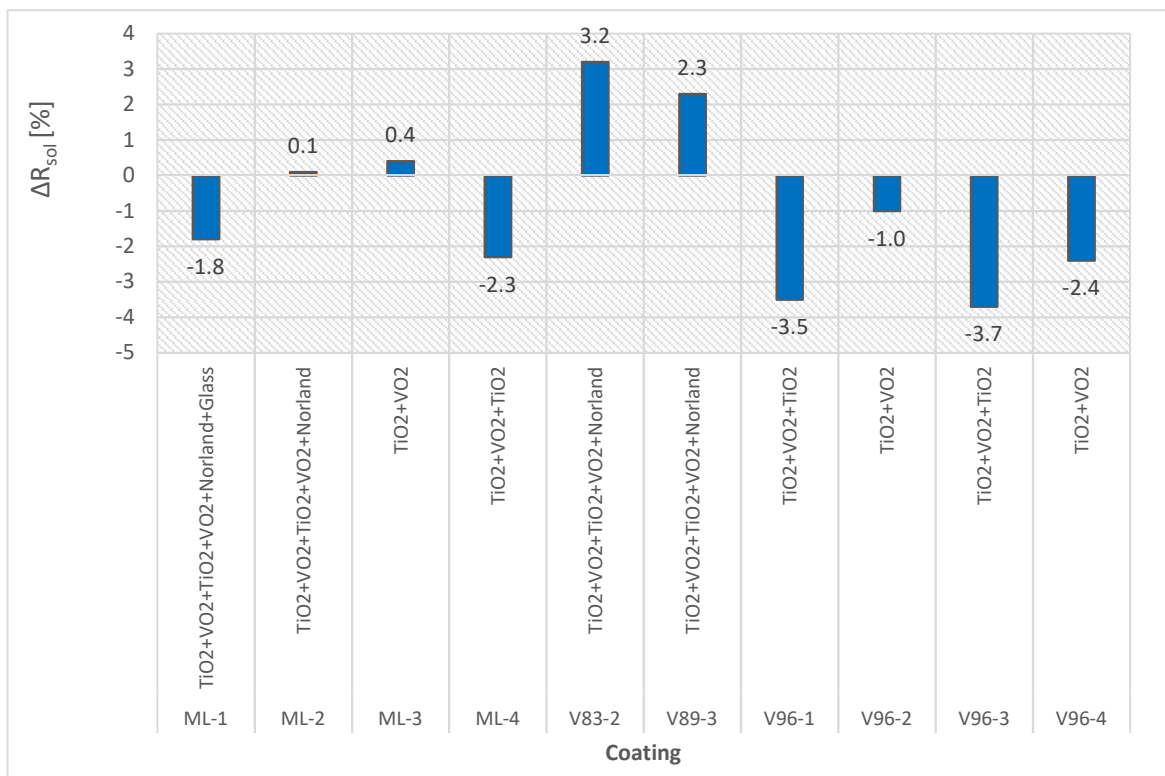
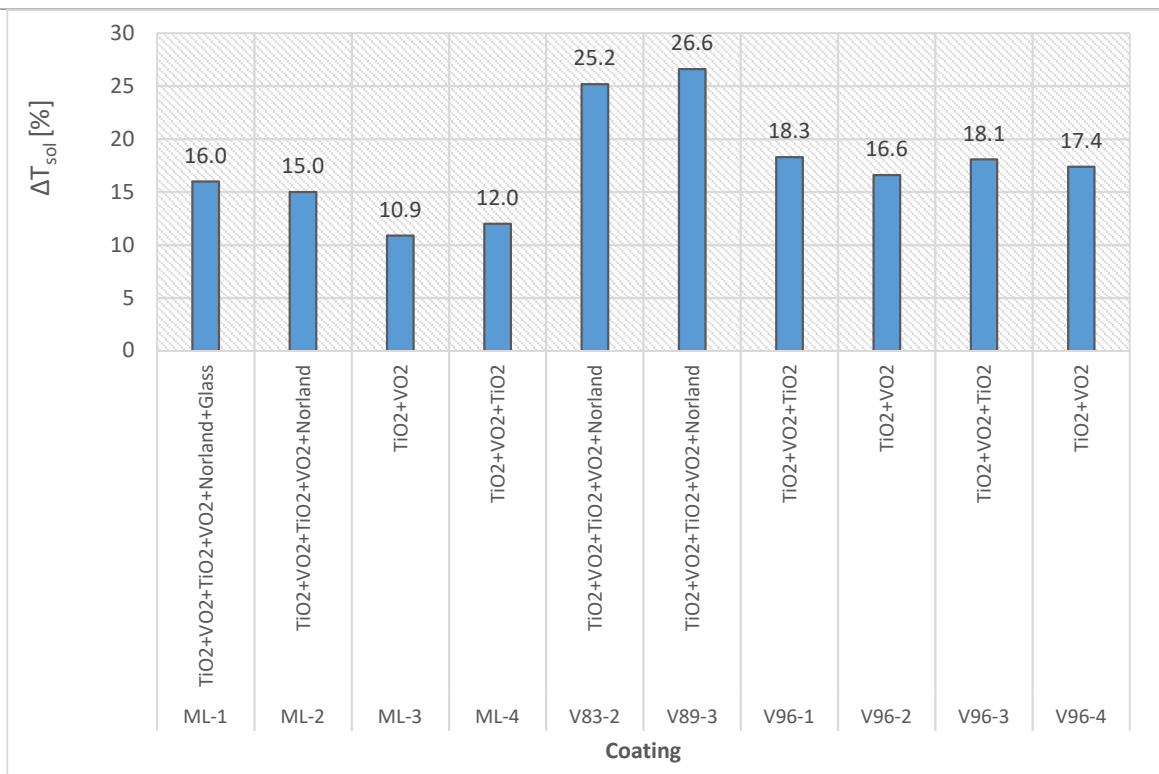Figure 70. Solar modulation ability ΔR_{sol}
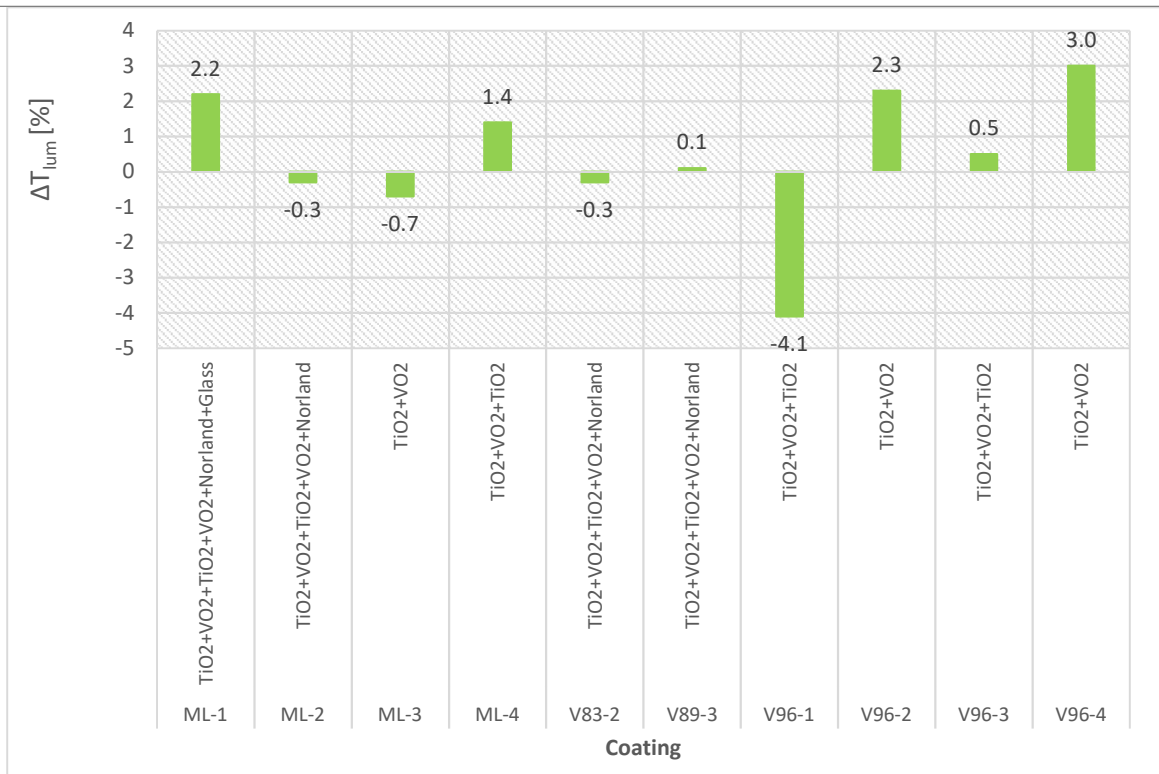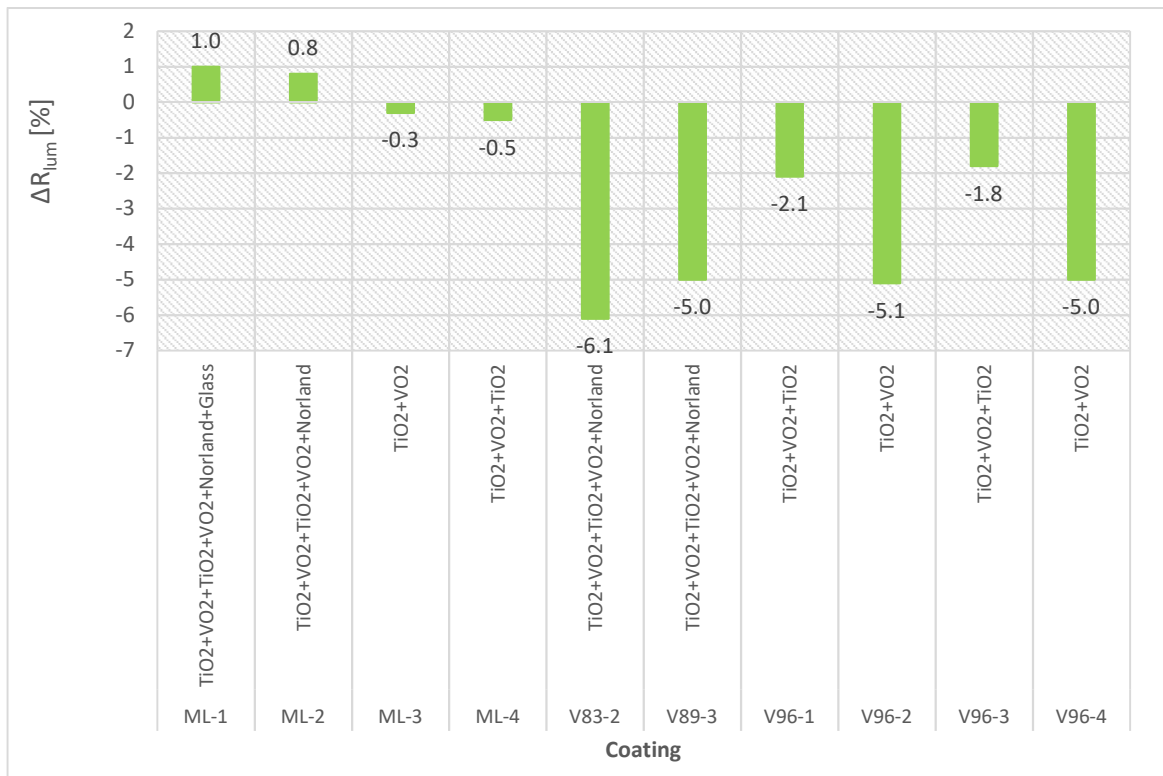
Figure 71. Luminous modulation ΔR_{lum}

4 Durability testing

4.1 Introduction

Specific accelerated ageing procedures have been developed to evaluate the durability of the stimuli-sensitive solar reflective glass coating. The main objective here was to evaluate the effect of ageing on the radiative properties (solar reflectance and thermal emittance) and therefore on the dynamic response of the coating to the environmental changes, taking into account also the soiling effect due to dust, soot deposition and biological growth.

None of the standard accelerated test methods can be applied since they only take into account UV radiation, temperature and moisture factors completely neglecting the effect of soiling.

The accelerated ageing procedures have been developed in three steps:

1) natural ageing tests on standard glazed assembly;
2) optimization of the accelerated procedure using outdoor exposure data;
3) application of the accelerated procedure to the new products.

4.2 Natural ageing test

One of the objective of this analysis is to understand the impact both of the soiling and the weathering agents like UV radiation, temperature and relative humidity on changing transmittance and reflectance properties of the thermochromic glass samples.

A first preliminary test has been performed on traditional building covering materials with the aim of providing background information on some basic ageing mechanisms. 2 thermochromic glass samples (sample 6 of series 1 and sample 3 of series 2) have been exposed for 6 Months to outdoor weather in

Ancona, Italy (Latitude 43.58, Longitude 13.51) from May to October 2019. Exposure conditions have been defined in agreement with standard ASTM G7 [14].

The sample 6 has external dimensions of 20 mm × 20 mm × 4 mm (height × width × thickness) and is coated with vanadium dioxide films (VO2) while the sample 3 has a semi-circular shape with a thickness of about 0.5 mm and is coated with VO_2+SiO_2 (see Figure 72).

(a)		(b)	
	VO$_2$		**VO$_2$ + SiO$_2$**
Sample 6		**Sample 3**	
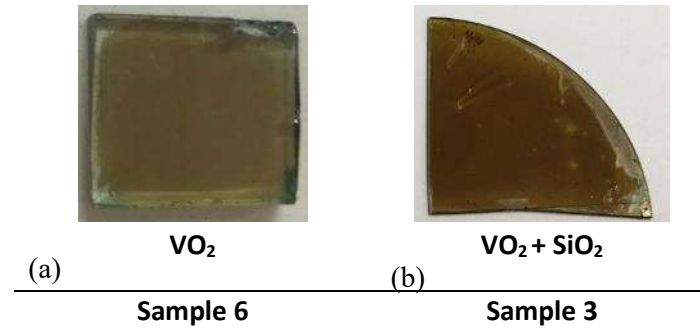
Figure 72. Samples used for natural aging test

The glasses were positioned with the surfaces facing south to maximize the effect of solar radiation and in a vertical position to simulate the installation in buildings (see Figure 62). Exposure racks have been installed at the height of 2.5 m near a lamppost positioned on a wall in the vicinity of a UNIVPM laboratory.
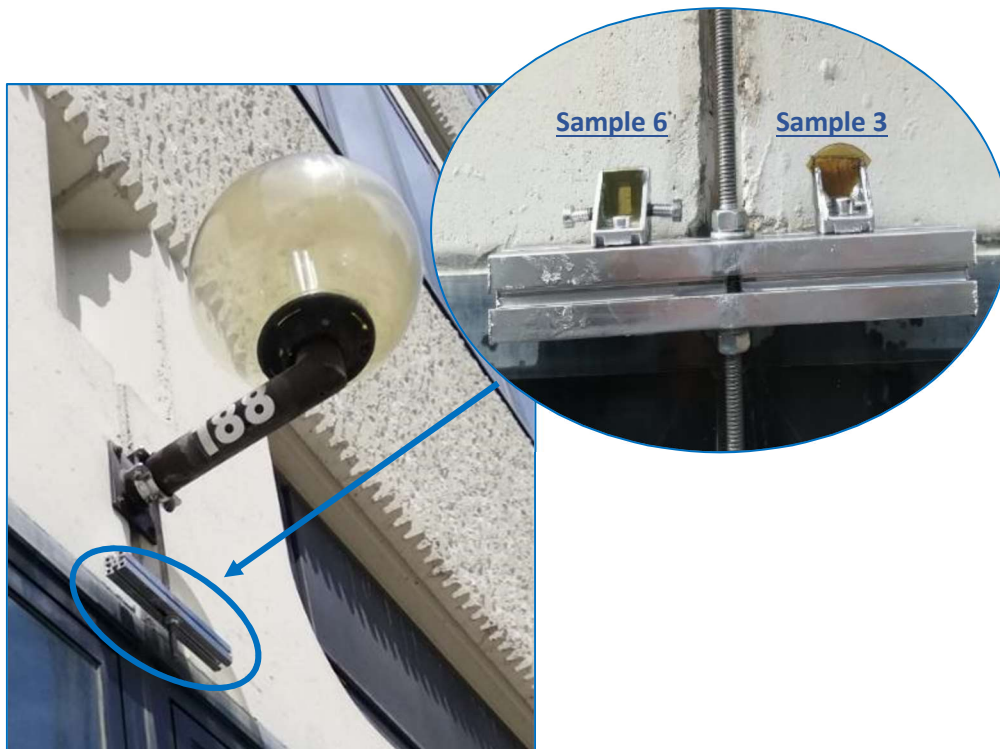
Figure 73. Picture of samples exposed on the wall at UNIVPM

The hysteresis loops given in terms of transmittance at 2000 nm and of luminous and solar transmittance have been measured after 4 and 6 months of natural exposition; they are reported in Figure 74 and Figure 75 for the sample 6 of set n. 1 and for the sample 3 of set n. 2. It is evident that in the case of sample without protection (sample 6, set n. 1) after 6 months the transmittance modulation ability had disappeared this

testifying that the thermochromic coating has stopped working. The sample 3 of set n. 2, which is protected with a silica layer preserved its modulation property albeit reduced.

| Transmittance hysteresis loop @2000 nm | Solar averaged transmittance T_{sol} | Photopically averaged transmittance T_{lum} |
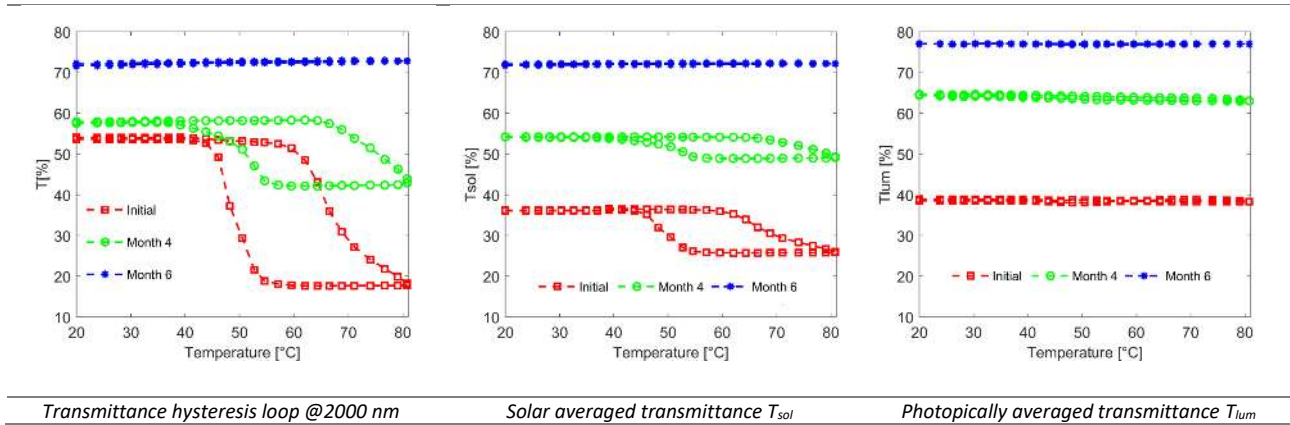
Figure 74. Thermochromic optical properties measured for the sample 6 - set n. 1

| Transmittance hysteresis loop @2000 nm | Solar averaged transmittance T_{sol} | Photopically averaged transmittance T_{lum} |
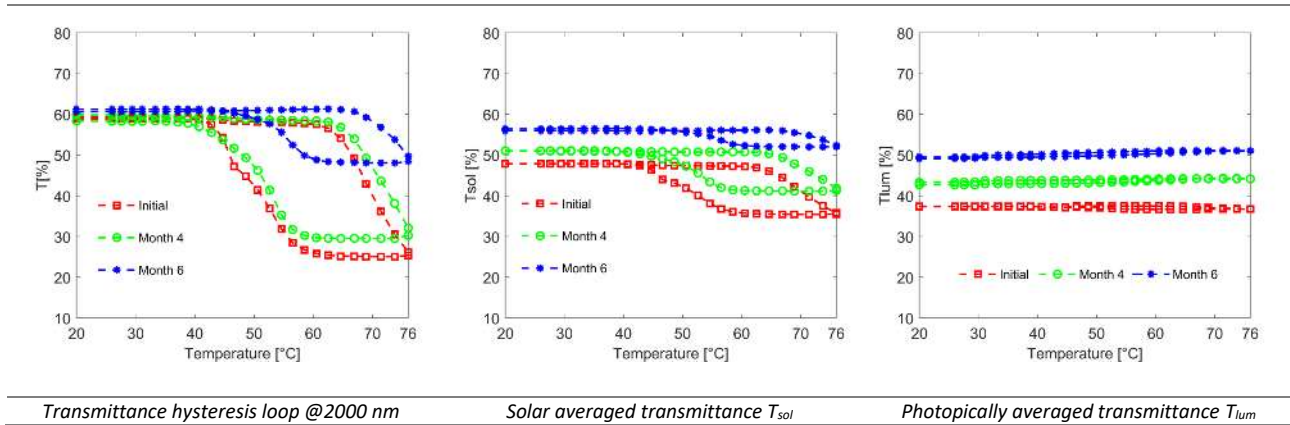
Figure 75. Thermochromic optical properties measured for the sample 3 – set 2

From February 2020, a second campaign of natural aging tests was launched on glass samples ML-4, ML-3 and V96-2 (see Figure 76).
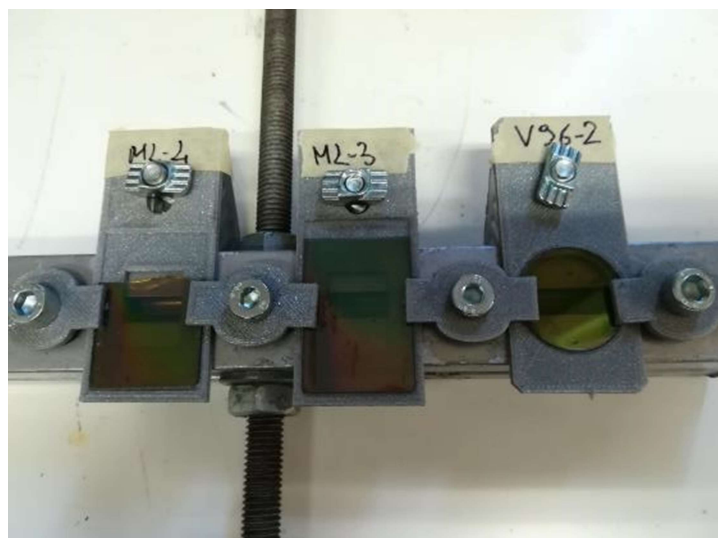
Figure 76. Installation of three samples of the set n. 3 for natural aging tests

4.3 Accelerated ageing tests

Accelerated methods for durability assessment are well known in the industry and are widely applied in different sectors: plastics, bituminous materials, polymeric coatings, woods. The objective is to hasten the material degradation by inducing the same ageing phenomena occurring under natural exposure but at higher intensity. Defining adequate methods for each materials is a very hard task since many factors have to be taken into account:

- Accelerated methods aim at simulating the effect of many years of environmental exposure on materials. The first issue concerns the variability of the natural stress factors that not only depends on the particular exposure site but, for a given region, different weather conditions can occur in different years.
- Due to the inherent variability of climatic conditions and materials to be tested most of existing standards do not recommend the definition of accelerated factors that correlate the duration of the artificial exposure to a certain durability (number of months) under natural exposure. Instead a comparative approach is suggested and the change of a certain property (weathering evaluation criterion) is quantified with respect to the change that occurs on a reference material (which is teste under natural ageing and is assumed as control point).
- Accelerated methods shall not alter the natural degradation mechanisms. Increasing the maximum temperature and resorting to very short UV wavelengths generate a significant reduction of material service life but, if not adequately controlled, it might activate different degradation processes with respect to those occurring during operative conditions.

Several accelerated weathering procedures have been developed and standardized for different materials and end-use environment. Most common methods are based on a specific test chamber that artificially reproduces natural stress factors (temperature, humidity, UV radiation, condensation and in some cases salt deposition and biological growth) with an higher intensity with respect to what happens outdoor. Some "hybrid" methods have been also defined and are based on a specific apparatus that maximize the effect of sunlight by focusing sun rays towards the test specimen. The EMMA (Equatorial Mounts with Mirrors for Acceleration) and EMMAQUE (Equatorial Mounts with Mirrors for Acceleration with a water spray cycle) are sun light concentrators that increase nine times the amount of received solar radiation and can develop temperatures up to 150°C resulting in a 5-6 times faster properties loss [15].

Figure 77. Equipment used to accelerate ageing phenomena: left EMMAQUE device, middle: weatherometer (sometimes called QUV chamber), Right: Xenon tester

Following these criteria dozens of accelerated standards have been developed for different materials (some examples relative to building envelope materials is presented in Table 12.

Table 12. List of standard accelerated methods for ageing resistance evaluation

Standard		Application
ASTM E3119 – 17	Standard Test Method for Accelerated Aging of Environmentally Controlled Dynamic Glazing	Thermochromic Dynamic Glazing
ASTM E3119 –20	Standard Specification for Evaluating Accelerated Aging Performance of Environmentally Controlled Dynamic Glazings	Thermochromic Dynamic Glazing
ISO 18543:2017	Glass in building — Electrochromic glazings — Accelerated ageing test and requirements	Electrochromic glazings
ASTM G151	Standard Practice for Exposing Nonmetallic Materials in Accelerated Test Devices that Use Laboratory Light Source	General - nonmetallic materials
ASTM G154	Standard Practice for Operating Fluorescent Light Apparatus for UV Exposure of Nonmetallic Materials	General - nonmetallic materials
ASTM G155	Standard Practice for Operating Xenon Arc Light Apparatus for Exposure of Non-Metallic Materials	General - nonmetallic materials
ASTM D4587	Standard Practice for Fluorescent UV-Condensation Exposures of Paint and Related Coatings	Paint and related coatings
ASTM D4329	Standard Practice for Fluorescent UV Exposure of Plastics	Plastics
ASTM D1435	Standard Practice for Outdoor Weathering of Plastics	Plastics
ASTM D4798	Standard Practice for Accelerated Weathering Test Conditions and Procedures for Bituminous Materials (Xenon-Arc Method)	Bituminous roofing
ASTM D4799	Standard Practice for Accelerated Weathering Test Conditions and Procedures for Bituminous Materials (Fluorescent UV, Water Spray, and Condensation Method)	Bituminous roofing
ISO 11341	Paints and varnishes – artificial weathering and exposure to artificial radiation – exposure to filtered xenon-arc radiation	Paint and varnishes
ISO 11507	Paints and varnishes – exposure of coatings to artificial weathering – exposure to fluorescent UV lamps and water	Paint and varnishes
ISO 1296	Flexible sheets for waterproofing: Bitumen, plastic and rubber sheets for roofing. Method of artificial aging by long term exposure to elevated temperature	Bituminous materials
ISO 1297	Flexible sheets for waterproofing: Bitumen, plastic and rubber sheets for roofing. Method of artificial aging by long term exposure to the combination of UV radiation, elevated temperature and water	Bitumen or plastic or rubber sheets for roof waterproofing

However all of these standards have been optimized considering the traditional failure criteria for coverings such as embrittlement, discolouration, chalking, loss of gloss.

Unfortunately, in the case of thermochromic glazing components, the most important functionality is represented by optical properties and mainly solar transmittance and its change over the time due to stress factors (UV radiation, temperature and humidity) but also soiling. The development of an accelerated weathering procedure for thermochromic glazing materials requires therefore an alternative approach that is capable of reproducing also the effect of pollutants, hydrocarbons and biological growth on tested samples. In order to separate the effect of different factors to the thermochromic glass aging tests based on thermal stress or fatigue and on soiling have been designed and applied to some of the samples provided by UCL as reported in Section 3.2.1 .

4.3.1 Accelerated ageing tests procedure – Thermal fatigue

Table 13 summarize the protocol followed to perform accelerated aging tests to mimic one-year outdoor exposure of thermochromic glazing samples and considering only a thermal stress exposure reproduced on a thermal controlled chamber or climatic chamber, see Figure 78. The sample was exposed to 86 cycles and then the thermal transmittance modulation was measured. The sample was therefore exposed to a second conditioning of 86 cycles and its transmittance modulation measured again. 172 cycles were performed in order to simulate the exposure of the samples to the effects of thermal fatigue that would occur on site over the course of a year.

Table 13. Accelerated aging laboratory protocol to mimic one-year outdoor exposure of thermochromic glazing samples

86 h total duration (86 cycles)	**1 cycle** = ramp up from 50 to 80 °C in 30 minutes and ramp down from 80 to 50 °C in 30 minutes for a total duration of 1 h Relative humidity fixed at 35%
	Transmittance measurements

(a)   *(b)*

Figure 78. (a) Climatic chamber used for accelerated aging tests and (b) samples installed in the chamber

The tested samples were: sample 4 of set n. 1 (coated with VO_2), sample 4 of set n. 2 (coated with VO_2 and silica protective layer), sample V96-4 (coated with TiO_2 and VO_2) and sample ML4 (coated with two alternate layer of TiO_2 and one of VO_2 and with a Norland protective layer).

Figure 79 compares the hysteresis curves evaluated for the samples 4 of set n.1 and 2 before and after the conditioning cycles calculated in transmission mode at the wavelength of 2000 nm, averaged in the solar spectrum and averaged in the visible spectrum respectively.. It is evident that the coating lost completely its thermochromic properties after the conditioning, also summarized in

Table 14 .

Solar averaged transmittance T_{sol}

Photopically averaged transmittance T_{lum}
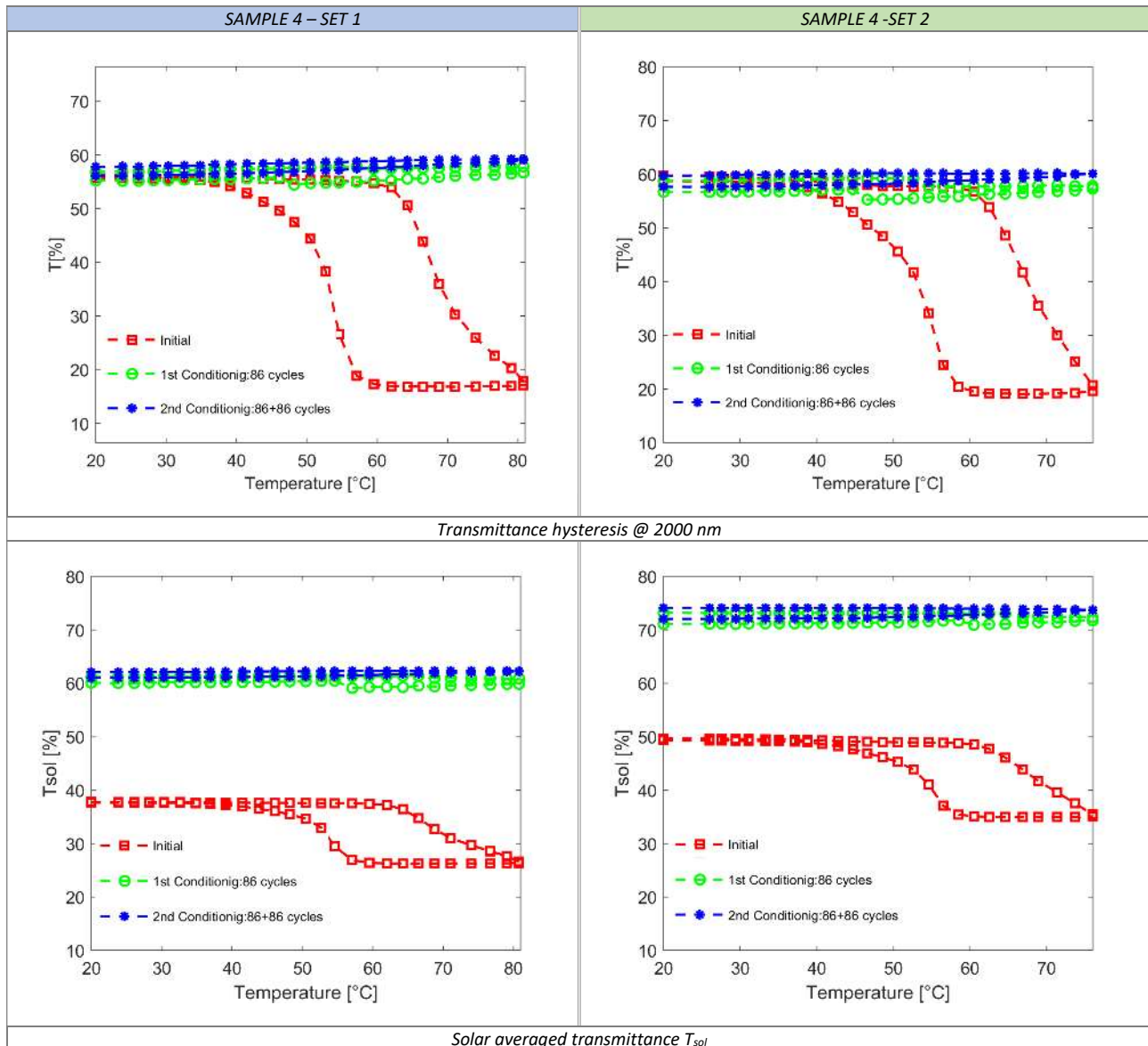
Figure 79. Thermochromic optical properties measured during the accelelerated aging tests in transmission mode for the sample 4 (set n. 1) and the sample 4 (set n. 2)

Table 14. Luminous, solar transmittance and transmittance @ 2000 nm of the samples 4 belonging to set n. 1 and 2

Samples	Coating	Conditioning	hot state		cold state		ΔT_{sol}	ΔT_{lum}
			T_{sol} [%]	T_{lum} [%]	T_{sol} [%]	T_{lum} [%]	[%]	[%]
4 – set 1	**VO$_2$**	Not conditioning	26.4	39.5	37.7	40.5	11.3	1.0
		86 h	59.9	65.4	60.2	66.5	0.3	1.1
		172 h	62.3	66.3	62.1	68.2	-0.1	1.9
4 - set 2	**VO$_2$ – SiO$_2$**	Not conditioning	35.1	40.7	49.4	42.5	14.3	1.8
		86 h	72.4	75.1	73.2	75.8	0.8	07
		172 h	73.6	76.1	74.1	76.8	0.5	0.7

The samples ML-4 and V96-4 of set n.3 showed a slight deviation between the first and second conditioning and therefore the hysteresis loops are reported for the initial condition, the one after 86 cycles and after 172 cycles in Figure 80. Observing the hysteresis loops it can be concluded that the ML-4 sample does not undergo alterations as the curves are comparable and therefore that the coating protection is essential to assure the thermochromic property durability. As for the samples 4 of the set n. 1 and n. 2, the sample V96-4 after the first 86 cycles undergoes an important deterioration of the coating, the curve flattens out, no longer showing the temperature switching.

Sample ML-4 – SET 3	Sample V96-4 - SET 3

Transmittance hysteresis @ 2000 nm

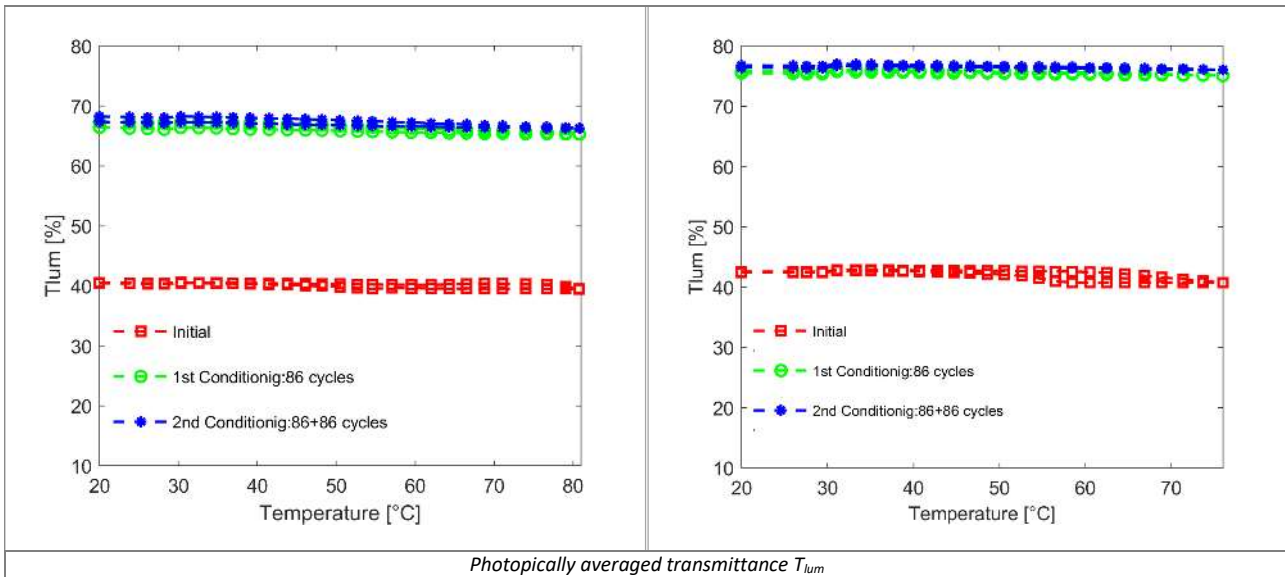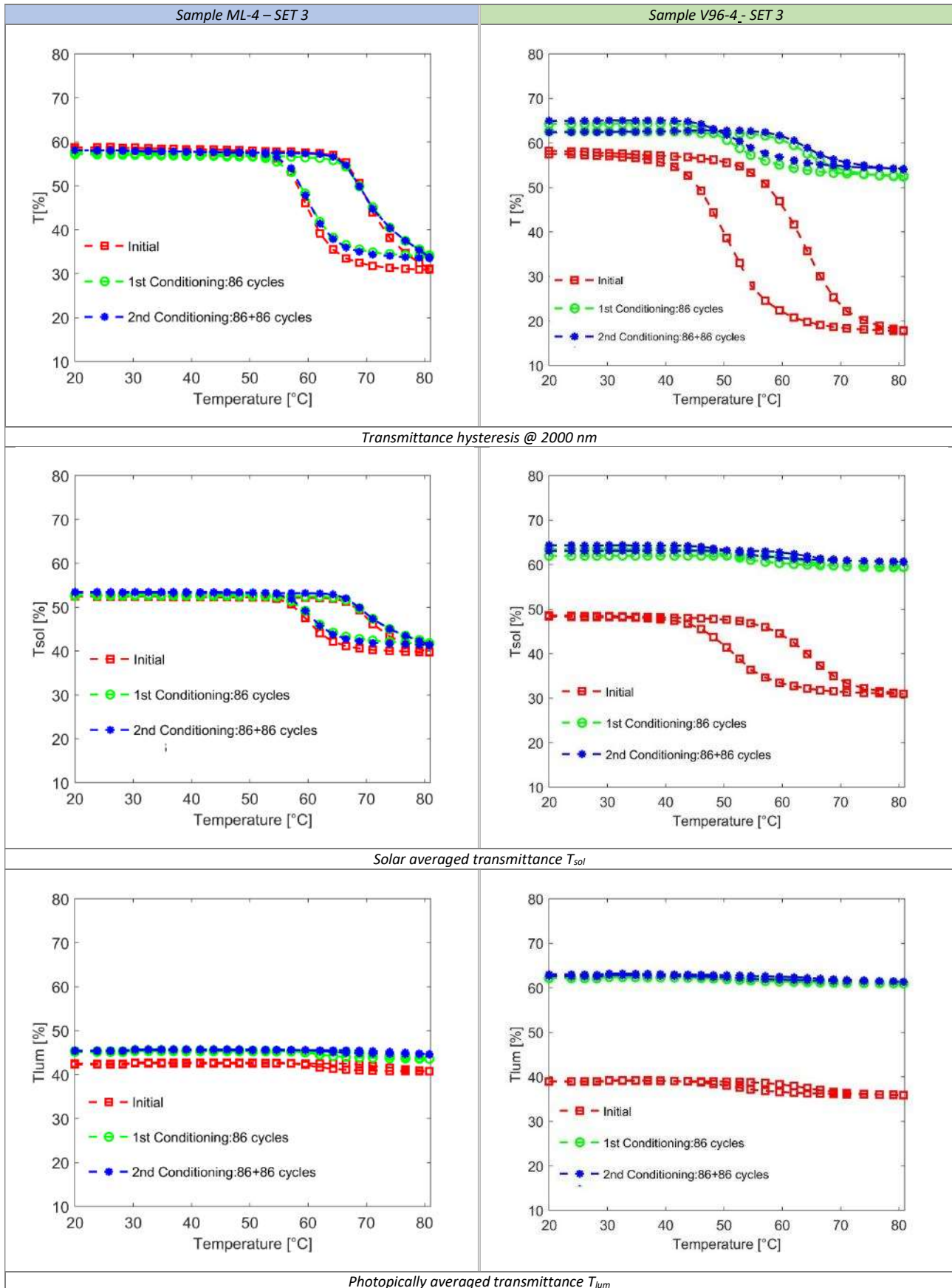*Solar averaged transmittance T_{sol}*

Photopically averaged transmittance T_{lum}

Figure 80. Thermochromic optical properties measured during the accelelerated aging tests in transmission mode for the samples ML-4 and V96-4 (set n.3)

Table 15. Luminous, solar transmittance and transmittance of the samples ML-4 and V96-4 to set n. 3

Samples	Coating	Conditioning	hot state		cold state		ΔT_{sol}	ΔT_{lum}
			T_{sol} [%]	T_{lum} [%]	T_{sol} [%]	T_{lum} [%]	[%]	[%]
ML-4 set 3	$TiO_2+VO_2+TiO_2$	Not conditioning	39.8	40.7	52.6	42.5	12.8	1.8
		86 h	41.8	43.6	52.9	45.2	11.1	1.6
		172 h	41.5	44.6	53.3	45.5	11.8	0.9
V96-4 set 3	TiO_2+VO_2	Not conditioning	40.0	35.9	48.4	39.0	8.4	3.1
		86 h	59.5	61.0	63.5	62.6	4.0	1.6
		172 h	60.6	61.3	64.4	63.1	3.8	1.8

4.3.2 Accelerated ageing tests procedure – Soling and weathering conditions

Deposition of atmospheric particulate matter is the dominant source of soiling agents accumulating on exposed building surfaces [16],[17]. The main particulate emitted by human activities, generated by natural processes, and formed in the atmosphere in Europe are dust minerals (28–66 wt %, percentage in weight), black carbon(4–12 wt %), organic matter (8–36 wt %) and soluble salts (18–27 wt %) [16].

While commercial weatherometers (weathering test chambers) are commonly used by industry to simulate the effect of weathering on material durability, widely accepted methods to simulate soiling have not been developed. Various dirt pick-up methods created by industrial R&D centers are used for in-house testing, [18][19]. UNIVPM has developed an accelerated laboratory method for simulating both soiling and weathering of building envelope based on Cool Roof Rating Council (CRRC) ratings of products naturally exposed for 3 years. This method will be applied also to test the durability of thermochromic coated glass in terms of optical properties when exposed to weathering and soiling conditioning.

The accelerated test protocol is based on the one proposed by the Heat Island Group of the Lawerence Berkeley National Laboratory (LBNL) [20], [21], [22]. UNIVPM has cooperated with LBNL to test the reproducibility of the tests by performing an interlaboratory study of the accelerated aging method for roofing materials, [23]. With respect to the LBNL protocol the one proposed for the glass coating accelerated test has been changed in the conditioning phase, due to the fact that the thermochromic coating is sensitive to the whole solar spectrum (300 -2500 nm) and not only to the UV range. A weathering tester equipped with a xenon arc light source has been therefore exploited to condition the samples. Specifically it has been reproduced the cycle 9 prescribed by the standard ASTM G155 (table X3.1), with the only difference in the black panel temperature which has been set to 80°C. This increase in temperature is due to the fact that the thermochromic coating switching temperature is of 68-70°C and therefore if the temperature had been set as required by the standard (63°C), the coating would never have switched.

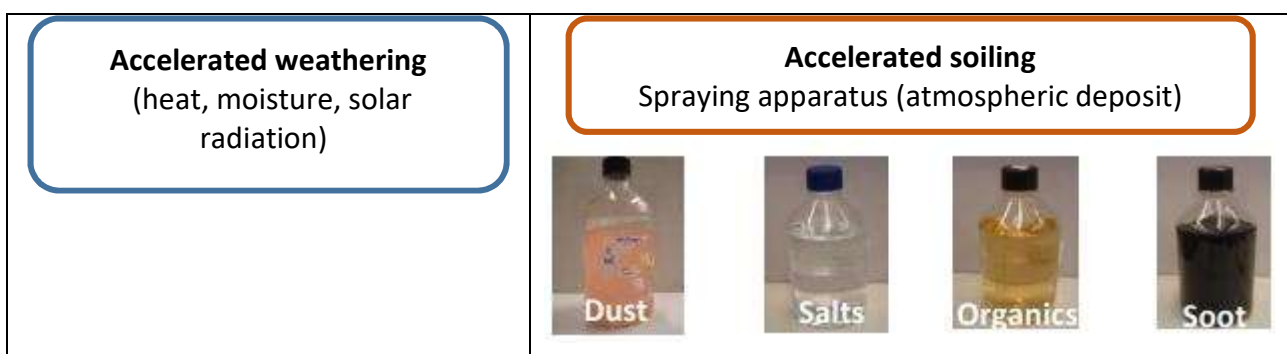The procedure consists of four main steps described in Table 16:

Table 16. Accelerated aging protocol

1. Conditioning	Daylight filter, irradiance= 180W/m^2 (300-400nm) in light at 80°C black panel temperature, light and water spray (temperature not controlled), dark at 40 °C and 90% RH
2. Soiling	Spray a mix of black carbon, humic acid, dust, and salts Target wet soiling coverage of 10 mg/cm2 Evaporate water by heating with IR lamp
3. Conditioning	Daylight filter, irradiance= 180 W/m2 (300-400nm) in 102 min light at 80°C black panel temperature, 18 min light and water spray (temperature not controlled), 60 min dark at 40 °C and 90% RH
4. Measurement	Transmittance/Reflectance

The most critical phase of the procedure is the deposition of the soiling mixture on the surface. This process determines in most cases the largest drop in reflectance. The composition of the solution has been chosen aiming at representing the standard US climates and is a mix of the following constituents [20]:

- **Black carbon (5%):** commercially available hydrophilic black carbon
- **Mineral Dust (47%):** mixture of ferritic oxide and two natural clays, montmorillonite K10 and hydrophilic betonite
- **Salts (20%):** solution containing sodium chloride, sodium nitrate and calcium sulphate dehydrate
- **Organics(28%):** humic acid.

A fixed amount of this aqueous suspension (about 7.7 - 9 mg/cm^2) is finely sprayed on the specimen through a soiling apparatus (Figure 81) consisting in a pressurized vessel connected to a wide angle nozzle at the top of a plexiglas box. An initial calibration is required to ensure the proper amount of soiling mixture is deposited. During this phase a reference coupon is used and the spraying duration is adjusted till the difference of weight before and after the treatment on the reference correspond to the value specified by the procedure (7.5-9 mg/cm^2).

Accelerated weathering
(heat, moisture, solar radiation)

Accelerated soiling
Spraying apparatus (atmospheric deposit)

Dust   Salts   Organics   Soot
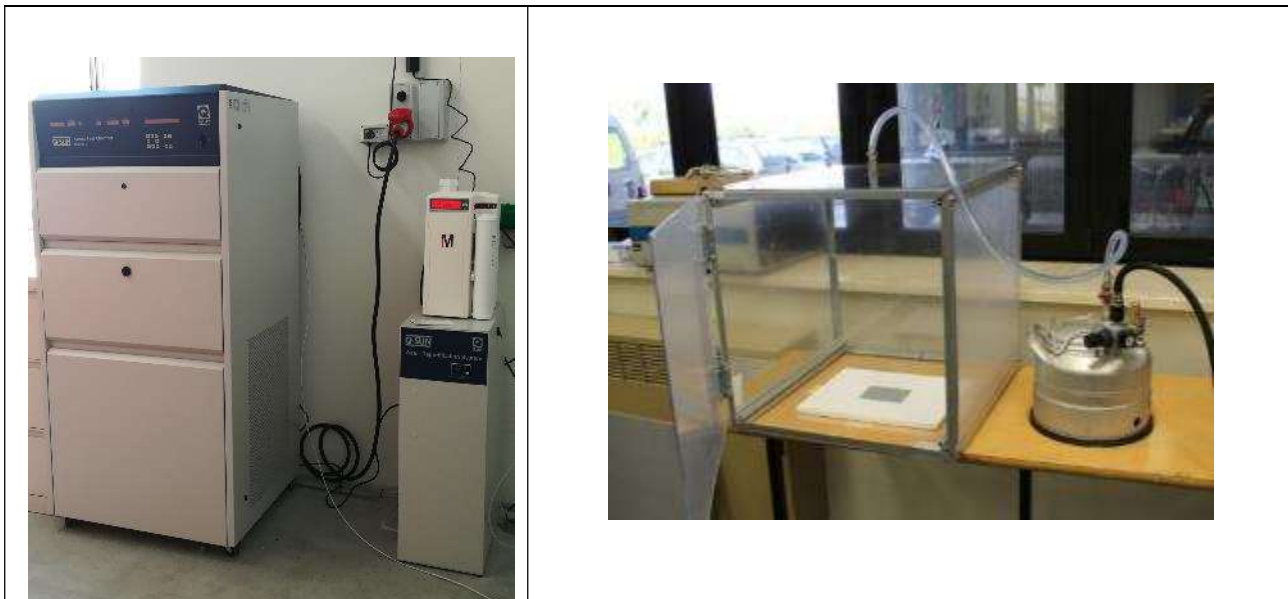
Figure 81. Apparatus for accelerated aging test (left) and soiling(right)

Figure 82. Samples after soiling

In order to maintain the correlation with natural ageing tests and to guarantee the repeatability of the method, the soiling pattern sprayed on the surface has to be kept under control. In particular two conditions have to be respected:

- The amount of sprayed soiling solution should not significantly differ from the value specified by the procedure in terms of wet mass.
- Soiling pattern should be uniform on the surface. Proper nozzle and spraying pressure should be selected to obtain finely dispersed drops on the surface. However this requirement cannot always be matched since the drop distribution also depends on the specific material and particularly on its hydrophobicity characteristics (contact angle).

The first samples exposed to artificial soiling are shown in Figure 82.

5 Compliance of design and manufacturing for retrofitting strategy

Additionally to the test already performed and above mentioned, some further actions are necessary to demonstrate the compliance of the VIG design and manufacturing for retrofitting. Some specific VIG compliances should be considered:

- Safety;
- Impact resistance;
- Acoustic performance;
- Fire resistance.

A fist relevant element is related to the protection for individuals from injury and falls, in particular considering two aspects:

- preventing the risk of injury caused by sharp pieces of glass;
- preventing the risk of falling through the glass (defenestration).

In the case of VIG the first risk has already been solved. Indeed, the utilization of 2 toughened 6 mm glass panes already comply with this first also for the application. Indeed in case of glass breakage of the VIGs' glass panes, the numerous small glass components will decrease the injury caused by sharp pieces typical of annealed glass; the utilization of a laminated glass will further reduce the injury which will occur.

On the other side, the VIG design has not considered in a first phase to prevent the falling through the glass. The falling can be prevent by the utilization of a laminated glass and this is necessary especially for public space compliances. For this reason the Task 4.1 for VIG scale up is including also the lamination of a glass on the VIG to allow a full compliance with this safety issue.

For what concerns VIG impact resistance, acoustic insulation and fire resistance, specific tests will be conducted to demonstrate the compliance with norms (impact resistance), with design specifications (acoustic insulation) or with performances not mandatory, but relevant for future construction scenarios (fire resistance). In particular these activities will be conducted in the frame of testing activities held in Task 4.4 of WP4 during prototyping and testing of Eensulate façade module. Indeed, the Eensulate façade module integrate the VIG has one of its main components and the tests will demonstrate the compliance with the norms especially for their applications in real cases.

Three tests will be conducted whose results will useful to demonstrate the compliance with norms of the general behaviour of the VIG test, see Table 17 for details:

- **Performance Mock-up (PMU)** – test to demonstrate the achievements of CE marking standard classification for façade under EN 13830:2005;
- **Acoustic Mock-up (AMU)** – test to identify the acoustic insulation of Eensulate façade;
- **Fire Mock-up (FMU)** – test to demonstrate the behaviour under fire actions, but not the the standard fire curve provided in the EN 1363-1: Fire resistance tests, Part 1.

Table 17. VIG prototype test details

Test name	Reference Norms	VIG tests	Description
Performance Mock-up (PMU)	EN 13830:2005 – CE marking	*Reference to Table 4 of PMU method statement (WP4)* Impacts for maintenance Impactor: spheroconical bag as per CWCT TN 76 Exposure category: F as per CWCT TN 75 (areas more than 1.5m above ground, wall surfaces at higher position than 6m)	Test conducted to demonstrate: - Serviceability: Class 1 (TN 76-Table 1) - Safety: Negligible risk (TN 76-Table 2) - Exceptional: Impact energies due to exceptional operation situations shall be sustained safely without disengagement of any component from their fixings

Acoustic Mock-up (AMU)	EN 16283-3	The acoustic insulation is relevant for a system integration and VIG is therefore tested within the Eensulate façade module. Field measurement of the apparent airborne sound insulation in accordance with standards UNI EN ISO 16283-3:2016/EC 1-2016/EC 2-2016 and UNI EN ISO 717-1:2013	The test will be conducted on the Eensulate façade which should achieves 52 dB of acoustic insulation. The role of vacuum is relevant
Fire Mock-up (FMU)	EN 1363-1	Fire test in medium scale to perform science oriented measurements. Specific fire temperature curve will be used until VIG fail from the Eensulate module's frame or VIG crack or break	Use the standard fire curve provided in the EN 1363-1: Fire resistance tests, Part 1 is no possible due to too high temperature achieved because the VIG is going to fail/break/crack before 200°C so there is no point to increase the temperature according to the standard temperature curve. A slower rate temperature increase instead of the standard testing curve. We could instead gradually increase temperature until cracking occurs.

The tests results will be reported in *D4.4 Outcomes of testing activities*, lead by Focchi and due in M48.

6 References

[1]   R. J. Corruccini; Vacuum [7–8], pages 19–29 (1957)

[2]   J. Crank, "The Mathematics of Diffusion", Clarendon Press, 1979.

[3]   L. M. Robeson, B. D. Freeman, D. R. Paul and B. W. Rowe, "An empirical correlation of gas permeability and permselectivity in polymers and its theoretical basis", J. Membr. Sci., 341, 178. B (2009)

[4]   L. K. Massey, "Permeability Properties of Plastics and Elastomers: A Guide to Packaging and Barrier Materials", Plastics Design Library, 2nd Edition (2002).

[5]   H. Beese, W. Grahlert, S. Kaskel, J. Grubler, J. Koch, K. Pietsch, "HiBarSens: Measurement of barrier properties by tunable diode laser absorption spectroscopy (TDLAS)", Web Coating & Handling Conference 2012. Vol.2 : Myrtle Beach, South Carolina, USA, 21 - 24 October 2012, Red Hook, NY: Curran, 2013 ISBN: 978-1-622-76950-6 pp.848-866.

[6]   A. Khawam, and D. R. Flanagan, "Solid-State Kinetic Models: Basics and Mathematical Fundamentals" J. Phys. Chem. B, 110 (35), 17315-17328 (2006).

[7]   M. Righetti, P. Manini, "High pressure quadrupole mass spectrometer for residual gas analysis in fluorescent lamps", Proc. 8th Int.Symp. Sc. And Techn. of L. Sources 378 (1998).

[8]   M. Currie, M. A. Mastro, and V. D. Wheeler, ''Characterizing the tunable refractive index of vanadium dioxide'', Vol. 7, No. 5 | 1 May 2017 | OPTICAL MATERIALS EXPRESS 1697.

[9]   Y. Jung-Hoon, N. Sang-Hun, L. Ji, B. Jin-Hyo, "Enhanced Visible Transmittance of Thermochromic VO2 Thin Films by SiO2 Passivation Layer and Their Optical Characterization", Materials 9(7):556, July 2016.

[10] M. Currie, M. A. Mastro, and V. D. Wheeler, "Characterizing the tunable refractive index of vanadium dioxide," Opt. Mater. Express 7, 1697-1707 (2017).

[11] A. Taylor, I. Parkin, N. Noor, C. Tummeltshammer, M. S. Brown, and I. Papakonstantinou, "A bioinspired solution for spectrally selective thermochromic VO2 coated intelligent glazing", Opt. Express, vol. 21, pp. A750–A764, Sep 2013.

[12] T. Smith and J. Guild, "The C.I.E. colorimetric standards and their use", Trans. of the Opt. Soc. 22, 73 (1931).

[13] American Society for Testing and Materials, "ASTM G173-03 reference spectra," (2013), http://rredc.nrel.gov/solar/spectra/am1.5/ASTMG173/ASTMG173.html.

[14] ASTM Standard G7 (2011) Standard practice for atmospheric environmental exposure testing of nonmetallic materials.

[15] Johnson, B.W., McIntyre, R., 1996. Analysis of test methods for UV durability predictions of polymer coatings, Progress in Organic Coatings 27, 95-106

[16] O. Favez, H.Cachier, A.Chabas, P.Ausset, R.Lefevre, Crossed optical and chemical evaluations of modern glass soiling in various European urban environments,Atmos.Environ.40(2006)7192–7204.

[17] M. Ferm ,J.Watt, S.O'Hanlon, F.DeSantis, C.Varotsos, Deposition measurement of particulate matter in connection with corrosion studies, Anal.Bioanal. Chem. 384(2006)1320–1330.

[18] BASFSE, Compositions with improved dirt pickup resistance comprising layered double hydroxide particles, Patent WO2011022175, /http://patent-scope.wipo.int/search/en/WO2011022175S, 2011.

[19] Dow Construction Chemicals, Elastomeric roof coatings: the use of elastomeric acrylic roof coatings to reduce the air conditioning load of low-slope-roof buildings. ⟨http://www.dowconstructionchemicals.com/na/en/pdfs/832-00209. pdf⟩, 1994.

[20] Sleiman, Kirchstetter, T.W., Berdahl, P., Gilbert, H.E., Quelen, S., Marlot, L., Preble, C.V., Chen, S., Montalbano, A., Rosseler, O., Akbari, H., Levinson, R., Destaillats, H., 2014. Soiling of building envelope surfaces and its effect on solar reflectance - Part II: Development of an accelerated ageing method for roofing materials. Solar Energy Materials and Solar Cells 122, 271-281.

[21] Paolini, R., Poli T., Fiori, M., Mainini, A.G., 2012. Valutazione delle prestazioni di cool materials esposti all'ambiente urbano: sporcamento e invecchiamento accelerato. Report Ricerca di Sistema Elettrico 2012/114.

[22] Sleiman M., Destaillats H., Kirchstetter, T., Gilbert H., Berdahl P., Akbari H., Marlot L., Quelen S., Preble C., Spears M., Ban-Weiss, G., Levinson. R., 2011. Accelerated Aging Protocols for Roofing Materials: Version 1.0, in Proc. of International Workshop on Advances in Cool Roof Research, Berkeley, CA – July 28 & 29, 2011

[23] Sleiman M., Chen S., Gilbert H. E., Kirchstetter T. W., Berdahl P., Bibian E., Bruckman L. S., Cremona D.,. French R. H., Gordon D. A., Emiliani M., Kable J., Ma L., Martarelli M., Paolini R., Prestia M., Renowden J., Revel G. M., Rosseler O., Shiao M., Terraneo G., Yang G., Yu G., Zinzi M., Akbari H., Levinson R., Destaillats H., Soiling of building envelope surfaces and its effect on solar reflectance – Part III: Interlaboratory study of an accelerated aging method for roofing materials, Solar Energy Materials and Solar Cells, Volume 143, 2015, Pages 581-590